Title

Investigating the Molecular Mechanisms Involved in the Mechanosensation of Neural Stem Cell Differentiation

Author

Lopez, Paola Andrea

Publication Date

2022

Peer reviewed|Thesis/dissertation

Investigating the Molecular Mechanisms Involved in the Mechanosensation of Neural Stem Cell Differentiation

By

Paola Andrea Lopez

A dissertation submitted in partial satisfaction of the

requirements for the degree of

Joint Doctor of Philosophy
With the University of California, San Francisco

in

Bioengineering

in the

Graduate Division

of the

University of California, Berkeley

Committee in charge:

Professor Sanjay Kumar, Co-chair
Professor David V. Schaffer, Co-chair
Professor Sandrine Dudoit

Spring 2022

Abstract

Investigating the Molecular Mechanisms Involved in the Mechanosensation of Neural Stem Cell Differentiation

by

Paola Andrea Lopez

Joint Doctor of Philosophy in Bioengineering with the University of California, San Francisco

University of California, Berkeley

Professor Sanjay Kumar, Co-chair
Professor David V, Schaffer, Co-chair

Since it was discovered that neural stem cells (NSCs) have the capacity to self-renew and produce progenitor cells beyond development, there has been increasing interest in harnessing these endogenous processes for repairing the injured or disease brain. Specifically, the hippocampus is one of the few areas of the brain that continue to produce neurons postnatally. A decrease in neurogenesis in this region of the brain is associated with not only aging, but also with a rise in neurodegenerative disorders such as Alzheimer's disease. Elucidating the regulation of neurogenesis is crucial for understanding adult brain function, as well as for treating neurodegeneration using cell replacement therapy.

The local microenvironment of the NSCs, also known as the neurogenic niche, is composed of a complex network of signaling mechanisms that strongly regulate NSC function, and recapitulating this network in vitro is a major barrier to neuronal cell replacement therapy. One such signaling mechanism is mechanotransduction of biophysical cues from the extracellular matrix (ECM) into cytoskeletal changes that influence whether NSCs differentiate into neurons, astrocytes, or oligodendrocytes. However, our understanding of the underlying mechanism still largely derives from focused studies on a limited set of molecular candidates. Therefore, the focus of my dissertation has been on probing mechanosensitive lineage commitment in a more unbiased-fashion using high-throughput sequencing technology.

In the first chapter of this dissertation, I conducted whole-transcriptomic RNA sequencing to NSCs cultured on soft (500 Pa) versus stiff (73 kPA) substrates, which we previously showed bias NSCs towards neuronal and astrocytic fates, respectively. Importantly, we conducted our studies 12-36 hours after cells were seeded and exposed to differentiation cues, a window where we have shown NSC fate is maximally sensitive to mechanical cues. While we identified a large number of differentially expressed genes in NSCs cultured on soft vs. stiff substrates, eukaryotic translation elongation factor 1 alpha

1 (eEF1A1) stood out in its high differential expression and established contributions to F-actin bundling and protein synthesis. To demonstrate the functional importance of eEF1A1 to mechanosensitive lineage commitment, we suppressed its expression with shRNAs, which resulted in an increase on both soft and stiff substrates. Rescue of full eEF1A1 on top of the knockdowns concomitantly reduced neurogenesis on both soft and stiff substrates. We further determined that eEF1A1 is regulating fate commitment by controlling Yes-Associated Protein (YAP) levels, and Rho-GTP levels. Thus, eEF1A1 is a novel mechanoregulators of NSCs that plays an important role in NSC fate commitment.

In the second chapter, we used the RNA-sequencing results from Chapter 1 and determined that substrate stiffness is regulating the usage of different alternative polyadenylation sites in the 3'UTR of mRNA during NSC differentiation. This difference in usage results in different mRNA isoforms that have the same coding region but vary in 3'UTR length in NSCs differentiating on soft versus stiff substrates. Interestingly, we show that most of the 3'UTR isoforms identified in soft substrates have a longer 3'UTR relative to NSCs differentiating on stiff substrates. A longer 3'UTR results in a higher chance of the mRNA to degrade in the cytoplasm through microRNA interactions. Furthermore, we show that there are higher expression levels of the Cleavage Factor Im 25 (CFIm25) protein in NSCs differentiating on soft substrates relative to stiff, which may be the cause of the difference in 3'UTR length. Lastly, suppression of CFIm25 suppresses overall neurogenesis, thus establishing its important functional role in fate commitment. Overall, this work integrates systems level measurements with biophysical approaches to identify the novel roles of eEF1A1 and 3'UTR lengthening and shortening in controlling stem cell mechanosensitive lineage commitment.

Table of contents

Abstract 1

Table of contents i

Table of Figures iv

List of tables vi

Acknowledgments vii

Chapter 1: Investigating the mechanosensation of adult neural stem cell differentiation 1

1.1. The significance of adult hippocampal neurogenesis 1

1.2. Elucidating the mechanism regulating NSC behavior 2

1.3. Overview of mechanotransduction pathways regulating NSC fate commitment 5

1.4. Scope of dissertation and impact 5

Chapter 2: eEF1A1 mediates the mechanosensation of NSC differentiation 8

2.1. Introduction 8

2.2. Results 9

Substrate stiffness influences gene expression 12-hours post differentiation 9

Loss of eEF1A1 increases neurogenesis 12

eEF1A1 is necessary and sufficient for inhibiting neurogenesis 13

eEF1A1 regulates neurogenesis through changes in Rho-GTP signaling 15

eEF1A1 regulates YAP levels during early neurogenesis 17

2.3. Discussion 18

2.4. Materials and Methods 22

Neural Stem Cell Culture 22

Polyacrylamide gel synthesis and protein functionalization 22

RNA sequencing sample preparation 23

RNA sequencing analysis 23

Quantitative Real Time PCR 23

Knockdown and overexpression vectors 24

Viral transduction 24

Immunofluorescence staining and imaging 24
Western blot and RhoA Activation Assay (G-Elisa) 25
TCF Luciferase Assay 25
Overall Nascent Protein Synthesis Assay 26
2.5. Acknowledgements 26
Chapter 3: Substrate Stiffness influences the alternative polyadenylation of mRNA transcripts during NSC differentiation 27
3.1. Introduction 27
3.2. Results 28
Determining 3'UTR isoform enrichment using CSI-UTR 28
Substrate Stiffness leads to alternative PAS usage in the 3'UTR of mRNA during NSC differentiation 30
Substrate Stiffness regulates the expression of CFIm25 32
Knockdown of CFIm25 suppresses neurogenesis 33
3.3. Discussion 34
3.4. Materials and Methods 36
Neural Stem Cell Culture 37
Polyacrylamide gel synthesis and protein functionalization 37
Identifying 3'UTR isoforms using CSI-UTR 37
Identifying Differentially Expressed 3'UTR isoforms 37
Quantitative Real-Time PCR 38
Western Blot 39
Knockdown Vector 39
Viral Transduction 39
Immunofluorescence staining and imaging 39
3.5. Acknowledgements 40
Appendix A: Supplementary Material for Chapter 2 41
Appendix B: Supplementary Material for Chapter 3 47
Appendix C: Application of CRISPRi genome screen to identify novel factors involved in the mechanosensing of NSCs 50

C.1 Background 50
C.2 Generating cell lines for performing CRISPRi knockdown screen 50
Development of mouse reporter line for selecting GFP+ (neurons) cells 50
Lentiviral packaging of plasmid(s) encoding dCas9-KRAB fusion protein and the single guide RNA library 55
C.3 In vitro selection screen for sgRNAs that knockdown genes that either enhance or suppress neurogenesis 56
C.4 Discussion and Future work 60
C.5 Supplementary Material 61
References 63

Table of Figures

Figure 1.1: A schematic illustration of the NSC microenvironmental niche in the SGZ. .. 3

Figure 1.2: NSCs are regulated by cues from the microenvironment. 3

Figure 1.3: Overview of the two main chapters discussed in this dissertation 7

Figure 2.1: RNA-Seq analysis during mechanosensing window of NSCs. 11

Figure 2.2: eEF1A1 is necessary for inhibiting neurogenesis 13

Figure 2.3: eEF1A1 is necessary and sufficient for inhibiting neurogenesis, particularly through interactions in Domain III. 14

Figure 2.4: Domain III region of eEF1A1 regulates Rho GTPase activity. 17

Figure 2.5: eEF1A1 regulates YAP protein levels through its Domain III 18

Figure 2.6: eEF1A1 upregulation on stiff substrates leads to a suppression of neurogenesis by increasing RhoA activity and YAP protein levels 22

Figure 3.1: Example of CSI significance calculation. 28

Figure 3.2: Read coverage track of two genes identified in the CSI-UTR analysis. 30

Figure 3.3: Scatter plot of RNA-seq data. 31

Figure 3.4: Experimental verification of 3'UTR analysis of RNA-seq results. 32

Figure 3.5: CFIm25 levels increase in NSCs seeded on soft substrate relative to stiff during differentiation. 33

Figure 3.6: Knocking down CFIm25 (by targeting *NUDT21* gene) suppresses expression 34

Figure A.1: Principal Component (PCA) and Pathway Analysis of RNA-sequencing results. 41

Figure A.2: phospho-AMOT and Overall Protein Synthesis measurements. 42

Figure A.3: Structured Illumination Microscopy (SIM) images of NSCs post 24 hours differentiation. 43

Figure B.1: Determining the change in 3'UTR length in NSCs in response to differentiating on a stiff substrate. 47

Figure B.2: There are more 3'UTR isoforms of eEF1A1 that are shorter in NSCs differentiating on stiff substrate relative those on soft. 48

Figure B.3: Treating NSCs for 24 hours with Torin1, mTOR inhibitor. 49

Figure C.1: Strategy for sorting neurons from population of differentiated NSCs. 51

Figure C.2: Strategy to inserting GFP downstream of Tubb3 endogenous gene. 52

Figure C.3: Strategy for genotyping clonal cells for generating reporter line. 52

Figure C.4: Verifying genotyping results using Sanger Sequencing and PCR. 54

Figure C.5: FACS results verifying reporter line. 54

Figure C.6: Immunostaining images of NSCs differentiating after 6 days. 55

Figure C.7: Selection strategy for CRISPRi genome wide screen to determine genes that enhance neurogenesis. 56

List of tables

Table 3.1: Results of CSI-UTR Analysis 29

Table 3.2: Results from determining the lengthening and shortening of the 3'UTR region of the mRNAs that had differentially expressed 3'UTR isoforms (from the CSI-UTR analysis) 30

Table A.1: List of genes found in each Cluster Group (from Figure 1.1.b) 44

Table C.1: Expected primer size of each of the primer sets used to genotype clonal cell lines. 52

Table C.2 Gene identity, function, and phenotype score of the most enriched genes from the GFP- population 58

Table C.3 Gene identity, function, and phenotype score of the most enriched genes from the GFP+ population 59

Table C.4: Primer sequences used to generate and verify reporter line 61

Table C.5: Primer sequences used for genotyping analysis 61

Acknowledgments

First off, I would like to give a huge thanks to my co-chairs of my dissertation committee, Professor David Schaffer and Sanjay Kumar, for their never ending support these past years. I am truly amazed, not just only by their vast scientific accomplishments, but also their extremely empathetic, and caring persona that made every interaction with them a delight. I have learned so much from them these past few years, and extremely grateful for not only the opportunities they both have given me, but also for encouraging me to pursue a variety of creative research directions. Both of them played instrumental roles in the scientist I am today and hope to one day emulate their scientific insightfulness.

I also want to give a shout-out to the members of my qualifying exam and dissertation committee – Professor Mohammad Mofrad, Professor Todd McDevitt, Professor Andrew Dillin, and Professor Sandrine Dudoit. All the meetings we had throughout the years were extremely insightful and played a crucial role in the development of my thesis work.

Like any other position, the lab environment plays a huge role in the well-being and happiness of any researcher. First off, I want to thank the lab managers of each of the labs - Katherine Patterson, Ruby Nelson and Noem Noiwangklang - for making the labs run smoothly and functionally. I want to also thank my NSC mechanotransduction subgroup – Serah Kang, Phillip Kang, Rocio Sampayo, Eric, Qiao, and Jieung Baek – for all the scientific discussions we had throughout the years, the reagents I 'borrowed' from you all, and for listening to me rant about the tiniest little things. I would also like to give a huge shout-out to some of my 'unofficial' mentors I had these years, particularly Kayla Wolf, Stacey Lee, Joseph Chen, Jasmine Hughes, and Kira Mosher for being extremely patient with me, especially during my younger PhD days, teaching me the simplest protocols, and all your scientific wisdom. I also want to give a shout-out to some of the lab members who made working in the lab these past few years a joyful one - Erin Akins, Cameron Morley, Kwasi Amofa, Ana Carniero, Hunter Johnson, Kaz Lewis, and Vivien Tran. From our 'failed' running groups, to random happy hours, thank you guys for making lab not just a place to work, but a place where I got to make some of the closest friendships during my PhD tenure.

I want to also thank Nick Fahrenkrog, for not just hearing me complain about when an experiment went wrong or for your free dog-sitting services, but also making sure I remember there is more to life than lab. Truly the best years of my PhD have been the last few years we spent together.

I am also extremely thankful for the endless love and support my parents, Jenny and Gustavo Lopez, gave me these past few years as I pursued my graduate degree. Without you both, I (literally) would not be here today and I owe all my academic success and accomplishments to both of you. I also want to thank my younger siblings, Kelsey and Carlos Lopez, who inspire me to be the best role model a person can be. They both are smarter, more creative, and more insightful than I am. I am really excited to hear about all the things they will accomplish in the future.

Last, and certainly not the least, I want to give a shout-out to my dog Yoda. I got Yoda the first year of my PhD and he has not left my side since day one. He truly made every bad day go away with his smile and joyful attitude. I could not have gone on this journey without him. Thank you for being the best furry cheerleader a girl can ask for.

Chapter 1: Investigating the mechanosensation of adult neural stem cell differentiation

1.1. The significance of adult hippocampal neurogenesis

Within our body, adult stem cells have the ability to replace injured or damaged cells to maintain tissue homeostasis. However, it was not until that scientists discovered regions of the brain that contained stem cells (termed neural stem cells) that have the ability to generate neurons beyond development and into adulthood. The generation of neurons from neural stem cells is referred to as neurogenesis. The first evidence of this phenomena was in the 1960's when scientists injected thymidine-H3 was into young rats and found granule cells labeled in the dentate gyrus of the hippocampus[1], thus demonstrating that there are stem cells within the brain that can self-renew and differentiating beyond development. However, this study was met with skepticism, mostly due to the lack of understanding as to how this labeling technique work.

It was not until 20 years later, that scientists used another thymidine analog, bromodeoxyuridine (BrdU), in pulse-chase experiments on post-mortem brain slices of cancer patients to show adult neurogenesis may occurs[2]. This discovery shifted the central dogma of developmental biology, which had the belief that the generation of neurons halted after development. However, some recent work presented data that shows neurogenesis does not at all exist in adults.[3] This work was met with some criticism as it did not discuss patient information nor other possible variables that could result in the lack of neurogenesis (i.e. underlying illnesses).[4] Furthermore, there was no information about how the tissues were preserved, and the timing between sample acquisition and labeling as the antigen binding region of cells from brain slices decays rapidly. Thus the lack of signal could have attributed to no protein present to begin with.

Further studies were later conducted to contradict this work[5], with the authors showing that neurogenesis does persist in adulthood and fully disclosing that the samples were acquired from healthy individuals and were fixated immediately to preserve the cell's protein binding regions[6]. While the paper does show the rate of neurogenesis does decline in adults relative to adolescence and is nearly non-existent in patients with neurodegenerative disorders like Alzheimer's (more discussed below), the general consensus is now that adult neurogenesis does occur in the brain.

As discussed above, one of the regions the neural stem cells reside in is within the hippocampus region of the brain. The hippocampus is important for both learning and memory, and thus, it is speculated that neurogenesis is necessary for maintenance of hippocampal capacity for memory[7]. One study has showed that when adult-born hippocampal neurons are ablated, there is an impairment of spatial memory, which supports a capacity for flexible, inferential, memory expression[8]. Furthermore, the adult hippocampus is one of the regions that is most affected by Alzheimer's Disease[9], which is characterized by decline in function and memory loss. Interestingly, it has been shown that the number and maturation of immature neurons declined rapidly as the progression of Alzheimer's patients advanced[6]. This was the first study linking the impaired neurogenesis as a relevant mechanism to the decline in cognitive function in Alzheimer's

patient, thus opening doors for therapeutic interventions. However, there is still a great deal of progress to be made to fully dissect the mechanism that regulates neurogenesis, which in turns influence the structural and functional plasticity in the regions where the NSCs reside in.

1.2. Elucidating the mechanism regulating NSC behavior

As discussed above, these neural stem cells (NSCs) reside in the dentate gyrus region of the hippocampus. Specifically within the dentate gyrus, they reside in the subgranular zone (SGZ) layer. In addition to residing in the SGZ, NSCs reside in the subventricular zone (SVZ) of the lateral ventricles[10]. Within the microenvironmental niche of the NSCs, there are various factors or cues that regulate neurogenesis, which differ from NSCs that reside in the SGZ or in the SVS. In this dissertation, we focus our attention primarily in the cells that reside in the SGZ but would be intrigued as to whether similar results translate to cells located the SVG.

Within the SGZ, NSCs not only interact with other support cell types such as microglia and endothelia cells, but also neurons, astrocytes, and oligodendrocytes[11]. The latter group of cells arise from NSCs themselves. The cells (classified as Type-II cells, and also referred in other contexts as neural progenitor cells (NPCs)) initially arise from activated quiescent radial glial-like cells, referred to as Type I cells. Both Type I and Type II cells reside in the SGZ prior to differentiation. Through various signaling mechanisms, the NPCs then migrate into the granule cell layer and generate into neuroblasts which in turn differentiate into new immature neurons, and maturate into adult-born dentate granule cells and extend dendritic arborizations and axonal projections[12].

There are various signaling mechanisms arising from the microenvironmental niche of the NSC that dictate this neurogenesis process. Our focus for this dissertation is on what specifically dictates whether NSCs (specifically the Type II NPCs) generate neurons, self-renew, or other differentiate into other lineages, specifically astrocytes or oligodendrocytes (Figure 1.1).

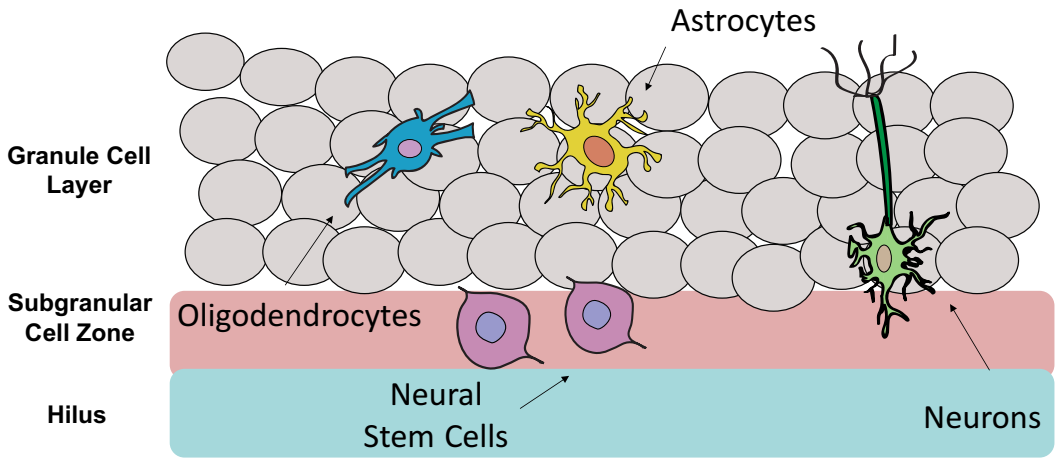

Figure 1.1 : A schematic illustration of the NSC microenvironmental niche in the SGZ. NSCs reside in the SGZ and then environmental cues influence whether they shall self-renew or differentiate into other lineages. Once it progresses to another lineage, the cells migrate into the granule cell layer which consists of mature granule cells

Within the microenvironmental niche, the cells are exposed to a host of biochemical and biophysical signaling factors such as cell-to-cell dependent cues, secreted paracrine signals, and lastly, the extracellular matrix (ECM) signals[13] (Figure 1.2).

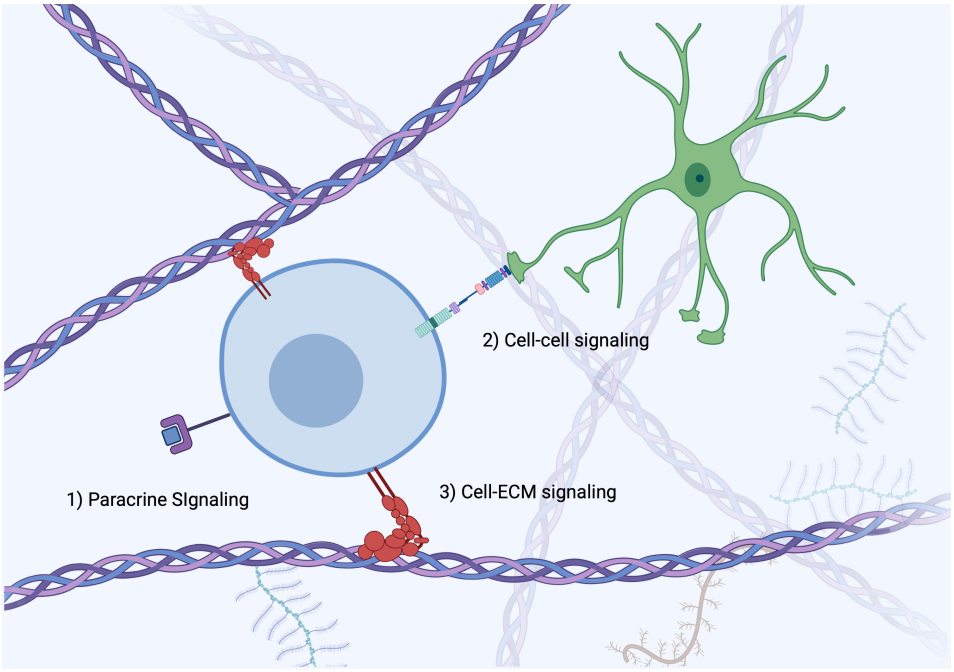

Figure 1.2: NSCs are regulated by cues from the microenvironment. NSCs receive multiple cues from their environment that regulate their behavior. These signals include 1) paracrine signals, 2) cell-cell signaling cues, and 3) cues from the extracellular matrix (ECM).

Cell-to-cell dependent cues are those that regulate juxtracrine signaling between membrane-bound ligands from one cell to receptors from other neighboring cell type. One of the main pathways affected by paracrine signals that has a significant effect in neurogenesis is the Wnt signaling pathway[14]. Wnt-3 is secreted by astrocytes residing in the niche, which in turn initiate a cascade of signaling mechanisms that activates ß-catenin signaling and induce neurogenesis. This secretion is shown to decreasing during aging, thus may contribute to the overall decrease in neurogenesis in adulthood [15]. Other paracrine signaling pathways have a more inhibitory role in neurogenesis such as bone morphogenic proteins (BMPs)[16], specifically BMP2, BMP4 and BMP6, which are part of the SMAD pathway and secreted by the endothelial cells[17] residing in the brain. The expression of both BMP4 and BMP6 have been shown to increase during aging[16,18], and inhibition partially rescued age-associated neurogenesis[16]. Interestingly, mice with decreased BMP signaling showed remarkably an increase in neurogenesis and cognitive

function, similar to the effects of exercise[19]. Thus further examination into the interplay into these pathways and contribution in neurogenesis is needed.

Two example juxtracrine signaling pathways, Notch[20] and Ephrin[21], have been identified to heavily influence NSC behavior and fate. Specifically, the two Ephrin classes have different effects on NSC fate commitment. Some work has been shown that when astrocytes present Ephrin-A2 and -A3 ligands, which are linked to the membrane by glyosylphosphatidylinositol linkage, and bind to the EphA7 receptors present in NSCs, they negatively regulate adult neurogenesis[22]. Interestingly, when astrocytes present Ephrin-B2 ligands and interact with EphB4-expressing NSCs, there is an increase in overall adult neurogenesis[21]. Thus targeting the Ephrin/Eph interaction is a proposed therapeutic intervention for regulating neurogenesis. Other studies focusing on the influence of Notch signaling have shown that without the Notch receptor that binds to the secreted ligand (e.g. Delta 1) in NSCs, there is a transient increase in overall neurogenesis followed by a complete depletion of all NSCs, and thus neurogenesis[20].

While manipulating signaling pathways in vivo is more feasible with the advancements in gene editing and delivery, most research continues to rely on manipulating NSC behavior in vitro to study NSC biology. This is mostly done using biomaterial platforms due to the ease of manipulation and reduced economic burden. Thus, there has been research in the past few years dedicated to understanding how the biochemical and biophysical cues emitted from the ECM regulate NSC proliferation and differentiation. ECM matrix proteins such as reelin[23], heparan sulfate proteoglycan[24], laminins[25], and hyaluronic acid[26] have previously been shown to interact with NSC receptors and influence overall fate commitment through emitting biochemical cues. The study of these matrix proteins and which property is important to enhance proliferation, and differentiation have aided in engineering more bio-mimetic materials to not only study NSC behavior, but also improve the viability[27] and engraftment[28] of stem cells for cell replacement therapies. While biomaterials do not recapitulate the all the signaling mechanisms from the ECM introduced to NSCs *in vivo*, they allow us to present NSCs to one or multiple of these cues, and see the degree of impact these cues have on their behavior. These biomaterials are thus engineered to recapitulate one or more properties of the extracellular niche NSCs reside in.

One of the biophysical cues of the environment that is proposed to play an important role in dictating cell behavior is the stiffness of the niche. NSCs are exposed to different stiffnesses as they migrate into the granule cell layer. Specifically, the elastic modulus of the SGZ differs from the elastic modulus from the granule cell layer, indicating that the NSCs are exposed to different elastic moduli when migrating from one region to another. Previous work in our lab has shown that as NSCs migrate into the granule cell layer, they are exposed to an increase of substrate stiffness, ranging from around 50 Pa to about 120 Pa[29]. However, these measurements were done using rat 2D brain slices and may not recapitulate what the cells are exposed to in vivo. Furthermore, the measurements were conducted using Atomic Force Microscopy, which results acquired from this approach do not always agree with one another.[30,31] Other work using ferrule-top dynamic indentation showed more consistent results from sample to sample, and verifies the consensus that cells are exposed to different moduli during migration into granule cell layer[32,33]. Lastly, the stiffness in the subgranular zone, the granule cell layer,

all increase during maturation, resulting in decrease of NSCs and immature neurons[34]. Thus, understanding how the biophysical properties is crucial in understanding the decrease in overall neurogenesis in adults

1.3. Overview of mechanotransduction pathways regulating NSC fate commitment

Using in-vitro biomaterial platforms, our labs have shown that the substrate stiffness of the environment regulates NSC fate commitment[35,36]. Specifically, when NSCs are cultured on a softer substrate (100 Pa – 500 Pa), there is a higher percentage of them that differentiate into neurons. When cultured on a stiff substrate, there is a higher percentage of NSCs that differentiate into astrocytes (1000 Pa >). This impact of substrate stiffness on NSC fate commitment has been proven to occur on both 2D and 3D substrates[37]. Further work has shown that changes in substrate stiffness result in changes in RhoA/Cdc42 activity[36], which are GTPases involved in regulating cellular contractor forces in NSCs. Specifically, RhoA and Cdc42 are part of the group of G-proteins that regulate F-actin dynamics and thus crucial in regulating intracellular forces[38]. As a GTPase, RhoA actively signals downstream targets only in the GTP-state, which our lab has shown is more active in NSCs differentiating on stiff substrates. Interestingly, modulating RhoA activity *in vivo* showed differences in neurogenesis as in *in vitro* results did. Thus the NSCs transduce the biophysical cues to biochemical cues to regulate their internal mechanical properties, and overall fate commitment.

Recent findings have shown that stem cells exhibit 'mechanical memory' which is when mechanical cues presented to the cells during early differentiation impact future cell behavior[39]. One notable example is done with human mesenchymal stem cells (MSCs) with YAP serving as a intracellular mechanical rheostat – which stores the information of the cell's past physical environment, and in turn, influence cell fate. When human MSCs are cultured on stiff substrates for longer than 7 days, there is an increase in YAP localization into the nucleus, even if they are cultured on soft substrates after being seeded on stiff substrates for longer than 7 days. Vice versa, if the cells are cultured on soft substrates, or on stiff substrates for less than 7 days then on soft substrates for any time after that, there is less YAP localization into the nucleus.

Motivated from this study, our lab determined that adult hippocampal NSCs also demonstrate some mechanical memory but through different mechanisms and time durations. Specifically we have shown that stiffness cues influence NSC fate commitment 12-36 hours[40] after initiating differentiation. During this early time window, NSCs respond to the changes in stiffness cues by regulating RhoA/Cdc42 activation, then YAP protein levels, which then modulates Wnt pathway/β-catenin, and thus neurogenesis.

1.4. Scope of dissertation and impact

Previously, we chose specific candidates and pathways to study how NSCs transduce biophysical cues based on prior literature and their involvement in mechanotransduction. For example, YAP was shown to be regulated by mechanical signals exerted by ECM stiffness and cell shape.[41] This candidate-to-candidate approach

in studying NSC mechanobiology biases our pool of candidates by eliminating those that have not been implicated in either the field of NSC biology or mechanotransduction.

To have a more unbiased perspective as to how NSCs respond to mechanical cues, and how these mechanical cues regulate NSC fate commitment, we turned to using more high-throughput sequencing approaches (such as RNA-seq) to see how NSCs respond to changes in substrate stiffness. Previous work using RNA sequencing technology have shown substrate stiffness regulates the gene expression of mesenchymal stem cell immunomodulatory markers in response to cytokine stimulation[42]. Other work also shows that substrate stiffness, coupled with different adhesion ligands, influence the cytokine secretion of these mesenchymal stem cells to regulate hematopoietic stem cell differentiation.[43]

Motivated by the results acquired from these studies, the focus of this dissertation is to use these high-throughput sequencing approaches to understand how NSCs respond to stiffness cues, and how these responses lead to the mechanotransduction of NSC fate commitment. The two chapters can be summarized in the Figure 1.3 below:

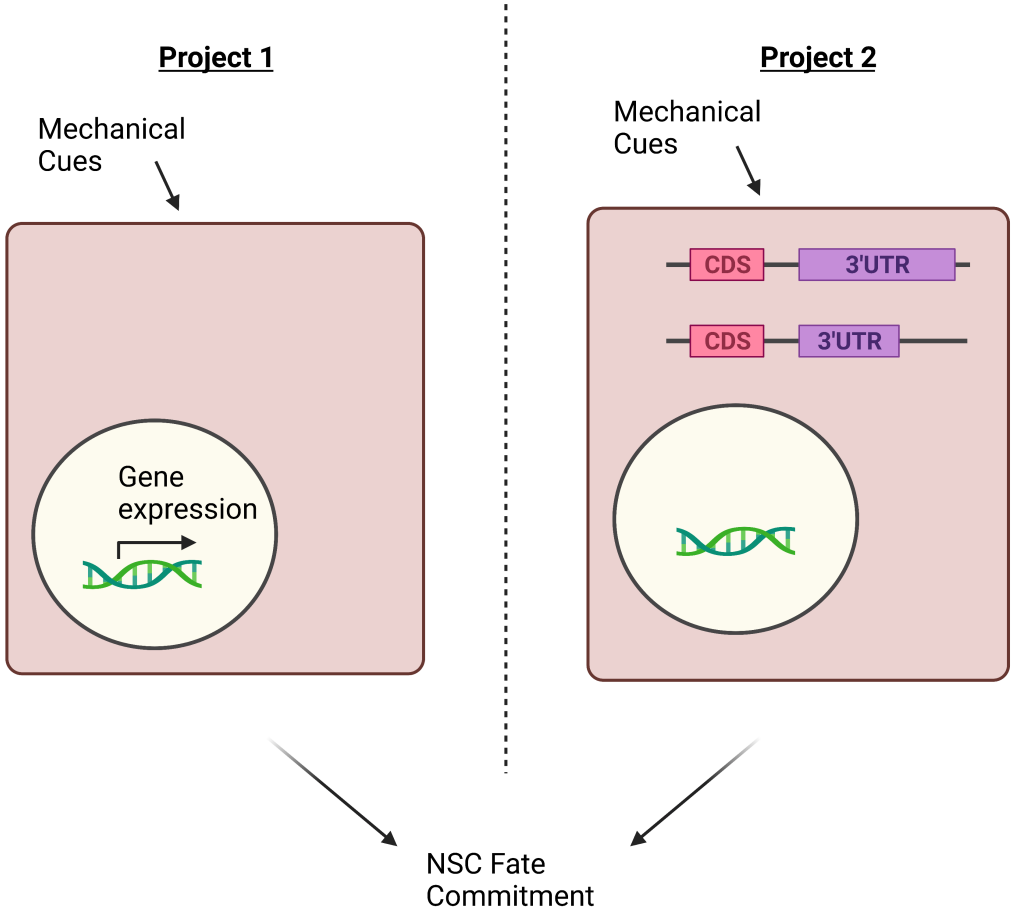

Figure 1.3: Overview of the two main chapters discussed in this dissertation. This first chapter explores how substrate stiffness influence NSC transcriptome, which leads to changes in NSC fate commitment. The last second chapter explores how substrate stiffness influences the post-transcriptional medications of mRNA.

For our first chapter, we focus our attention on studying one protein, eEF1A1, and how it regulates the mechanosensation of neural stem cell differentiation. We identified eEF1A1 as potential regulator of NSC mechanosensation from performing an unbiased RNA-sequencing experiment on neural stem cells differentiating on soft and stiff substrates. For our next chapter, we explored how ECM cues dictate the expression of not just eEF1A1 but other mRNA transcripts that showed up in the RNA-sequencing analysis from Chapter 1. Some recent work has led to linking stiffness cues to post-transcriptional regulation of gene expression, particularly through changes in the alternative polyadenylation of the 3'Untranslated region (UTR) of mRNA transcripts. Interestingly, our RNA-seq work gives evidence that stiffness cues may regulate the lengthening and shortening of 3'UTR of mRNA, adding another layer of complexity as to how stiffness transduces mechanical cues to biophysical signals. Thus, the second chapter focuses on exploring this relationship and how stiffness may regulate this behavior.

Chapter 2: eEF1A1 mediates the mechanosensation of NSC differentiation

2.1. Introduction

The generation of neurons from neural stem cells (NSCs), also known as neurogenesis, contributes to brain plasticity in the developing and adult brain.[44,45] NSCs reside in two regions of the mammalian brain: the subventricular zone (SVZ) and the subgranular zone (SGZ) of the dentate gyrus of the hippocampus. Particularly, adult hippocampal NSCs are important for memory, mood regulation, and learning.[46,47] Additionally, decreased neurogenesis in the hippocampus contributes directly to cognitive functional decline, as seen in aging[47], and progressive neuronal death in degenerative disorders such as Alzheimer's Disease.[46] Therefore, many have sought to harness neurogenesis to replenish these damaged cells and repair the diseased or injured brain.

NSCs can not only self-renew, but also differentiate into progenitor cells, including neuronal, astrocyte, and oligodendrocyte progenitors.[46] Like other stem cells, the processes ranging from initial fate decision and final commitment of NSCs are highly regulated by the extracellular microenvironment, here known as the neurogenic niche.[13] Incomplete understanding of how the niche influences NSC behavior and how the stem cell integrates these mechanistic cues has limited the use of these cells as a potential stem cell based therapy for treating neurodegenerative diseases.

One parameter of the neurogenic niche that influences NSC behavior is the extracellular matrix. The extracellular matrix presents both biochemical and biophysical signals that alter the cytoskeleton architecture of the NSC, acting as epigenetic determinants of NSC fate commitment. Specifically, when NSCs are cultured on soft gels, they are strongly biased towards neuronal differentiation, but when cultured on stiff gels, neurogenesis decreases.[35,36] Further work using switchable-stiffening DNA-oligo polyacrylamide gels showed that there is a time window in which mechanical signals from the ECM dictate NSC fate commitment.[40] This time window, referred to as the mechanosensitive time window, occurs 12-36 hours after initiating differentiation. Within this time window, the Yes Associated Protein (YAP) is upregulated in NSCs differentiating on stiff substrates relative to those on soft only within this mechanosensitive time window. This YAP upregulation results in the decrease activity of ß-catenin, and thereby, results in a decrease of neurogenesis on stiff substrates.

Previous approaches to understanding the mechanisms linking stiffness cues to fate commitment have been purely phenomenological, For example, YAP and Angiomotin (AMOT) have been heavily explored in regulating the mechanosensing behavior in other cell types such as in mesenchymal stem cells[48] and cancer cells[49]. This biased approach in studying previously implicated mechanoregulators have limited our understanding of the true extent and vast number of mechanisms influenced by changes in mechanosignaling.

To get an unbiased, and a more broad perspective as to how stiffness is regulating NSC behavior, particularly in the gene expression level, we performed RNA sequencing analysis on NSCs differentiating on soft substrates and on stiff substrates. These results revealed that at 12-hours after initiating differentiation, we see the largest differences in gene expression between soft and stiff substrates. Specifically, we see most genes downregulated in NSCs seeded on soft substrates relative to those on stiff substrates, including our gene of interest, eEF1A1. eEF1A1 was chosen as a potential candidate linking stiffness to NSC fate commitment due to prior literature involving its role in F-actin polymerization[50], protein synthesis[51] and stability[52], and mRNA binding[53,54].

Functional analysis of eEF1A1 revealed that this protein is both necessary and sufficient for inhibiting neurogenesis. We further examined the mechanism through which this protein inhibits neurogenesis and determined that it regulates mechanosensing through regulating YAP protein levels, and mediates RhoA activity and its downstream effectors. Interestingly, we determined that the influence of eEF1A1 on NSC fate commitment is regulated through Domain III (amino acids 328-432) region of eEF1A, which previous studies have shown to be a direct binding site for F-actin[54,55] and regulator of F-actin polymerization[56]. Taken together, this study takes advantage of next generation sequencing to identify a novel candidate that plays a prominent role in NSC mechanosensing, further advancing our understanding of the intracellular mechanism linking stiffness cues to NSC fate commitment.

2.2. Results

Substrate stiffness influences gene expression 12-hours post differentiation

To analyze how the transcriptome of NSCs respond to stiffness cues in a global and unbiased manner, we performed RNA-seq on NSCs differentiating on soft (500 Pa) and stiff (73 kPa) laminin coated polyacrylamide substrates at time points 0-, 12-, 24-, and 36-hours after initiating differentiation (Figure 2.1.a). Using a likelihood ratio test (LRT)[57], we tested to see whether there are any differences in gene expression throughout time between NSCs differentiating on a 500 Pa (Soft) vs 73 kPA (stiff) substrates, Using R package DEGreport[58], we performed hierarchical clustering on differentially-expressed genes ($p_{adj} < 0.05$) identified by the LRT for stiffness. To calculate the distance matrix, the Kendall rank correlation coefficient was used[59]. We identified three clusters of genes that decrease (Cluster 1 – 133 genes), remain the same (Cluster 2 – 58 genes), or increase (Cluster 3 – 102 genes) throughout the time course analysis, but deviate in gene expression at the 12-hour time point between the two stiffness conditions. (Figure 2.1.b). A list of the genes in each cluster can be found in Table A.1. Principal Component Analysis (PCA) further corroborated the findings that gene expression only differed at the 12-hour time point (Figure A.1). Interestingly, all these clusters reveal a decrease in gene expression of NSCs on soft conditions relative to stiff conditions at the 12-hour time point, and that after the 12-hour time point, the genes expression levels converge back to similar levels to those on stiff conditions in all three clusters. This led us to hypothesize that stiffness is directly influencing gene expression at this 12-hour time, and that one, or potentially multiple, of these genes may be involved in linking the influence of stiffness cues to NSC fate commitment.

We then performed a pair-wise comparison between samples collected from soft and stiff substrates only at the 12-hour time using a Wald's test comparison (DEseq2). We identified 184 differentially expressed genes (DEGs) that were upregulated and 685 genes that were downregulated on cells seeded on soft gels versus stiff substrates (Figure 2.1.c) (adjusted *p*-value of 0.05). We verified some of the findings from the RNA-seq analysis using qPCR and verified a strong correlation using Pearson's Correlation Analysis[60] (Figure 2.1.d).

We then focused our attention on identifying which of the top DEG may play a role in linking mechanotransduction cues to NSC fate commitment. One top differentially expressed gene, elongation translation factor 1 alpha 1 (eEF1A1), which was highly downregulated on soft versus stiff substrates, stood out as candidate. eEF1A1 has a very well-defined role in the translational machinery in protein biosynthesis[51]and is also a direct binding partner to F-actin and regulates cytoskeleton polymerization[61,62]. Therefore, we speculate eEF1A1 may be an intermediate player in linking cues from substrate stiffness to NSC fate commitment.

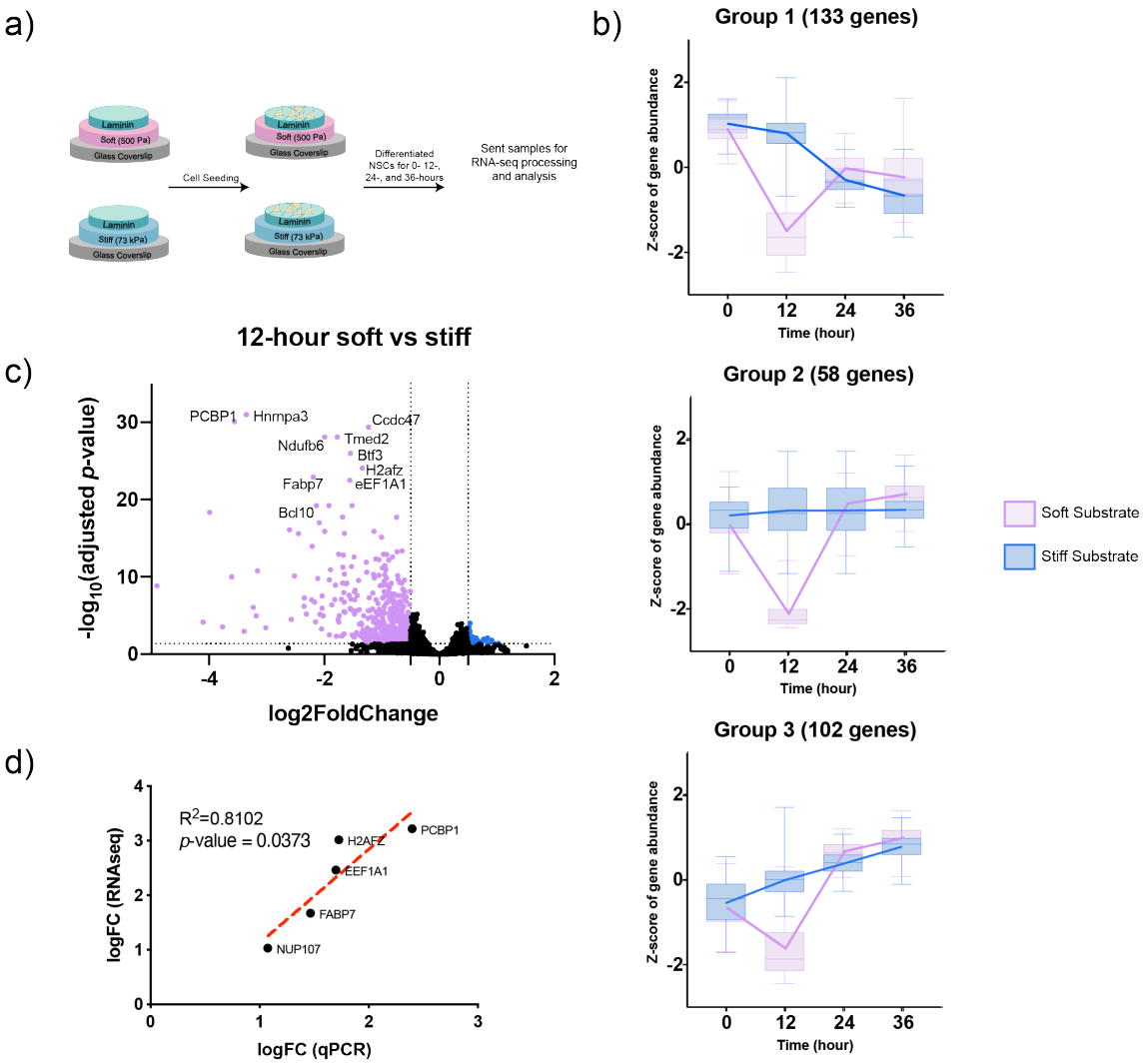

Figure 2.1: RNA-Seq analysis during mechanosensing window of NSCs. (A) Schematic of the RNA-Seq setup. Cells were seeded on soft and stiff matrices and RNA from cells from each condition was collected at 0-, 12-, 24-, and 36 hours (Mechanosensing Time Window) after initiating differentiation. Three biological replicates were collected for each condition, resulting in a total of 24 samples submitted for RNA-seq analysis. (B) Box plots of gene expression of cells differentiating on soft and stiff matrices. Statistical significance was assessed using DESeq2 Likelihood Ratio Test ($p_{adj} < 0.05$). Clusters were produced using the degPatterns function on the regularized log transformation of the normalized counts from the statistically significant genes. (C) Volcano plot of differentially expression analysis of genes in the cells seeded on soft versus stiff gels at the 12-hour time point. Purple and blue points mark the genes with significantly decreased or increased expression (respectively) in cells differentiating on soft versus stiff gels (Wald's Test, p_{adj}-value < 0.05, logFC>0.5. D) Pearson's Correlation Analysis between the relative quantification of RNA-seq and qPCR results

Loss of eEF1A1 increases neurogenesis

To test the functional importance of this gene on neurogenesis, we generated two short hairpins (shRNA-1 and shRNA-3) to target eEF1A1 at different sites within the coding region. We packaged the plasmid encoding these hairpins (along with a scramble control) into lentiviruses and infected into NSCs. These hairpins efficiently reduced eEF1A1 expression levels relative to the scramble control as seen in Figure 2.2.a. We then seeded the knockdown and scramble cells on soft and stiff substrates in mixed differentiation conditions (1% FBS and 1 uM retinoic acid) and differentiated for 6 days. The cells were then immunostained for Tuj1% to measure the overall neurogenesis effect as seen in Figure 2.2b-c. Knocking down eEF1A1 overall increased neurogenesis on cells seeded on soft and stiff conditions by approximately 10% and 30%, respectively (Figure 2.2.b-c). These results implicate that the upregulation of eEF1A1 on stiff substrates within the temporal mechanosensitive time window results in a suppression of neurogenesis.

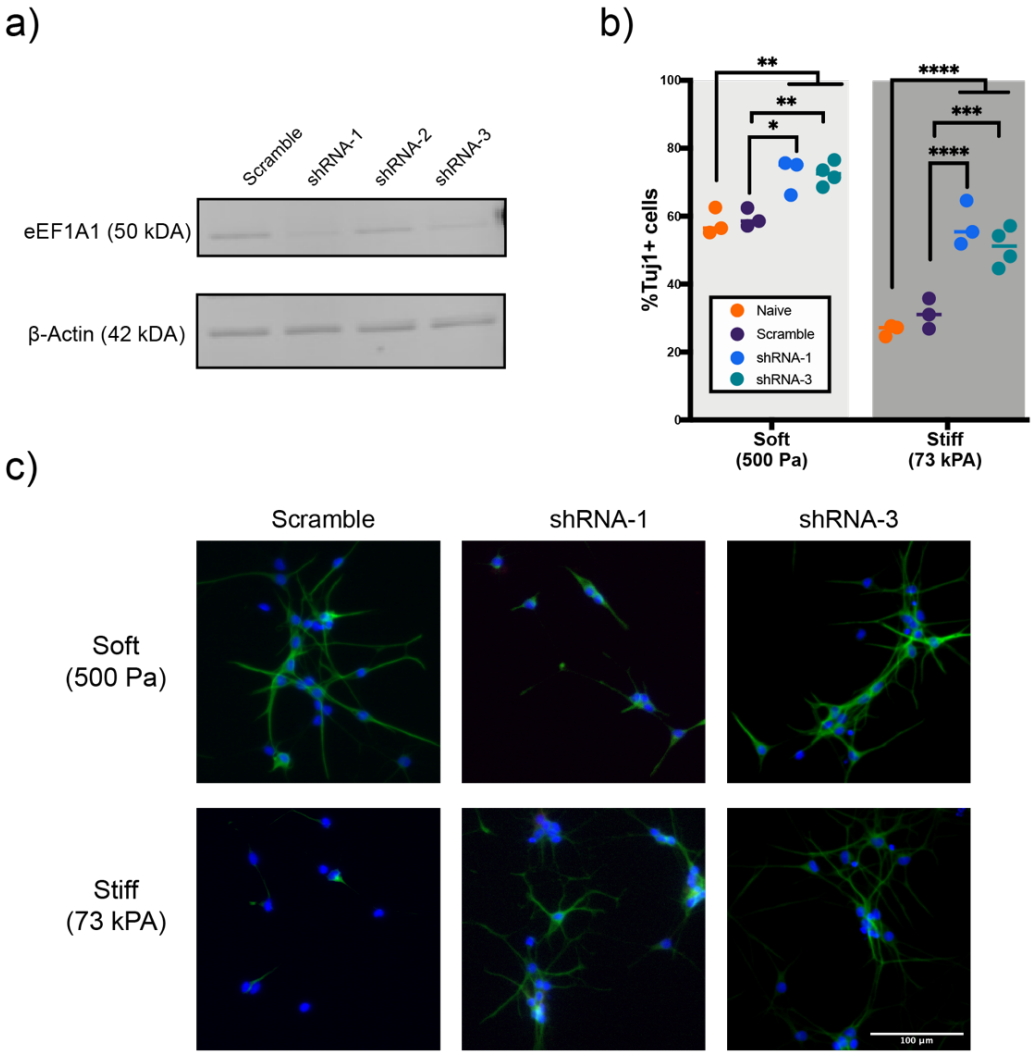

Figure 2.2: eEF1A1 is necessary for inhibiting neurogenesis: (A) Western blot validating the shRNA knockdowns (B) Representative immunofluorescent images of Scramble, eEF1A1 KD's (shRNA-1 and shRNA-3) NSCs after culture in mixed differentiating conditions (1 uM retinoic acid + 1% Fetal Bovine Serum) on soft (500 Pa) or stiff (73 kPA) gels for 6 days. Cells were fixed and stained for DAPI (blue) and Tuj1 (Green), a neuronal marker. Bar = 100 uM. (C) Immunostaining results of knockdowns. *p < 0.05, **p < 0.005, ***p< 0.001, ****p < 0.0001 by two-way analysis of variance (ANOVA) followed by Tukey's post-hoc test.

eEF1A1 is necessary and sufficient for inhibiting neurogenesis

To verify the specificity of the shRNA construct, we performed a rescue strategy where we transduced NSCs containing the eEF1A1 knockdown with retroviruses containing plasmids encoding the human WT eEF1A1 cDNA (shRNA-3 + WT eEF1A1). We used human WT eEF1A1 cDNA rather than rat cDNA for the rescue studies since there are a few base pair mismatches in the regions in the rat eEF1A1 cDNA relative to the human cDNA. Therefore, the knockdowns do not target the human eEF1A1 cDNA. We also generated a mutant form of the eEF1A1 protein which did not contain the region (Domain III) that reportedly binds to and induces F-actin bundling[56] (shRNA-3 + ΔDIII eEF1A1) (Figure 2.3.a-b). Structured Illumination Microscope (SIM) images demonstrate that eliminating this Domain III region reduces the co-localization of eEF1A1 to F-actin, thus giving us insight that this region of eEF1A1 may bundle F-actin in our NSCs (Figure A.2).

Our lab has previously shown that changes in the cellular contractility through modulating levels of Cdc42 and RhoA influences NSC fate commitment[36]. These players polymerize F-actin filaments[63], which are then bundled up by actin bundling proteins such as eEF1A1 to give rise to the mechanical properties of the cytoskeleton of the cell. Because of this, we hypothesize that through this Domain III region, eEF1A1 plays an important role in the mechanosensing of NSCs.

To test the hypothesize, we performed differentiation experiments analogous to the knockdown experiments. shRNA-3 + WT eEF1A1 NSCs show a reduction of neurogenesis of NSCs differentiating on both soft and stiff substrates (Figure 2.3.c). Interestingly, shRNA-3 + ΔDIII-eEF1A1 cell lines doubled the amount of neurogenesis based on the Tuj1% staining on soft and stiff substrates relative to the shRNA -3 + WT eEF1A1 cell lines (Figure 2.3.c). These results demonstrate that eliminating Domain III of eEF1A1, a region prior literature states plays an important role in regulating F-actin polymerization, eradicates the ability of eEF1A1 to inhibit neurogenesis on both soft and stiff substrates.

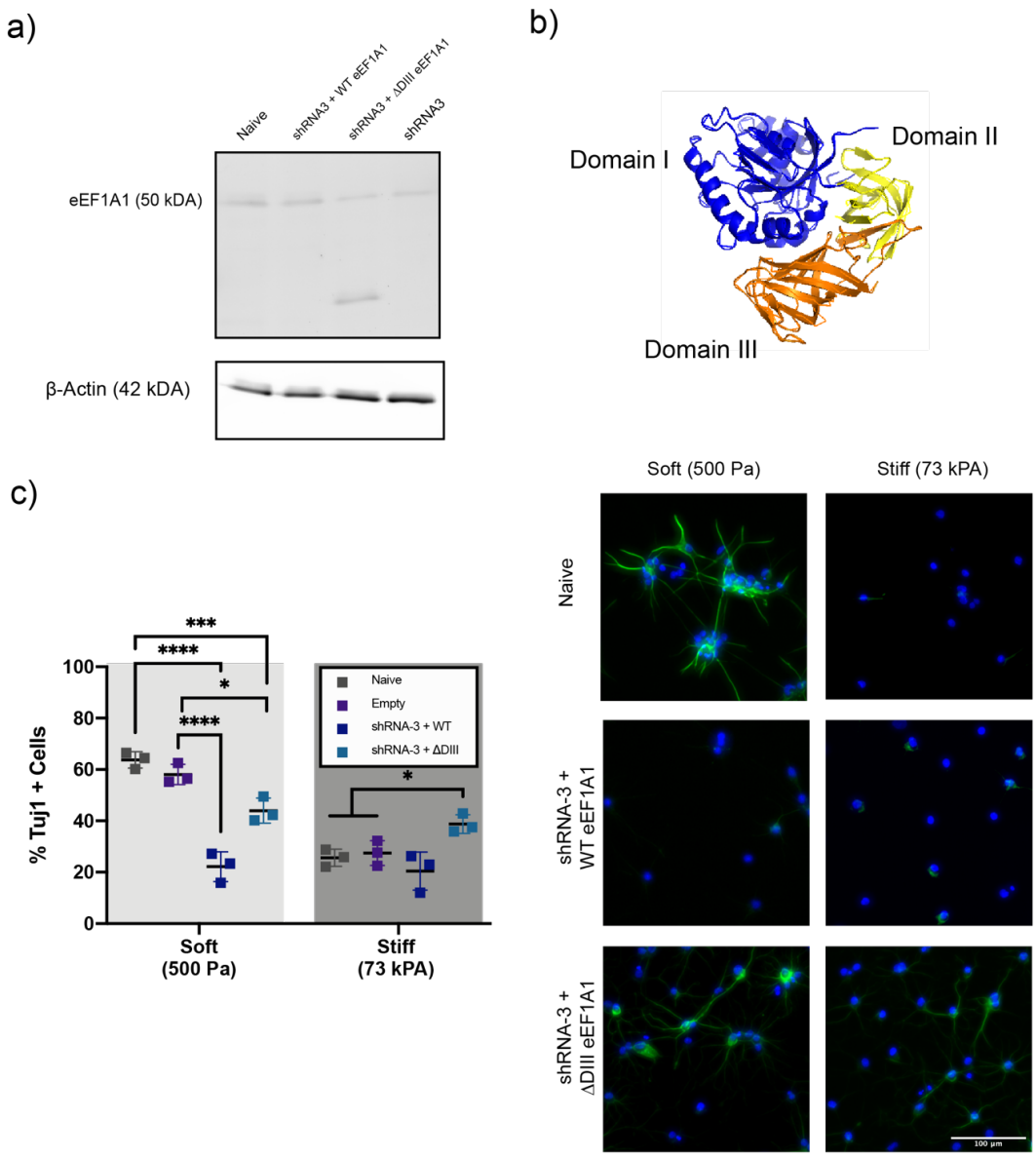

Figure 2.3: eEF1A1 is necessary and sufficient for inhibiting neurogenesis, particularly through interactions in Domain III. (A) Western blot results demonstrating the introduction of recombinant eEF1A1 DNA to knockdown cell lines. (B) Three-dimensional (3-D) model of eEF1A1 structure (PDB: 1SYW) with each domain highlighted. Blue = Domain I, Yellow = Domain III, and Orange = Domain III. B) Immunocytochemistry results of eEF1A1 mutants differentiation on soft and stiff substrates. (C) Representative immunofluorescent images of Scramble, eEF1A1 KD's (shRNA-3 + WT eEF1A1 and shRNA3+ΔDIII eEF1A1) NSCs after culture in mixed differentiating conditions (1 uM retinoic acid + 1% Fetal Bovine Serum) on soft (500 Pa) or stiff (73 kPA) gels for 6 days. Cells were fixed and stained for DAPI (blue) and Tuj1 (Green), a neuronal marker. Bar = 100 uM. Error bars represent standard deviation (n=3). *p < 0.05, ***p< 0.001, ****p < 0.0001 by two-way ANOVA followed by Tukey's post-hoc test.

eEF1A1 regulates neurogenesis through changes in Rho-GTP signaling

We next wanted to further examine the mechanism through which eEF1A1 is regulating neurogenesis. We focused our attention as to whether eEF1A1 is involved in how NSCs transduce signals from the ECM to changes in cellular contractility that ultimate lead to changes in NSC fate commitment. Previous work has shown that eEF1A1 regulates F-actin stress fiber formation through regulating the activation of Rho-GTP in human keratinocyte cells[64]. Therefore, we wanted to test whether eEF1A1 is involved in activating Rho-GTPase signaling during early NSC neurogenesis.

We seeded the rescue, knockdown, and naïve NSCs on soft and stiff substrates, and differentiated them for 24 hours. We then collected the protein lysate and measured the relative amounts of activated RhoA (Rho-GTP) of all our samples using a G-Elisa assay. These results show an increase in Rho-GTP levels in naïve NSCs differentiating on stiff substrates relative to those on soft, which is an observation seen previously in other work[36] (Figure 2.4.a). When knocking down eEF1A1 we see a reduction of Rho-GTP levels in NSCs seeded on stiff substrates relative to the naïve control. Interestingly, we do see an increase when rescuing shRNA-3 NSC knockdowns with WT-eEF1A1 on both soft and stiff substrates. Thus, eEF1A1 is both necessary and sufficient for inducing Rho-GTP levels.

However, while we do not see an increase in Rho-GTP levels in shRNA-3 + ΔDIII eEF1A1 NSCs differentiating on soft substrates, we do still observe an increase in RhoA activation on stiff substrates with these cells. (Figure 2.4.a). As seen in the earlier fate commitment results (Figure 2.3.c), shRNA-3 + ΔDIII-eEF1A1 NSCs do not lead to the same level of suppression of neurogenesis as the WT eEF1A1 cell lines on both soft and stiff substrates. This indicates the possibility that there may other mechanisms downstream of activated RhoA signaling that require the presence of this DIII of eEF1A1 to fully suppress neurogenesis.

We also wanted to make sure the changes we see in activated RhoA is not due to differences in the total protein levels of RhoA. This is a concern as eEF1A1 plays a significant role in protein synthesis[51]. To test whether eEF1A1 regulates total RhoA protein levels, we measured Total RhoA levels 24 hours post initiating differentiation using western blot (Figure 2.4.b-c). These results show that there are no differences in Total RhoA among all our cell lines. Thus, the changes we see in Rho-GTP levels are not due to differences in the total levels of RhoA protein in our cells.

We then wanted to test whether the changes in activated RhoA signaling regulated by eEF1A1 lead to changes in NSC fate commitment. To do so, we transiently treated naïve NSCs, shRNA-3 + WT eEF1A1, and shRNA-3 + ΔDIII eEF1A1 cell lines differentiating on stiff substrates (73 kPA) with Blebbistatin and Y-27632, which inhibit the activity of Rho GTPase effectors Rho Kinase (ROCK)[65] and myosin II[66], respectively, for the first 48 hours of their 6-day differentiation period. We chose to only treat the cells for 48 hours so that we do not affect any other biological processes outside the mechanosensitive time window. Similarly to the naïve cells, we see that when we treat the shRNA-3 + WT eEF1A1 rescue cell line with Blebbistatin and Y-27632, we see a rescue of neurogenesis on stiff substrates (Figure 2.4.d-e). By contrast, when we treat the shRNA-3 + ΔDIII eEF1A1 with the drugs, we see no difference in fate commitment.

Therefore, while we do see an increase in RhoA in the shRNA-3 + ΔDIII eEF1A1 as seen in Figure 2.4.a, inhibiting the downstream effectors of this pathway does not lead to changes in fate commitment. These results suggest that on stiff substrates, eEF1A1 increases RhoA signaling and downstream effectors that ultimately leads to the inhibition of neurogenesis.

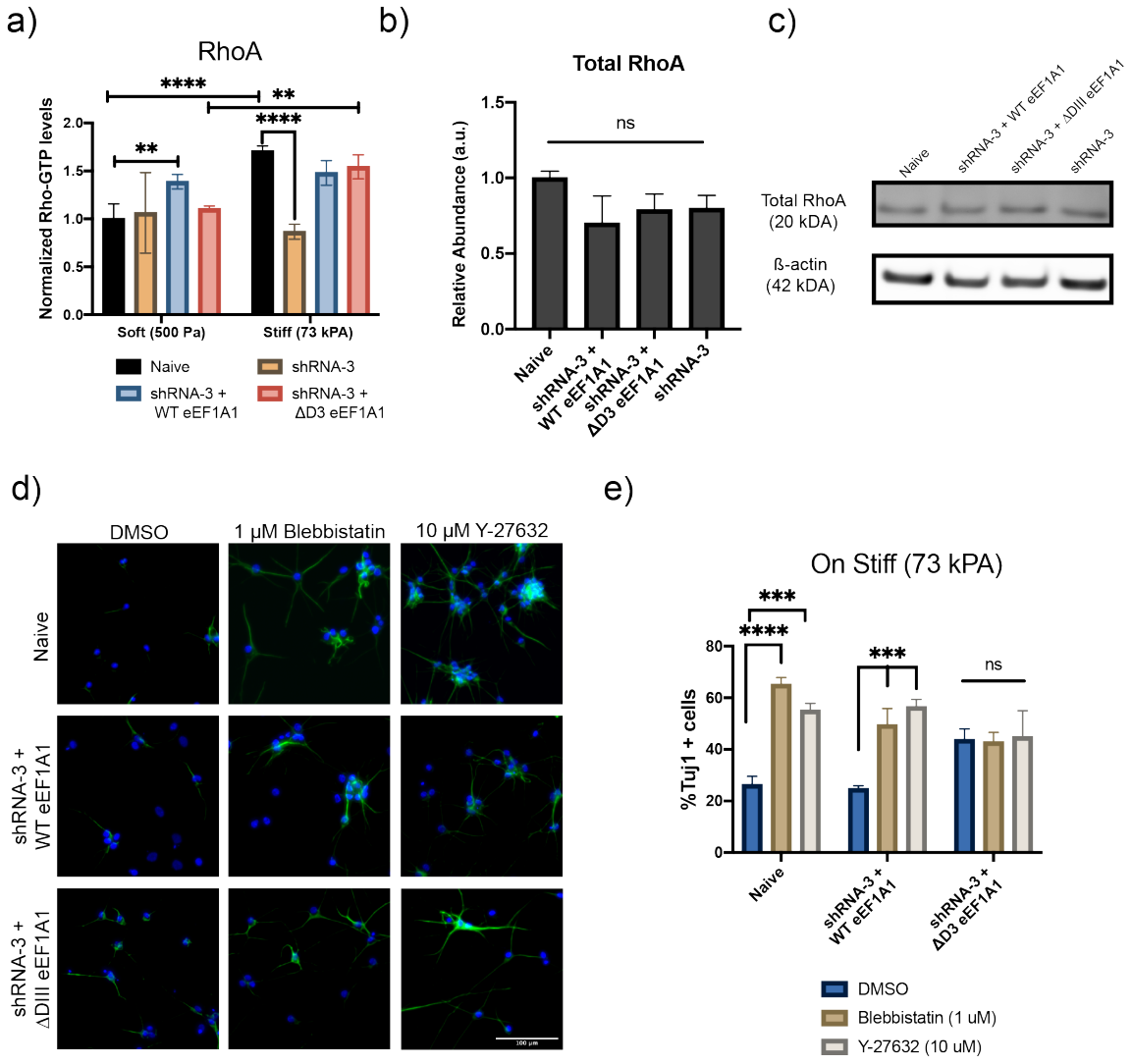

Figure 2.4: Domain III region of eEF1A1 regulates Rho GTPase activity. A) Rho-GTP levels normalized to the naïve soft substrate (500 Pa) value. B) Western Blot Results measuring total RhoA proteins from naïve, shRNA-3, shRNA-3 + WT eEF1A1, shRNA-3 + ΔDIII-eEF1A1 NSCs C) Quantification of western blot results. N=3. D) Immunocytochemistry results of eEF1A1 knockdown and mutant cell lines differentiating on soft and stiff substrates treated with either DMSO, Blebbistatin (1 uM) or Y-27632 (10 uM) for the first 24-hours of their 6-day differentiation period. E) Representative immunofluorescent images of Scramble, shRNA-3, and eEF1A1 rescue cell lines (shRNA-3 + WT eEF1A1 and shRNA3+ΔDIII eEF1A1) after 6-days of differentiation in mixed conditions. **p < 0.005, ***p< 0.001, and ****p < 0.0001 two-way ANOVA followed by Tukey's post-hoc test. ns = not significant.

eEF1A1 regulates YAP levels during early neurogenesis

We further wanted to determine whether eEF1A1 is influencing other players to influence neurogenesis. Previous work in our lab has shown that there is an increase YAP levels in NSCs seeded on stiff substrates relative to those on soft the first 24 hours of NSC differentiation. This increase in YAP leads to a direct reduction of β-catenin levels, resulting in an overall decrease in neurogenesis, in NSCs differentiating on stiff substrates[40]. Furthermore, our lab has shown that the increase in RhoA activation in NSCs seeded on stiff leads to the decrease in phosphorylation of angiomotin (phospho-AMOT)[67]. This increase of phospho-AMOT leads to the increase of YAP and decrease of β-catenin[40]. Therefore, we wanted to test if eEF1A1 is influencing neurogenesis through modulating YAP.

To first test this hypothesis, we measured YAP levels in the shRNA-3 knockdown and scramble control cell lines. We seeded these cells on soft and stiff substrates, differentiated them for 24-hours, and then collected their lysates for Western Blot analysis. The results show that by knocking down eEF1A1, there is a decrease amount of YAP on NSCs differentiating on stiff substrates, whereas there are no differences in YAP levels on soft substrates (Figure 2.5.a-b).

We also wanted to see if eEF1A1 levels correlate with β-catenin activity. We thus generated cell lines that contained both the eEF1A1 knockdown and a 7xTFP luciferase reporter which measures β-catenin/TCF/LEF transcriptional activity. We also generated cell lines containing the same luciferase reporter and a scramble knockdown. We then seeded these cells on stiff substrates, differentiated them for 24 hours, and collected and analyzed the lysate for luciferase expression. β-catenin/TCF levels were higher in the eEF1A1 knockdown relative to the scramble control only at 24 hours (Figure 2.5.c). We also measured the levels at the 0-hour time to assure that the differences we see only occur within the mechanosensitive window. There were no differences in the β-catenin/TCF levels between the scramble and the eEF1A1 knockdown. Taken together, these results indicate that the increase of eEF1A1 results in an increase of YAP thereby promoting β-catenin activity.

Furthermore, we wanted to see if YAP levels are rescued in the rescue cell lines (shRNA-3 + WT eEF1A1 and shRNA-3 + ΔDIII eEF1A1) relative to the knockdown cell lines. In a similar manner as described earlier, we collected western blot lysates from these cell lines seeded on stiff substrates 24 hours after initiating differentiation. Relative to the naïve controls, we see a rescue in YAP levels in the WT-eEF1A1 levels on stiff

substrates, indicating that eEF1A1 is necessary and sufficient for inhibiting YAP protein levels (Figure 2.5.d-e). However, ΔDIII eEF1A1 rescue lines do not result in similar YAP protein levels as the WT eEF1A1 cell lines. This interactions in this Domain III region result in the YAP levels that are needed for the suppression of neurogenesis.

Taken together, these experiments show that NSCs respond to differences in substrate stiffness during early neurogenesis by not only increasing Rho-GTP levels, but also YAP protein levels (Figure 6).

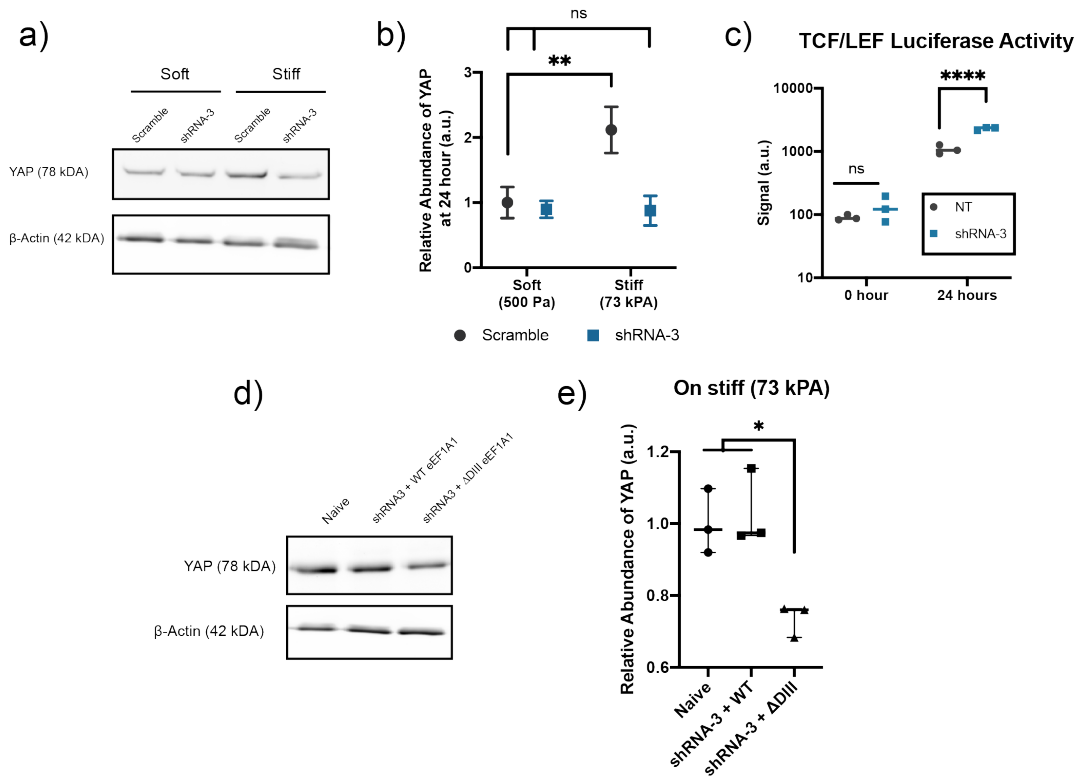

Figure 2.5: eEF1A1 regulates YAP protein levels through its Domain III. A) Western blot results of Scramble and shRNA-3 NSCs collected at the 24-hour time point. B) Western blot quantification results of YAP levels normalized to β-actin. N=3. C) TCF/LEF Luciferase Activity measuring β-catenin activity. D) Western blot results of the rescue samples (shRNA-3 + WT eEF1A1 and shRNA3+ΔDIII eEF1A1) collected at the 24-hour time point. E) Western blot quantification results of YAP levels normalized to β-actin. N=3. *p < 0.05, **p < 0.005, and ****p < 0.0001 two-way ANOVA followed by Tukey's post-hoc test. ns = not significant.

2.3. Discussion

Previous research shows that the extracellular matrix encodes mechanical cues that dictate adult hippocampal NSC fate commitment, but the intermediate mechanisms as to how the cells respond to these cues intracellularly remain unclear. Through an unbiased transcriptomic analysis of NSCs seeded on soft and stiff substrates during the early stages of differentiation, we identified eEF1A1 as a potential gene involved in linking mechanical cues to NSC fate commitment. Genetic perturbation of this gene

revealed its critical role in neuronal differentiation, and that it influences NSC mechanosensing through increasing RhoA activation and YAP protein levels. Interestingly, eEF1A1 influences these pathways specifically through interactions in a region of eEF1A1 that is proposed to regulate F-actin polymerization and bundling. These results elucidate the mechanism as to how NSCs respond to changes to stiffness cues, through regulating the expression of eEF1A1 and how this protein is involved in the transduction of mechanical signals in the cell to ultimately dictate fate commitment

The canonical function of eEF1A1 is, as a GTPase, to bind to the aminoacytelated tRNA at the GTP-bound state and deliver it to the ribosome during protein elongation[68]. Once eEF1A1 is bound to the ribosome, eEF1A1 becomes hydrolyzed, leaving it in the GDP state[69]. In addition to its role in protein elongation, eEF1A1 also binds to and co-localizes with actin cytoskeleton to mediate cytoskeletal organization[70]. In one study in particular, human keratinocytes were infected with human papillomavirus type 38, which then disrupts the actin stress binding formation and Rho-GTP activity by binding to eEF1A[64]. Interestingly, this study showed eliminating the Domain III disrupts F-actin architecture and reduces Rho-GTP levels. However, there is no work yet demonstrating whether eEF1A1 directly regulates RhoA activation as a GTPase.

Motivated by the results of this study, we sought to explore whether eEF1A1 has some effect on RhoA activation during early NSC differentiation. As we previously discussed, NSCs differentiating on stiff substrates result in higher Rho-GTP levels, thus increasing the internal stiffness of the cell. Interestingly, our results show that RhoA activation decreases when eEF1A1 is eliminated, and is rescued when the WT eEF1A1 protein is re-introduced. Furthermore, when inhibiting downstream activated RhoA effectors, ROCK (Y-27632) and myosin II (Blebbistatin), we saw a rescue of neurogenesis in the naïve and full WT eEF1A1 rescue cell lines. This indicates that eEF1A1 is regulating NSC lineage commitment into neurons through changes in Rho-GTP activation levels. Furthermore, we hypothesize the eEF1A1 is regulating Rho-GTP by inducing F-actin bundling. Preliminary SIM images show there is high co-localization between F-actin and eEF1A1 only when Domain III is present. However, more follow-up work is necessary to fully understand the impact eEF1A1 has on F-actin bundling.

When introducing the ΔDIII eEF1A1 mutant rescue to the knockdown cell lines, Rho-GTP levels increased only in NSCs differentiating on stiff substrates, and not on soft substrates. In addition, there were no changes in the percent of neurons when the cells were treated with Y-27632 and Blebbistatin. This could indicate the presence of the other domain regions (Domain I and II) in eEF1A1 coupled with other mechanisms upregulated on stiff substrates may also result in higher Rho-GTP levels. However this Rho-GTP increase does not lead to changes in NSC fate commitment to neurons. Future studies are needed to determine if whether the GTPase region in Domain I region of eEF1A1 coupled with other signaling pathways enhanced on stiff substrates may be involved with RhoA activation.

While these results demonstrate eEF1A1 may regulate NSC fate commitment to neurons through changes in Rho-GTP, there is the possibility that changes in NSC fate commitment are due to changes in protein synthesis. Interestingly, when NSCs begin to differentiate, there is an upregulation of protein synthesis which is then followed by cell

division and differentiation[71]. Using an using O-propargyl-puromycin (OPP) to label nascent proteins[72], we do see differences in protein synthesis in NSCs on soft versus stiff substrates, with higher protein synthesis on soft substrates relative to stiff substrates (Figure A.3). We also see an overall reduction in the knockdown and rescue eEF1A1 cell lines relative to the naïve. However, we no longer see the differences between soft and stiff substrates in both the knockdown and rescue eEF1A1 cell lines as we do in naïve NSCs. While we did not entirely capture the dynamics of protein synthesis during the NSC mechanosensitivity time window since we are only measuring nascent protein synthesis at 24-hours post differentiation, these results demonstrate that modulating eEF1A1 may influence protein synthesis in addition to changes in Rho-GTP and YAP levels during NSC differentiation. Interestingly, there is work indicating that eEF1A1 is a main player in linking the influence of substrate stiffness to overall protein synthesis[73]. Interestingly, previous work has shown that changes in the F-actin bundling properties of eEF1A1 also lead to chances in the aminoacyl-tRNA binding of protein synthesis[74]. Thus, further work exploring the relationship between eEF1A1, F-actin, and protein synthesis is needed.

As mentioned above, eEF1A1 plays an important role in protein elongation and modulating the expression levels of eEF1A1 may also influence protein synthesis. Even before exploring eEF1A1, we saw differences in YAP protein levels on stiff relative to soft substrates in the mechanosensitive time window, but the phenomena as to why we see differences in YAP levels remain unclear. In this study, we determined that eEF1A1 suppression reduced YAP expression and increased ß-catenin activity on stiff substrates. Rescue of eEF1A1 conversely increased YAP on stiff substrates, whereas rescue of ΔDIII-eEF1A1 mutant did not. These results suggest that eEF1A1 influences the overall YAP levels during this mechanosensitive time window.

To determine whether eEF1A1 is potentially influencing YAP through changes in Rho-GTP levels or protein synthesis, we also measured the levels of phospho-angiomotin, which previous work in our lab shows is upregulated on soft substrates, and interacts with YAP to prevent it from interacting with ß-catenin[67]. On stiff substrates, phospho-AMOT level decreases as a result of higher Rho-GTP levels. Interestingly, on stiff substrates, we see a decrease in phospho-AMOT in the knockdown cells and the ΔDIII eEF1A1 rescue lines relative to naïve and WT eEF1A1 rescue lines (Figure A.2) . Thus, this provides more evidence that eEF1A1 may be regulating YAP levels through changes in Rho-GTP levels and phospho-AMOT. However, more follow up studies are necessary as to whether eEF1A1 is regulating phospho-AMOT through influencing Rho-GTP levels or total AMOT levels, and whether these changes in phospho-AMOT is leading to the differences in YAP.

A novel part of this study is initial unbiased transcriptomic analysis of the NSCs differentiating on soft and stiff substrates during the early mechanosensitive time window. We chose our focus at the 12-hour time point after observing a large deviation in gene expression between soft and stiff substrates. However, we still do not know what results in these differences in transcript levels. Recent work has shown that microRNAs, which are a class of non-coding RNAs that regulate gene expression by binding to specific elements in mRNA, are sensitive to mechanical stiffness cues[75]. If bound to a mRNA, microRNAs can result in mRNA destabilization[76]. Thus, it would be interesting

to explore, in the context of adult hippocampal NSCs, whether microRNAs or other post-transcriptional modifiers regulate the gene expression differences between NSCs differentiating on soft versus stiff substrates.

Furthermore, we have yet to explore how the changes in gene expression throughout early differentiation (as seen from our initial hierarchical clustering analysis) impact fate commitment. Our focus of this chapter was on eEF1A1, which besides the 12-hour time point, had no changes in transcript level from 0-hour and 36-hour post differentiation in NSCs seeded on both soft and stiff substrates (eEF1A1 was part of Cluster 2, Table A.1). Cluster Group 1 and group 3 groups showed decrease and increase transcript levels, respectively, over time in both soft and stiff substrates. Interestingly, genes such as *Orc6*[77], and *Cdk2*[78], showed up in Group 1 (Table A.1), both of which have important roles in cell cycle regulation. One example to take these results further (based on seeing these two genes in this clustering analysis) would be to explore if stiffness is impacting cell cycle regulation, which is important in the context of neurogenesis[79], during this early mechanosensitive time window. Overall, these observations lead us to believe that matrix stiffness is impacting the expression of genes involved not just in regulating in neurogenesis, but also impacting genes that normally would not change during neurogenesis (specifically Group 2).

The exact mechanisms underlying how the mechanotransduction of biophysical cues from the extracellular matrix into cytoskeletal changes influences NSC lineage commitment remains unknown. This project utilizes RNA-seq analysis to identify candidate genes involved in mechanotransduction that are differentially expressed in NSCs differentiating on soft and stiff substrates. Our focus of this work is on one of those candidate genes, eEF1A1, which regulates neurogenesis through modulating Rho-GTP levels during the mechanosensitive time window. This integration of stem cell biology, mechanobiology, and novel genetic technologies promises to advance our fundamental understanding of the impact of tissue mechanics on stem cell behavior, which has widespread implications for both basic science/biology and therapeutic translation.

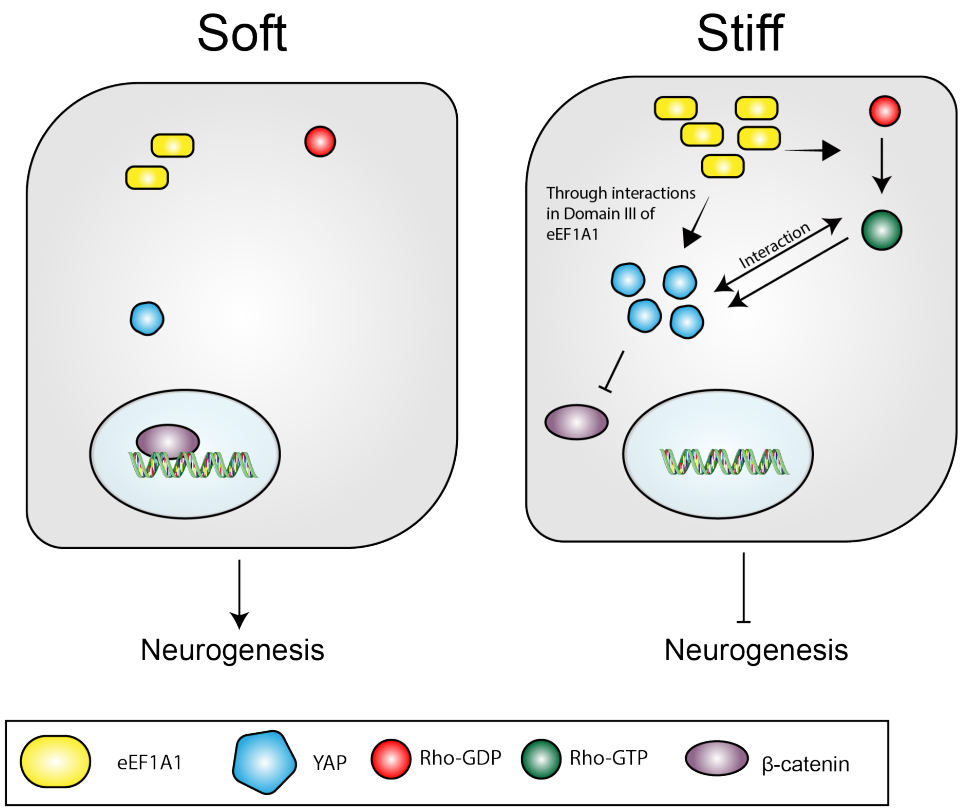

Figure 2.6: eEF1A1 upregulation on stiff substrates leads to a suppression of neurogenesis by increasing RhoA activity and YAP protein levels

2.4. Materials and Methods

Neural Stem Cell Culture

Adult rat hippocampal cells were extracted and cultured as discussed previously[35,80]. Briefly, the cells were cultured in DMEM/F12 supplemented with N2 Supplement (Invitrogen) and 20 ng/ml of FGF-2 (Proteintech) (proliferation conditions) and seeded on plates coated with poly-L-ornithine and laminin. The media was changed every two days to maintain the cells in a proliferative state. For differentiation studies, the cells were initially seeded at a density of 25,000 cells/cm^2 and maintained in proliferation conditions for 16-18 hours to allow the cells to attach to the substrate. The cells were then switched to differentiation conditions, which consists of DMEM/F12, 1% fetal bovine serum (FBS) and 1 uM retinoic acid. The media was changed every two days for a total of 6 days.

Polyacrylamide gel synthesis and protein functionalization

The initial polyacrylamide precursor solution is composed of a mixture of acrylamide monomer and bisacrylamide crosslinker. The concentration for the 500 Pa (soft) gel precursor solution is 3% acrylamide + 0.1% bisacrylamide, whereas for the 73

kPA (stiff), the gel solution consists of 10% acrylamide + 0.3% bisacrylamide. The concentration of each component varies and is dependent on the final desired polyacrylamide gel stiffness[36]. To initialize the gel polymerization, the precursors solution was mixed with 1% ammonium persulfate and 0.1% tetramethylethylenediamine (TEMED) and synthesized on 12-, 18-, or 25 mm glass coverslips. Sulfo-sanpah solution (5 ul/ml) was added to the polymerized gels to functionalize the gels Laminin (25 ug/ml).

RNA sequencing sample preparation

RNA from NSCs differentiating on soft and stiff substrates was collected at 0-, 12-, 24, and 36- hours after initiating differentiation. RNA was lysed and purified using RNAeasy Minikit (Qiagen). A total of three biological replicates were collected for each condition. Total RNA samples were checked on the Bioanalyzer (Agilent) to assure each sample had an RIN > 8. The samples were then sent off to the UC Davis Genome Center for library preparation. The preparation was done using the QuantSeq 3' mRNA Library Prep Kit FWD for Illumina (Lexogen) and sequenced through the HiSeq 4000 Illumina Sequencer using 90 bp single-end reads.

RNA sequencing analysis

The read quality of each sample was done using FastQC[81]. The Phred scores of each sample were equal to or greater than 28. Adapter trimming was done using a BBTools package called BBDuk and ribosomal RNA contaminants were removed using BBtools package called BBSplit[82]. Sequences were then aligned to the rat reference genome Rattus Norvegicus (rn6) using HiSat[83]. Read count was done using htseq-count[84] and the differentially expression analysis was conducted with the DESeq2 R package[57], which normalizes counts using the median of ratios method. Initial time series analysis was done using the likelihood ratio test (LRT), using a significance threshold of adjusted *p*-value of < 0.01, which lead to a total of 293 genes differentially expressed between soft and stiff conditions. Genes passing this threshold were then scaled to z-scores and clustered using DEGreports R package. The clusters identified were then retained for downstream gene ontology analysis which was done using DAVID version 6.8[85], with those further explored having an adjusted *p*-value < 0.01.

Pairwise comparison of NSCs seeded on soft versus those on stiff substrates at the 12-hour time point to determine differentially expressed genes was done using Wald's test from the DESeq package[57] using a adjusted *p*-value of 0.05 (184 upregulated and 685 downregulated genes on soft versus stiff). The identified differentially expressed genes were then used for further gene ontology analysis also using DAVID version 6.8[85], with those further explored having an adjusted p-value < 0.01.

Quantitative Real Time PCR

The Total RNA was isolated using RNeasy Mini Kit (Qiagen), which was further treated with DNAse digest enzyme from the RNAse-Free DNase Set (Qiagen) to remove and single or double stranded DNA. The 1 ug of total DNase treated RNA was reverse

transcribed using Superscript III Reverse Transcripted (Thermo Fisher Scientific) along with a mix of random hexamer and oligo(dT)$_{20}$ primers (Thermo Fisher Scientific). Quantitative PCR reactions were done in CFX Connect Real-Time PCR System (Bio-Rad), with three replicates conducted per sample.

Knockdown and overexpression vectors

For generating the knockdowns, 21-mer siRNA constructs (shRNA-1: GGAAGTCAGCACCTACATTAA, shRNA-2:GCCAACTCGTCCAACTGACAA, shRNA-3: GCTCCAGTCAATGTAACAACT) were designed to target the rat eEF1A1 cDNA region using the online InvivoGen siRNA Wizard Software, along with a scramble control (GGTAGGAAATG TTT AGAGTCTCGAGA). The final shRNA construct consists of the siRNA-sense + loop+ siRNA antisense sequences, with EcoRI and AgeI restriction enzyme sticky ends, allowing insertion to the pLKO.1 vector. The pLKO.1 – TRC cloning vector was a gift from David Root (Addgene plasmid # 10878).

pGBDUC2 plasmids containing either the full human eEF1A1 cDNA, and Domain 1+ Domain cDNA sequences were a generous gift from Charlotte Knudsen (Aarhus University, Denmark). The eEF1A1 cDNA sequences were PCR amplified (KAPA HiFi HotStart PCR Kit) with SfiI and PmeI digest sites to allow for insertion into the pCLGPIT Vector

Viral transduction

HEK 293T cells were seeded one day prior at approximately 90% confluency on a 10cm plate. To package the pLKO.1 vector into lentiviruses, 10 ug of the pLKO.1 vector along with 7.5 ug of psPAX2 packaging plasmid and 2.5 ug of pMD2.G envelope plasmid were mixed along with 120 ul of polyethylenimine (PEI). This mixture was added dropwise to the cells. The supernatant was collected 48- and 72-hours post transfection and was filtered and pooled prior to ultracentrifugation. The viral particles were resuspended using cold PBS. The CLGPIT/CLPIT vectors were packaged similarly as the lentiviruses but were packaged into retriviruses. 10 ug of the pCLGPIT/pCLPIT vectors were used along with 6 ug of the pCMV gag-pol packaging plasmid and 4 ug of pcDNA3-IVS-VSV-G envelope plasmid.

The NSCs were transduced in all cases at a multiplicity of infection of 1. Cells transduced with the lentivirus containing the pLKO.1 vector were selected with 0.6 ug/ml puromycin[86] for 4 days or until the negative control were dead. To rescue eEF1A1 on top of the knockdown, Cells with the shRNA constructs were transduced again but with the pCLGPIT vectors. These cells became GFP+ which were sorted from the GFP- population using FACS.

Immunofluorescence staining and imaging

The cells were fixed in 4%(vol/vol) paraformaldehyde (Alfa Aesar) for 20 minutes at room temperature, permeabilized with 0.5% Triton-X for 10 minutes, and blocked in 10% goat serum for 1 hour. Between each step, the cells were washed twice

with phosphate-buffered saline (PBS). Following the blocking, the cells were stained with primary antibodies overnight at 4C, and then with secondary antibodies for 1 hour at room temperature. After additional washes, 4'6-diamidino-2-phenylindole (DAPI) was added as the nuclear marker. The primary antibody used was Tubb3 (1:1000; Biolegend 801201). Secondary antibodies from Life Technologies were obtained using the appropriate species conjugated to either an Alexa-488 or -633 fluorophore.

Epifluorescence images were taken using Zeiss Axio Observer epi-fluorescent microscope (CIRM/QB3 Shared Stem Cell Objective, with a 10x objective. Samples were submerged in PBS during image acquisition. Image processing, including stitching and z-slice projection, and analysis was carried out using either Fiji[87] or CellProfiler[88]. Structured Illumination (SIM) epifluorescnce images were taken in the Elyra PS.1 using 60x objective and analyzed using Zeiss imaging software.

Western blot and RhoA Activation Assay (G-Elisa)

For Western blot assay, cells were first lysed in HALT Protease Inhibitor Cocktail and RIPA Buffer (Thermo Fisher) for 5 minutes in 4C. The protein concentration was determined using a bicinchonic acid (BCA) assay. Lysates were mixed with LDS and reducing agent, and then heated for 5 minutes in 95C. The samples were then run on a 4-12% Bis-Tris gel and transferred onto nitrocellulose membrane (Licor). The membrane was blocked for one hour (Licor), and then incubated with primary antibody overnight. The next day, the membrane was washed with twice with TBST (5 minutes per wash), then incubated with IRDye secondary antibodies (Licor). The membrane was imaged using the Licor Odyssey 9120 Imaging System. The following antibodies were used: anti-eEF1A1 (1:1000; abcam ab157455), ß-actin (1:20000, Sigma Aldrich A2228), anti-Yap (1:1000; Cell Signaling 4912S), and anti-c-Myc (1:1000; Cell Signaling 2276S).

RhoA Activity was determined using the RhoA G-elisa Activation Assay (Promega, Cat # BK124), which measured the active form of RhoA in the cells (RhoA-GTP levels). Briefly, the cells were seeded overnight, and differentiated for 24-hours prior to sample collection. Cells were lysed for 10 minutes, which afterwards the total protein concentration was determined using Precision Red. Absorbance for measuring RhoA activity was read at 490 nm using a plate-reading luminometer

TCF Luciferase Assay

The shRNA-3 eEF1A1 knockdown and scramble NSC control were further transduced with a lentiviral construct expressing a 7xTFP TCF/LEF luciferase reporter. This reporter is response to ß-catenin-TCF/LEF-based transcription. The cells transduced with the reporter were selected with hygromycin 100 ug/ml for one week prior to performing experiments. The cells were then seeded and differentiated on stiff substrates for 24 hours in mixed differentiation conditions before lysates were collected. The lysis buffer used came from the Luciferase Assay System kit (Promega), and the assay was carried out with a plate-reader luminometer.

Overall Nascent Protein Synthesis Assay

Overall nascent protein synthesis was analyzed using nonradioactive metabolic labeling (Click-IT OPP Alexa Fluor 568 Protein Synthesis Kit). Briefly, NSCs were exposed to OPP reagent for about 30 minutes. The cells were then fixed (4% paraformaldehyde) and permeabilized (0.5% Triton) before OPP detection. The signal intensity of incorporated OPP was determined using a Nikon Eclipse TI Microscope, Hamamatsu Photonics K.K. C10600-10B-H camera, using 20x objective lens, and native Prairie View Software. The samples were analyzed by measuring the signal intensity emitting from the 568 channel within and surrounding the nucleus using Fiji software[87]. As a negative control, cells were pre-treated with cycloheximide (50 ug/ml) for 30 minutes prior to performing the experiment.

2.5. Acknowledgements

We kindly thank Dr. Charlotte Knudsen (Aarhus University, Denmark) for sharing his lab's pCDNA constructs encoding WT eEF1A1 and ΔDIII eEF1A1. We also thank Erin Tan (University of California, Berkeley) for her efforts in the cloning of the knockdown and immunostaining sample preparations. P.A.L. was supported by the National Science Foundation Graduate Fellowship. P.H.K. was supported by the Siebel Scholarship. P.A.L, P.H.K., S.K., and D.V.S. gratefully acknowledge grant support from the National Institutes of Health (grant #5R01NS074831: Mechanisms of Neural Stem Cell Mechanoregulation), awarded to S. K. and D.V.S. Research reported in this publication was supported in part by the National Institutes of Health S10 program under award number 1S10OD018136-01. The content is solely the responsibility of the authors and does not necessarily represent the official views of the National Institutes of Health.

Chapter 3: Substrate Stiffness influences the alternative polyadenylation of mRNA transcripts during NSC differentiation

3.1. Introduction

Prior to becoming fully mature messenger RNAs (mRNA), pre-mRNAs undergo several modifications that influence their ability to get translated into a functional protein[89]. One of the modifications is the addition of the poly-A tail to the pre-mRNA, a process referred to as polyadenylation[90–92].The process of polyadenylation is regulated by four distinct protein complexes, the cleavage and polyadenylation specificity factor (CPSF), the cleavage stimulation factor (CstF), the cleavage factor I (CFIm), and the cleavage factor II (CFIIm)[93]. Polyadenylation begins with these protein complexes first identifying polyadenylation signals (PAS) within the 3'UTR of pre-mRNA. These proteins then cleave the 3'UTR a few nucleotide downstream of the PAS, and synthesize the poly(A) tail at the end of the 3'UTR. Interestingly, 70% of genes[94] contain transcribe mRNAs that contain multiple PAS in the 3'UTR, thus resulting in the alternative usage of these PAS in the mRNAs that encode the same coding region but vary in 3'UTR length[95]. Having a longer 3'UTR results in more potential binding sites within the 3'UTR for microRNA and RNA-binding proteins (RBPs) to target. Specifically, microRNAs mostly target regions in the 3'UTR, promoting further mRNA degradation and decreased protein translation[96]. Thus, the sequence and composition of the 3'UTR region serve as another level of complexity in the post-transcriptional regulators of gene expression to determine the stability of mRNA, and overall cell behavior.

Intriguingly, recent work has shown that substrate stiffness influences usage of the proximal and distal usage of the PASs in the 3'UTR. When lung fibroblasts are exposed to a substrate stiffness that equals that of a fibrotic lung, these cells alter their extracellular matrix production (primarily collagen and fibronectin) to mimic that of their fibrotic environment. When cultured on a stiffness that emulates the fibrotic lung, there is an decrease in Cleavage Factor Proteins (CFIm25, CFIm68, and CFIm69), and thus favoring the usage of the proximal PAS in the 3'UTR[97]. This results in a shorter 3'UTR of collagen and fibronectin and overall higher protein expression. While there is an array of work discussing extracellular cues that regulate PAS usage[98], this is the first work showing how mechanical cues regulates the expression of the CFIm proteins, and thus the length of the 3'UTR region. In addition, pathways such as TGF-ß1[99,100] and mTOR[101,102] also have been shown to regulate CFIm protein expression and PAS usage. These pathways have been shown to be involved in orchestrating mechanotransduction cues in various cell types[103], and thus potential regulators in linking matrix cues to PAS usage.

Furthermore, CFlm proteins have been showing to dictate stem cell fate and neural behavior. Specifically, in induced pluripotent stem cells, reducing the expression of CFlm25 protein by suppressing the expression of the gene that transcribes it, *NUDT21*, results in the impaired differentiation of the pluripotent stem cell[104]. This study further elucidated that mechanism of CFlm25 in pluripotency and showing that by changing the expression of this CFlm25 protein there is an alternative usage of PAS of genes (thus

generating 3'UTR mRNA isoforms) involved in reprogramming such as integrin mediated and MAPK signaling pathways. Interestingly, inhibiting expression of *NUDT21* in human-stem cell derived neural cells also resulted in alternative PAS usage and protein dysregulation, resulting in cognitive impairment in mice[105].

Motivated by these studies, this work focuses on elucidating the relationship between substrate stiffness and the alternative polyadenylation usage of 3'UTR of mRNA, particularly in the context of adult neural stem cells differentiation. This study first begins by identifying 3'UTR isoforms in mRNA that are enriched in NSCs seeded on soft and stiff substrates using a method called CSI-UTR[106]. We then performed a more in-depth analysis on the alternative PAS usage and determined that distal PASs in the 3'UTR of mRNA are favored in NSCs seeded on soft substrate relative to stiff substrate. Lastly, we identified CFIm25 as a mechanosensitive protein in NSCs during early differentiation, thus providing more evidence that stiffness may regulate the alternative polyadenylation of mRNA to ultimately dictate NSC fate.

3.2. Results

Determining 3'UTR isoform enrichment using CSI-UTR

To explore whether we see 3'UTR isoforms enriched on soft (500 Pa) versus stiff (73 kPA) substrates, we used previously analyzed RNA-seq data of NSCs differentiating on soft and stiff substrates at time points 0-, 12-, 24-, and 36-hours post differentiation (from Chapter 2). Using this dataset, we determined which 3'UTR isoforms are differentially expressed between NSCs on soft versus stiff conditions using a method called CSI-UTR[106]. This method first identifies the total count data of reads that aligned to each of the 3'UTR isoforms of all the RNA transcripts in the transcriptome. Then, it compares the ratio of reads that belong to a specific 3'UTR region in NSCs seeded on soft to those seeded on stiff. This program does this for all the 3'UTR isoforms and a Fisher's Exact test (followed by Benjamini-Hochberg for False Discovery, FDR) is used to determine the *p*-value. An example of a CSI significance calculation is shown in Figure 3.1.

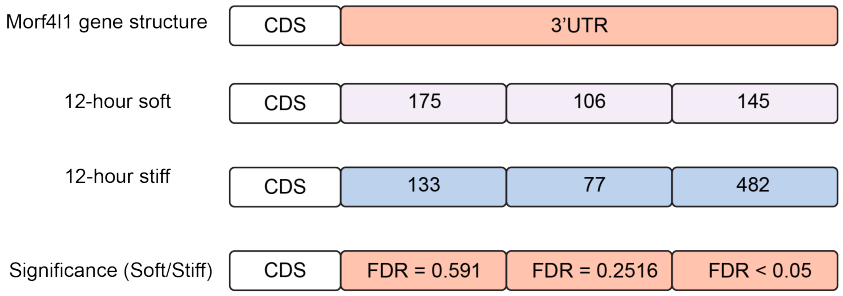

Figure 3.1: Example of CSI significance calculation. Shown is the calculation of the FDR-corrected significance for *Morf4l1* gene in NSCs seeded on soft versus stiff substrates at the 12-hour time point. The counts in each intervals are normalized to the total count in each dataset.

The total number of 3'UTR isoforms differentially expressed in NSCs seeded on soft versus substrates at each time point can be seen in Table 3.1:

Condition	# of Differentially Expressed 3'UTR isoforms	# of genes that transcribed Differentially Expressed 3'UTR isoforms
0 hour soft vs. stiff	27	13
12 hour soft vs. stiff	284	132
24 hour soft vs. stiff	2	2
36 hour soft vs. stiff	12	7

Table 3.1: Results of CSI-UTR Analysis

As seen in the table, most of the differentially expressed 3'UTR isoforms (and respective gene) occur at the 12-hour time point. This quantitative observation can be seen qualitatively in the alignment of RNA transcripts of two genes in particular, isopentyl-diphosphate delta isomerase 1 (*IdI1*) and Mortality Factor Like 4 Like 1 (*Morf4l1*) (Figure 3.2).

Idi1 is a gene involved in the synthesis of cholesterol[107], whereas *Morf4l1* is involved in regulating chromatin activity[108]. Neither of these genes have been involved in the context of neurogenesis or mechanobiology. However, as seen from Figure 3.2 for both *Idi1*and *Morf4l1* genes, a greater amount of transcripts are aligned to a shorter 3'UTR isoform in NSCs on soft substrates, resulting in favoring the proximal PAS, whereas in NSCs on stiff substrates, we see more transcripts aligned to a longer 3'UTR isoform, thus in favoring the distal PAS. These initial results indicate that substrate stiffness may be indirectly regulating the post-transcriptional modification of mRNA by influencing the usage of PAS and resulting in different 3'UTR isoforms.

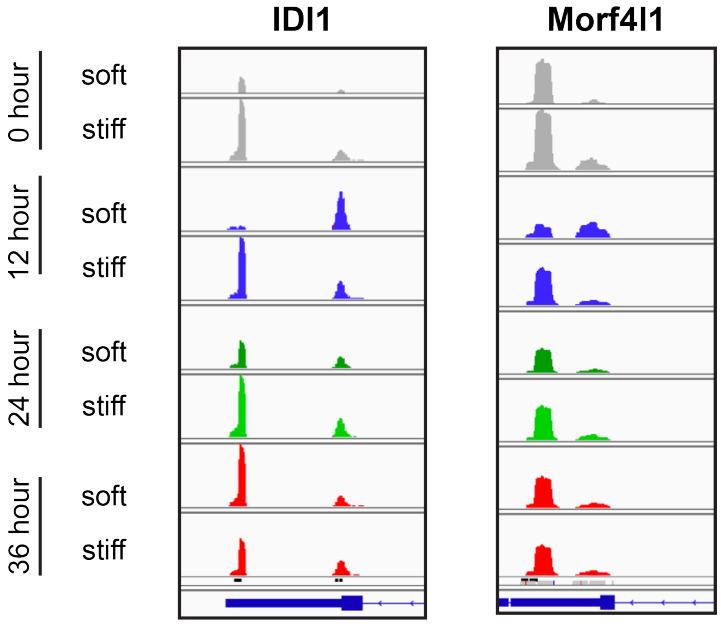

Figure 3.2: Read coverage track of two genes identified in the CSI-UTR analysis. Alignment was done using IGV software[109].

Substrate Stiffness leads to alternative PAS usage in the 3'UTR of mRNA during NSC differentiation

By knowing which 3'UTR isoforms are enriched in NSCs seeded on soft versus stiff substrates, we determined whether substrate stiffness promotes a shorter 3'UTR (proximal PAS usage) or longer 3'UTR (distal 3'UTR) by comparing the nucleotide lengths of the enriched 3'UTR isoforms on soft vs stiff substrates (Figure B.1). If $\varphi > 0$, there is an decrease in 3'UTR length of the mRNA on stiff versus soft substrate, and if $\varphi < 0$, there is a, increase in 3'UTR length on stiff versus soft. A table summarizing the 3'UTR lengthening and shortening of each mRNA transcripts of NSCs from each time point can be seen in Table 3.2.

	0 hour	**12 hour**	**24 hour**	**36 hour**
Increase in 3'UTR length (on stiff versus soft)($\varphi < 0$,)	5	21	0	2
Decrease in 3'UTR length (on stiff versus soft) ($\varphi > 0$),	8	111	1	5
Total Genes	13	132	2	7

Table 3.2: Results from determining the lengthening and shortening of the 3'UTR region of the mRNAs that had differentially expressed 3'UTR isoforms (from the CSI-UTR analysis)

Previously, we identified which genes are differentially expressed in NSCs differentiating on soft versus stiff substrates (results discussed in Chapter 2) based on comparing overall RNA transcript levels. As previously discussed, the lengthening and shortening of the 3'UTR region of mRNA may influence the stability of the mRNA, and thus its expression. To determine whether there is a relationship the lengthening and shortening of each 3'UTR and overall expression, we plotted the $-\log_{10}(FDR_{CSI})$ value on the x-axis, and the log fold change difference of the overall transcripts levels on the y-axis (Figure 3.3). The genes that had a longer 3'UTR isoform on soft versus stiff ($\varphi > 0$) were plotted on the left side of the graph where as those with a shorter 3'UTR isoform ($\varphi < 0$) were plotted on the right.

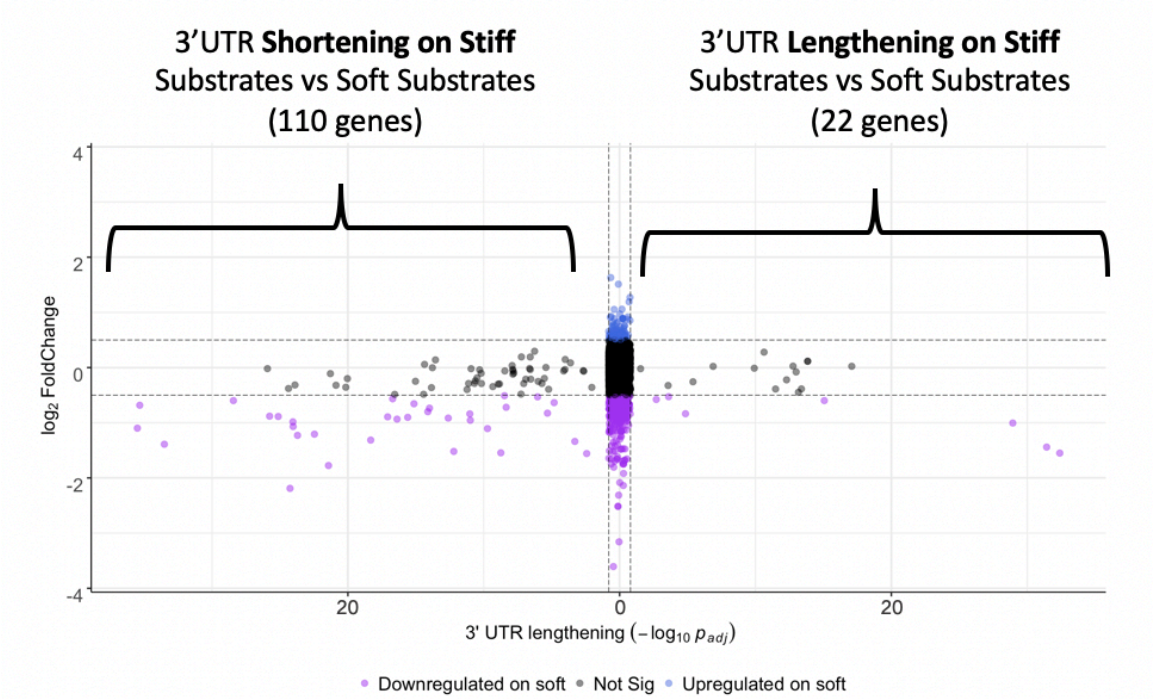

Figure 3.3: Scatter plot of RNA-seq data. Horizontal lines represent the cutoff value for one fold change in differential gene expression. Vertical line represent the cutoff value for the -$\log_{10}(p_{adj}$-value) of the 3'UTR shortening (1.3 represents p-value of 0.05) of NSCs in soft and stiff substrates which was determined using Fisher's Exact test.

As seen from this plot, it appears that most of the RNA transcripts have a longer 3'UTR on soft substrates versus stiff substrates. Out of all the X genes that, based on overall transcript count, were differentially expressed on soft versus stiff substrates (logFC>0.05 and $p_{adj} < 0.05$), 39 genes had transcripts that have a longer 3'UTR region on soft substrates relative to stiff substrates. A longer 3'UTR region may result in post transcriptional modifications of mRNA transcripts by including more microRNA and ribosomal protein binding sites that induce RNA degradation[110]. Thus, this is evidence that perhaps the length of the 3'UTR region may have some influence on whether an RNA is properly transcribed or not.

To experimentally verify the lengthening and shortening of the 3'UTR analysis of the RNA-seq analysis, we used a previously published method[102] to calculate the 'relative shortening index' (RSI) value. The equation used to calculate the RSI can be seen below along with Figure 3.4.a depicting the positioning of the primers used to amplify the total RNA and the long-specific region of the RNA transcript. The RSI of genes from conditions that either showed no difference in 3'UTR length, or an increase or decrease in 3'UTR length on soft versus stiff substrates was determined and can be seen in Figure 3.4.b. These results experimentally verify the observations seen from the computational analysis that shows differences in 3'UTR lengthening and shortening of certain mRNA transcripts.

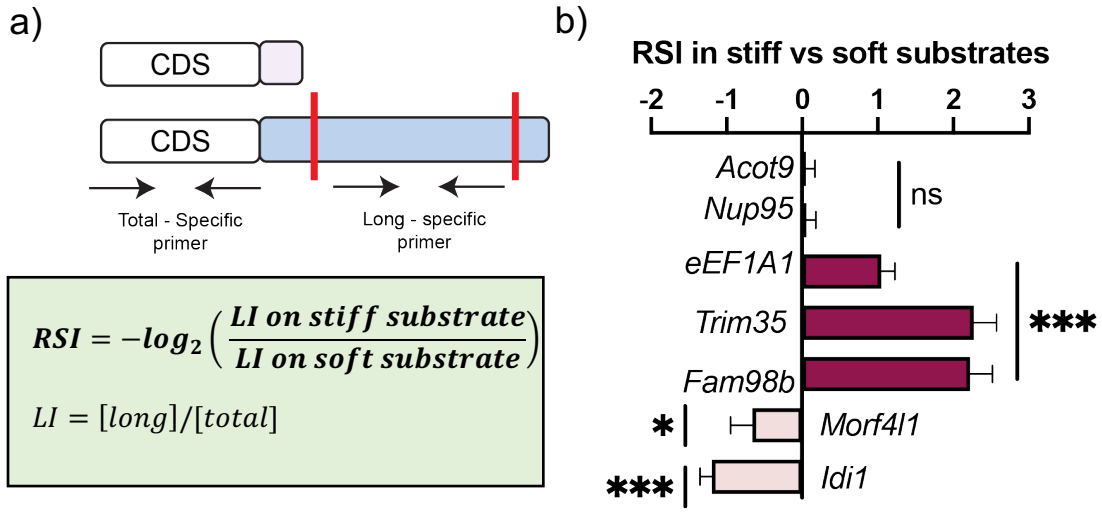

Figure 3.4: Experimental verification of 3'UTR analysis of RNA-seq results. (A) Primer design strategy to target the long 3'UTR region and the total primer to quantify total transcript levels. (B) RSI results of some of the genes identified in CSI-UTR analysis

Substrate Stiffness regulates the expression of CFIm25

Once we observed and verified that substrate stiffness influences the shortening and lengthening of the 3'UTR, we wanted to determine what intermediate players are involved in linking these two processes. Previous work has shown that a substrate stiffness regulates the expression of components of the mammalian cleavage factor I (CFIm), which in turn regulate the alternative polyadenylation usage of the PASs of mRNA[93]. Specifically, when cultured on stiff substrates, proximal PAS in fibroblasts, resulting in shorter 3'UTR and thus an increase in the overall protein production[97]. Furthermore, three components of the cleavage factor complex (CFIm68, CFIm59, and CFIm25) were upregulated in lung fibroblasts cultured on soft substrates versus stiff substrates, thereby regulating the distal usage of the PAS signals[97].

Motivated by this work, we studied whether substrate stiffness influences the protein abundance of any of the CFIm complexes listed above. We focused our attention first on measuring CFIm25 due to its strong relevance in pluripotent stem cell differentiation[104]. We seeded naïve NSCs on soft and stiff substrates in mixed differentiation conditions (1% FBS and 1 uM retinoic acid) and differentiated them for 24 days. We chose this time point as it is within the mechanosensitive time window in which mechanical cues have the largest influence on NSC fate commitment[40]. We then collected their lysates for Western Blot analysis. The results seen in Figure 3.5 indicate that at the start of differentiation (0 hour), we see no differences in CFlm25 expression in NSCs seeded on soft versus stiff substrates. However, during differentiation, we begin to see significant differences in expression levels, with a two fold increase on soft versus stiff substrate (Figure 3.5). Therefore, stiffness may be regulating the alternative polyadenylation, and thus the shortening and lengthening of 3'UTR regions of RNA transcripts by regulating the expression of CFlm25.

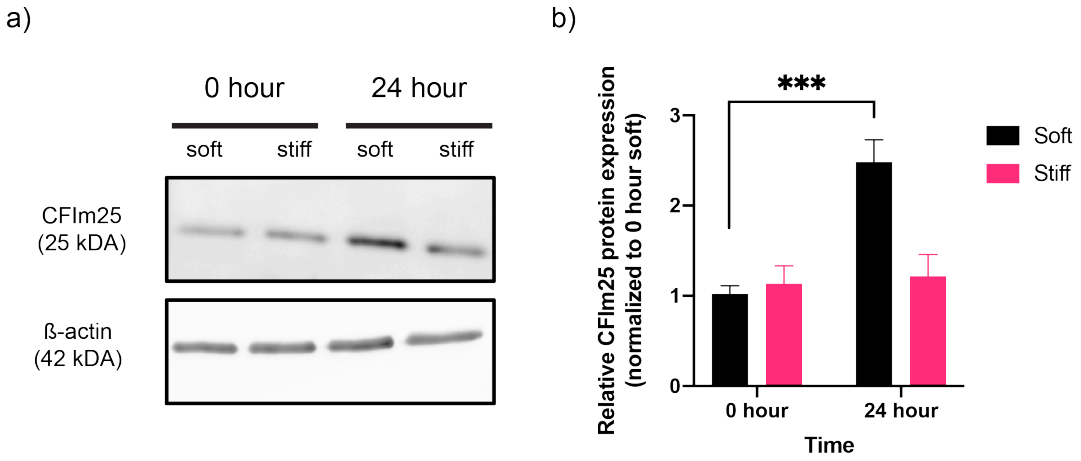

Figure 3.5: CFIm25 levels increase in NSCs seeded on soft substrate relative to stiff during differentiation. (A) Western blot results of naïve NSCs collected at the 24-hour time point. B) Western blot quantification results of CFIm25 protein levels normalized to β-actin. N=3

Knockdown of CFIm25 suppresses neurogenesis

To test the functional importance of CFlm25 on neurogenesis, we generated two short hairpins (shRNA-1 and shRNA-2) to target *NUDT21* gene (which expresses the CFIm25 protein) at different sites within the coding region (Figure 3.6.a). We packaged the plasmid encoding these hairpins (along with a scramble control) into lentiviruses and infected into NSCs. We then seeded the knockdown (only shRNA-1 and shRNA-2) and scramble cells on soft and stiff substrates in mixed differentiation conditions (1% FBS and 1 uM retinoic acid) and differentiated for 6 days. The cells were then immunostained for Tuj1% to measure the overall neurogenesis effect as seen in Figure 3.6.b. Knocking down CFIm25 decreased overall neurogenesis of NSCs differentiating on both soft and stiff substrates (on soft to 15% and on stiff to 10%) (Figure 3.6.c). These results indicate that CFIm25 is an important mediator of adult hippocampal neurogenesis.

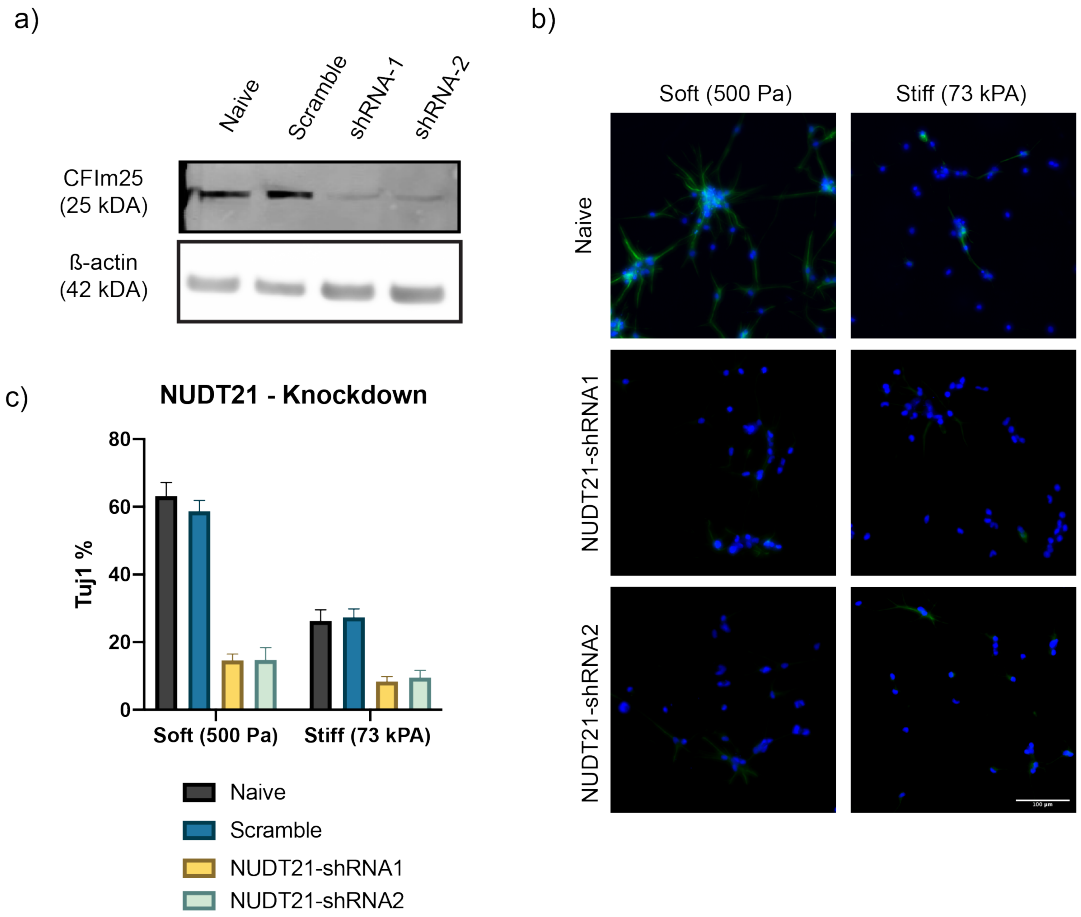

Figure 3.6: Knocking down CFIm25 (by targeting *NUDT21* gene) suppresses expression (A) Western blot validating the shRNA knockdowns (B) Representative immunofluorescent images of naive, NUDT21 KD's (shRNA-1 and shRNA-2) NSCs after culture in mixed differentiating conditions (1 uM retinoic acid + 1% Fetal Bovine Serum) on soft (500 Pa) or stiff (73 kPA) gels for 6 days. Cells were fixed and stained for DAPI (blue) and Tuj1 (Green), a neuronal marker. Bar = 100 uM. C) Immunostaining results of knockdowns. N=2.

3.3. Discussion

Throughout the past few years, our lab and others have shown that mechanical cues from the extracellular matrix influences NSC fate commitment, but the intermediate steps linking them together remain unclear. Previous bioinformatic results show that substrate stiffness influences transcript levels during NSC differentiation, and that these differences in mRNA transcript levels lead to differences in NSC fate commitment. However, the mechanism that leads to these differences in transcript remains unknown.

The overall focus of this study was to determine whether substrate stiffness influences the post transcriptional modification of mRNA, specifically the alternative polyadenylation of the 3'UTR of mRNA. The alternative polyadenylation of 3'UTR results in mRNA isoforms that have the same coding region but different 3'UTR lengths (referred to as 3'UTR isoforms). Within the mRNA transcript, there are multiple

polyadenylation signal sites (PAS) where polyadenylation can occur, thus allowing many genes to code for several mRNA that differ in their 3'end.

We first gained insight that substrate stiffness may regulate alternative polyadenylation of NSCs during differentiation after observing differences in the alignment of reads of previously acquired RNA-seq dataset. To gain a more unbiased perspective, we used a method called CSI-UTR[106] to allow us to determine which 3'UTR isoform is enriched on soft versus stiff substrates. These results show that there are different 3'UTR isoforms enriched in each condition and that these differences are mostly seen 12-hours after initiating differentiation. This initial bioinformatics study provides evidence that different PAS are used on soft versus to stiff, resulting in 3'UTR isoforms present in each stiffness condition.

For each mRNA that our study identified to have different 3'UTR isoforms on soft vs stiff, we compared the length of the 3'UTR isoform enriched on soft to that on stiff to see if substrate stiffness is influencing overall 3'UTR length. Interestingly, we see more usage of the distal PAS of 3'UTR in NSCs differentiating on soft versus those on stiff, resulting in longer 3'UTR isoforms. Previous work has shown that longer 3'UTR isoforms result in less mRNA transcript stability and overall protein production due to more binding sites for microRNAs and ribosomal binding proteins to target. Interestingly, mechanical cues also seem to regulate the expression of microRNAs[75], thus the interplay between microRNA expression and the alternative polyadenylation would be interesting to further explore. For example, in the gene eEF1A1, we see more usage of the distal, allowing more AU-Rich element binding sites for microRNA to target[111] (Figure B.2). Overall, the differences in the lengthening and shortening of the 3'UTR of mRNA may be the reason for transcript level differences in NSCs cultured on soft versus stiff substrates.

Furthermore, we determined a protein that is involved in the mammalian cleavage factor I (CFIm) complex which regulates the cleavage of the 3'UTR, is sensitive to mechanical cues. This protein, CFIm25 is upregulated in NSCs on soft versus stiff substrate during early neurogenesis. While we have not yet determined whether this difference is resulting in differences in the usage of PAS in NSCs differentiating on soft versus stiff substrates, other work has shown that the upregulation of CFIm25 results in longer 3'UTR of mRNAs encoding matrix proteins collagen and fibronectin[97]. While it is not clear as to how substrate stiffness is influencing the expression of CFIm25, other work has shown that TGF- ß1 signaling influences this proteins expression level[100]. TGF-ß1 signaling is also a pathway heavily studied in the field of mechanotransduction[112] but its involvement in NSC mechanosensing has yet to be explored.

Lastly, previous work has shown that suppression of CFIm25 levels results in impaired differentiation of pluripotent stem cells by enhancing the expression of genes involved in maintaining pluripotency during differentiation[104]. Similarly, knocking down CFIm25 in NSCs resulted in a decrease of neurogenesis on both soft and stiff substrates. However, we do not know whether reducing CFIm25 levels leads to changes in fate commitment, or just impairing differentiation. While these differentiation results are similar to those observed in pluripotent stem cells, we have yet to determine whether

these differences lead to changes in 3'UTR lengthening of pluripotent genes, or the genes found in the CSI-UTR analysis.

As discussed earlier, we used a method called CSI-UTR to identify the 3'UTR isoforms present in each of our RNA-seq datasets. CSI-UTR uses a more annotated rat genome that includes more information regarding the composition 3'UTR region, which was done using polyA seq data to annotate the regions between PAS. However, one drawback to this method is that it heavily relies on polyA seq data to annotate the 3'UTR isoforms of mRNA in the rat genome. Thus there may be some 3'UTR isoforms that are missed due to lack of polyA seq data. Over time, with more polyA seq data become available can we have more coverage of the 3'UTR isoforms that are present in our samples.

The main hypothesis as to how substrate stiffness is influencing the alternative polyadenylation of the 3'UTR of mRNA is through changing the expression level of CFIm25. While the functional results do show a drastic difference in fate commitment, we have yet to establish relevance to CFIm25 influence on 3'UTR composition. Thus, there is a possibility that CFIm25 may not have an impact on the lengthening and shortening of 3'UTR and may influence fate commitment through other means. If this is the case, there are other CFIm subunits (such as CFIm59 and CFIm68) that in other work are shown to be sensitive to stiffness cues and regulate 3'UTR shortening and stiffening. We are also interested in investigating whether the mTOR pathway may be regulating the lengthening and shortening of the 3'UTR in our NSCs. As discussed earlier, mTOR is also regulates the alternative polyadenylation of 3'UTR in other cell types[102]. Furthermore, treating our NSCs with mTOR inhibitor, Torin1, shows a drastic reductions of neurogenesis, while not impacting overall cell viability (Figure B.3). However, we have not tested whether mTOR activity differs in NSCs differentiating on soft versus stiff.

The alternative polyadenylation of the 3'UTR of mRNA has not only been recently been discovered to play a role in mechanotransduction, but also been connected to have heavy roles in in neurological disorders. One example is seen in patients with Huntington's disease where long 3'UTR isoform of the huntingtin gene is altered[113]. However, the mechanism as to how this gene is altered remains unknown. Another disease impacted by 3'UTR isoforms is myotonic dystrophy type I[114]. In this disease, there is a repeat expansion of the 3'UTR in the DMPK gene, which in turn prevents the gene from undergoing normal pre-mRNA processing. Furthermore, CFIm25 has been indicated as a potential diagnostic marker for glioblastoma multiforme[115]. Thus, understanding the regulatory mechanisms that modulate alternative polyadenylation can not only help us understand in a how stiffness is influencing NSC fate commitment, but also ways to treat diseases impacted changes in this mechanism for developing more effective treatments.

3.4. Materials and Methods

Neural Stem Cell Culture

Adult rat hippocampal cells were extracted and cultured as discussed previously[35,116]. Briefly, the cells were cultured in DMEM/F12 supplemented with N2 Supplement (Invitrogen) and 20 ng/ml of FGF-2 (Proteintech) (proliferation conditions) and seeded on plates coated with poly-L-ornithine and laminin. The media was changed every two days to maintain the cells in a proliferative state. For differentiation studies, the cells were initially seeded at a density of 25,000 cells/cm^2 and maintained in proliferation conditions for 16-18 hours to allow the cells to attach to the substrate. The cells were then switched to differentiation conditions, which consists of DMEM/F12, 1% fetal bovine serum (FBS) and 1 uM retinoic acid. The media was changed every two days for a total of 6 days.

Polyacrylamide gel synthesis and protein functionalization

The initial polyacrylamide precursor solution is composed of a mixture of acrylamide monomer and bisacrylamide crosslinker. The concentration for the 500 Pa (soft) gel precursor solution is 3% acrylamide + 0.1% bisacrylamide, whereas for the 73 kPA (stiff), the gel solution consists of 10% acrylamide + 0.3% bisacrylamide. The concentration of each component varies and is dependent on the final desired polyacrylamide gel stiffness[36]. To initialize the gel polymerization, the precursors solution was mixed with 1% ammonium persulfate and 0.1% tetramethylethylenediamine (TEMED) and synthesized on 12-, 18-, or 25 mm glass coverslips. Sulfo-sanpah solution (5 ul/ml) was added to the polymerized gels to functionalize the gels Laminin (25 ug/ml).

Identifying 3'UTR isoforms using CSI-UTR

The method, CSI-UTR, was used to determine the coverage of our reads that align to the cleavage site intervals (CSIs) of the Rattus Norvegicus (Rn6) genome. This method identifies a CSI as region in the 3'UTR that occur between two functional polyadenylation site (or a stop codon and a polyadenylation site) to determine 3'UTR isoforms in our sample[106]. Briefly, RNA-seq reads were mapped to the Rattus Norvegicus (Rn6) genome using HISAT aligner[83], which produced uniquely aligned reads in BAM format. These resulting BAM files from each sample were then mapped to the CSI of the Rn6 genome in BED format using BEDtools[82], which produced a raw CSI counts matrix. This matrix was then normalized to counts per million (CPM), which was used for further differential expression analysis.

Identifying Differentially Expressed 3'UTR isoforms

To determine the 3'UTR regions (CSIs) that are enriched, the normalized CSI counts of the reads mapped to a specific CSI is compared from one condition to another. This approach is labeled as the Within CSI Usage Differential Expression[106] and uses the normalization matrix acquired above of each sample set was used to identify differentially expressed CSIs.

Briefly. the percentage of the enriched CSI reads from the stiff condition (ψ_{A_i}) were compared to the enriched CSI reads from the soft condition (ψ_{B_i}) as seen in the equation below:

$$\psi_{A_i} = \frac{A_i}{\sum_{j=1}^{numCSI} A_j}; \psi_{B_i} = \frac{B_i}{\sum_{j=1}^{numCSI} B_j};$$

The difference in the percentage of read was calculated as:

$$\Delta\psi_i = \psi_{A_i} - \psi_{B_i}$$

To determine which CSIs (CSI_i) are significantly differentially expressed, a Fisher's exact test[117] was used to calculate the *p*-value:

$$(A_i, \left(\sum_{j=1}^{numCSI} A_j\right) - A_i, B_i, \left(\sum_{j=1}^{numCSI} B_j\right) - B_i)$$

The *p*-values were then corrected for false-discovery (FDR) using the Benjamin-Hochberg correction[118].

Quantitative Real-Time PCR

The Total RNA was isolated using RNeasy Mini Kit (Qiagen), which was further treated with DNAse digest enzyme from the RNAse-Free DNase Set (Qiagen) to remove and single or double stranded DNA. The 1 ug of total DNase treated RNA was reverse transcribed using Superscript III Reverse Transcripted (Thermo Fisher Scientific) along with an anchored oligo$(dT)_{20}$ Primer (Thermo Fisher Scientific). Quantitative PCR reactions were done in CFX Connect Real-Time PCR System (Bio-Rad), with three replicates conducted per sample.

To determine the relative shortening index (RSI) of each RNA transcript, different Primer sets amplifying 1) a long-specific region of the RNA, and 2) a common region within the cDNA to calculate total RNA were used for RT-PCR analysis. GAPDH was used as a housekeeping gene to compare among different conditions. The Ct value of each primer was converted to absolute value using the standard curve method[119]. The absolute value of each primer was normalized based on the absolute value of GAPDH of each condition.

Western Blot

For Western blot assay, cells were first lysed in HALT Protease Inhibitor Cocktail and RIPA Buffer (Thermo Fisher) for 5 minutes in 4C. The protein concentration was determined using a bicinchonic acid (BCA) assay. Lysates were mixed with LDS and reducing agent, and then heated for 5 minutes in 95C. The samples were then run on a 4-12% Bis-Tris gel and transferred onto nitrocellulose membrane (Licor). The membrane was blocked for one hour (Licor), and then incubated with primary antibody overnight. The next day, the membrane was washed with twice with TBST (5 minutes per wash), then incubated with IRDye secondary antibodies (Licor). The membrane was imaged using the Licor Odyssey 9120 Imaging System. The following antibodies were used: anti-NUDT21 (1:1000; Proteintech 10322-1-AP), and ß-actin (1:20000, Sigma Aldrich A2228).

Knockdown Vector

For generating the knockdowns, 21-mer siRNA constructs (shRNA1: GGGTC AACCAATTCGGTAACA, shRNA2: GGTCAACCAATTCGGTAACAA, and shRNA-3: AAACTACCTGGCGGTGAACTT) were designed to target the rat NUDT21 cDNA region using the online InvivoGen siRNA Wizard Software, along with a scramble control (GGTAGGAAATGTTTAGAGT). The final shRNA construct consists of the siRNA-sense + loop+ siRNA antisense sequences, with EcoRI and AgeI restriction enzyme sticky ends, allowing insertion to the pLKO.1 vector. The pLKO.1 – TRC cloning vector was a gift from David Root (Addgene plasmid # 10878).

Viral Transduction

HEK 293T cells were seeded one day prior at approximately 90% confluency on a 10cm plate. To package the pLKO.1 vector into lentiviruses, 10 ug of the pLKO.1 vector along with 7.5 ug of psPAX2 packaging plasmid and 2.5 ug of pMD2.G envelope plasmid were mixed along with 120 ul of polyethylenimine (PEI). This mixture was added dropwise to the cells. The supernatant was collected 48- and 72-hours post transfection and was filtered and pooled prior to ultracentrifugation. The viral particles were resuspended using cold PBS. The CLGPIT/CLPIT vectors were packaged similarly as the lentiviruses but were packaged into retriviruses. 10 ug of the pCLGPIT/pCLPIT vectors were used along with 6 ug of the pCMV gag-pol packaging plasmid and 4 ug of pcDNA3-IVS-VSV-G envelope plasmid.

Immunofluorescence staining and imaging

The cells were fixed in 4%(vol/vol) paraformaldehyde (Alfa Aesar) for 20 minutes at room temperature, permeabilized with 0.5% Triton-X for 10 minutes, and blocked in 10% goat serum for 1 hour. Between each step, the cells were washed twice with phosphate-buffered saline (PBS). Following the blocking, the cells were stained with primary antibodies overnight at 4C, and then with secondary antibodies for 1 hour at room temperature. After additional washes, 4’6-diamidino-2-phenylindole (DAPI) was

added as the nuclear marker. The primary antibody used was Tubb3 (1:1000; biolegend 801201). Secondary antibodies from Life Technologies were obtained using the appropriate species conjugated to either an Alexa-488 or -633 fluorophore.

Epifluorescence images were taken using Zeiss Axio Observer epi-fluorescent microscope (CIRM/QB3 Shared Stem Cell Objective, with a 10x objective. Samples were submerged in PBS during image acquisition. Image processing, including stitching and z-slice projection, and analysis was carried out using either Fiji[87] or CellProfiler[88].

3.5. Acknowledgements

We kindly thank Pratush Saravanan (University of California, Berkeley) for his experimental assistance. P.A.L. was supported by the National Science Foundation Graduate Fellowship. P.A.L., S.K. and D.V.S gratefully acknowledge grant support from the National Institutes of Health (grant #5R01NS074831: Mechanisms of Neural Stem Cell Mechanoregulation), awarded to S.K. and D.V.S.

Appendix A: Supplementary Material for Chapter 2

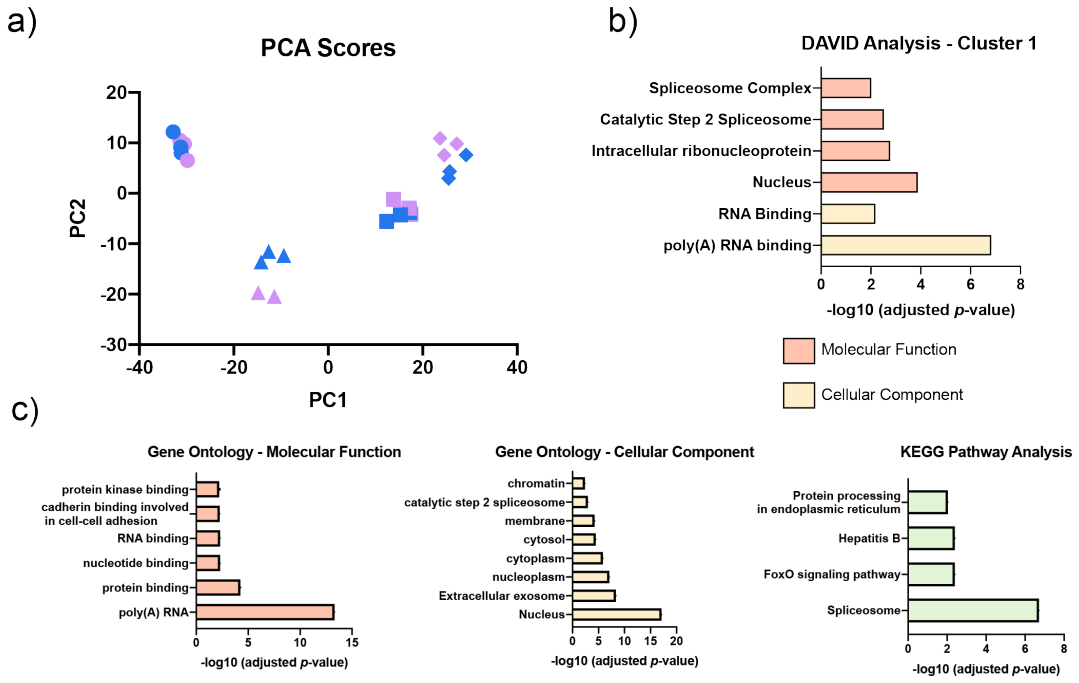

Figure A.1: Principal Component (PCA) and Pathway Analysis of RNA-sequencing results. (A) Principal component analysis of the samples collected at 0-, 12- , 24-, and 36-hour time point. Shapes correspond to time point (circle = 0 hour, triangle = 12 hour, square = 24 hour, and diamond = 36 hour), and colors correspond to stiffness (purple = soft, blue = stiff). (B) DAVID Pathway Analysis of Group 1 (Figure 1b). Enrichment analysis of Molecular Function and Cellular Component (C) DAVID Pathway Analysis of differentially expressed genes identified at the 12-hour time point (Figure 1C). Enrichment analysis of Molecular Function, Cellular Component, and KEGG Pathway Analysis.

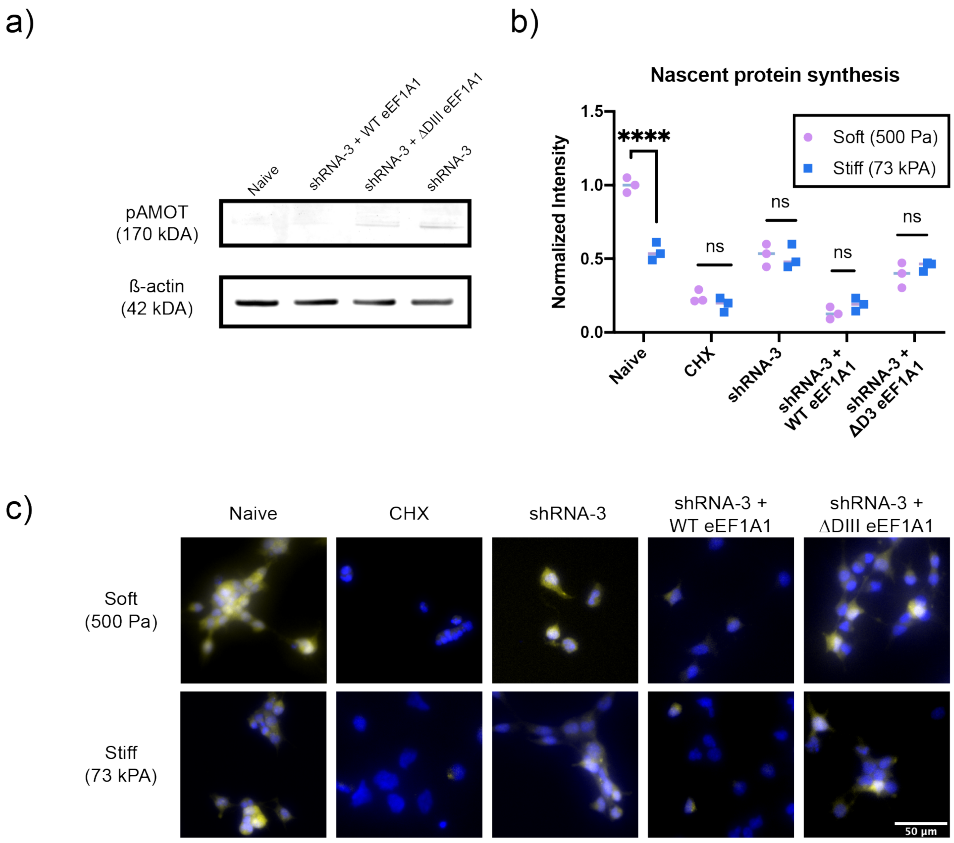

Figure A.2: phospho-AMOT and Overall Protein Synthesis measurements. (A) phospo-AMOT measured at 24 hours post differentiation collected from naïve, shRNA-3+WT eEF1A1, shRNA-3 +ΔDIII eEF1A1, and shRNA-3. (B) Nascent Protein Synthesis Assay Results at the 24 hour time point. A) Quantification of cell fluorescence following OPP incorporation Click-iT assay (n > 50 cells across three separate experiments) (C) Representative fluorescent images of naïve NSCs, cycloheximide (CHX)-treated NSCs, shRNA-3, shRNA-3 + WT, or shRNA3+ΔDIII eEF1A1, following incorporation of OPP to label nascent proteins (yellow) using a Click-iT assay and costaining of cell nuclei (DAPI; blue). Scale bars = 20 µm. ****$p < 0.0001$ two-way ANOVA followed by Tukey's post-hoc test. ns = not significant.

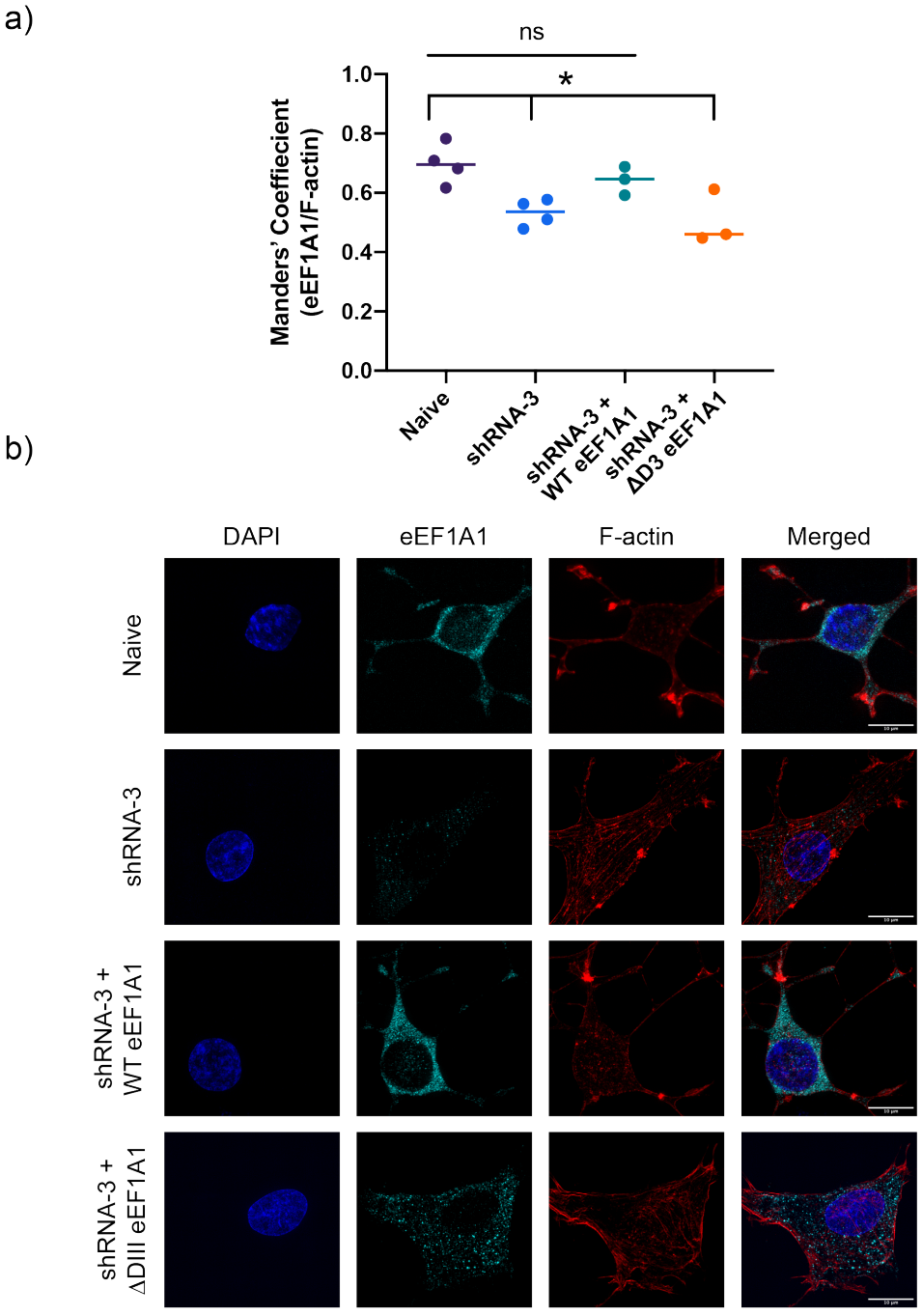

Figure A.3: Structured Illumination Microscopy (SIM) images of NSCs post 24 hours differentiation. (A) Quantification of the Mander's coefficient M1 (fraction of eEF1A1 colocalization with F-actin). N=3-4 biological replicates. 7-10 cells were imaged per replicate. (B) Representative SIM images of naïve, shRNA-3, shRNA-3 + WT eEF1A1, and shRNA-3 + + ΔDIII eEF1A1. Scale bar = 10 µm. *$p < 0.05$ by two-way ANOVA followed by Tukey's post-hoc test. n.s. = not significant

Table A.1: List of genes found in each Cluster Group (from Figure 1.1.b)

Group 1		Group 2	Group 3
Orc6	Uqcrc2	Mien1	Gnpda2
Pfdn2	Gap43	Glce	Med13l
Fam98b	Gtf2h5	Dync1li1	Klhl9
Magohb	Khdrbs1	Tgfa	Cog3
Arcn1	Gng5	Polr1d	Fyn
Bpnt1	Hnrnpd	Raf1	Galnt11
Spcs2	Ccdc47	Gnb2	Trim35
Rps27a-ps1	Acat1	Golga7	Dpm1
C1galt1c1	Sdhd	Hook1	Elf1
Rheb	Vdac1	Tsnax	Slc35e2b
Atxn2l	Psmd5	Lrp12	Rnf5
Timm23	Mrps31	Wsb1	Adam9
Armc8	Snrpf	Mex3b	Tgfbr2
Gtse1	Rpa3	Rtn4	Ctsl
Ppp4c	Wdr82	Ndufa4	Tusc3
Srp9	Cnn3	Mmadhc	Paip2
H2az1	Lsm6	Eef1a1	LOC100360087
Atp5pf	LOC100360750	Nrn1	Ftl1
Gpn3	Swap70	Bnip3	Maf1
Depdc1b	Rbl1	Bcl10	Dpy19l1
Eef1e1	Prpsap2	Rfk	Zdhhc8
Pfn1	Spcs3	Apod	Glyr1
Ndufc1	Wrnip1	Msx1	Ccng2
Hint1	Emc1	Elf2	Nkx2-2
Qsox2	Kif11	Chchd2	Ctnna1
Slc35a1	Pcgf5	Bbs5	Sgk3
Ramac	Map3k1	RGD1308706	Galnt2
Gabpb2	Dnajc19	Cyfip1	Cd164
Tmed7	Slc25a5	Sft2d1	Cpeb4

Mrpl33	Ndufb6	Atp1b3	Selenof
Pcgf6	Btf3	Zdhhc17	Grid1
Rnaseh1	LOC100911361	Plod2	Snx24
LOC100359574	Gclm	Fzd1	Tmem251
Zcchc9	Dpy30	Map2k1	Gltp
Gatad1	Pcna	Rev1	Usp19
Ankib1	Luc7l2	Ldb1	Crtc2
C2cd5	Rnf7	Gramd4	Gpm6b
Lsm7	Cycs	Capza1	Cyth1
Sh3bp4	Nr4a1	Rnf130	Wdr26
Eaf1	Fabp7	Zfp949	Slc35f5
Hif1a	Hnrnpk	Sec24b	Opcml
Nphp1	Nae1	Efcab7	Rnft1
Tma7	Pan2	Tgds	Copb1
Rps9l1	Bcas2	Ppfibp1	Cd9
Rps13	Lsm8	Tmed4	Dnaaf9
Micos10	RGD1308601	Sgk1	Uprt
Hsp90aa1	Cep85	Cox7c	Tex2
Idi1	Nup98	Ost4	Trappc8
Hdac2	Tp53rk	Gnas	Ndfip2
Zdhhc21	Rpl22l1	Rchy1	Yipf4
LOC108348989	Cdk2	Arf4	RGD1310352
Hnrnpa2b1	Acyp1	Cldnd1	Ddx6
Ola1	Snrpel1	Zfp266	Acap2
Cspg5	Med30	Eif4a2	Med13
Pabpc4	Dnajc24	Fam76a	Zkscan1
Rpl4	Tmcc3	Ndufc2	Etfdh
Rpl27	Ppp1r2	Dip2a	Pdia4
Ppia	Ctnnd1		Reep3
Tial1	Med23		Sbds
Nup107	Alg10		Sppl2a

Sumo2	Fam168b		Kdm7a
Cdkn2c	Memo1		Tob1
H2az2	Kpna2		Ireb2
Eloc	Rpf1		Mpc2
Pdpk1	Pole4		Stxbp3
LOC100362027	Tmed2		Trmt11
Pfdn4			Pnrc1
Dhx9			Anks1b

Appendix B: Supplementary Material for Chapter 3

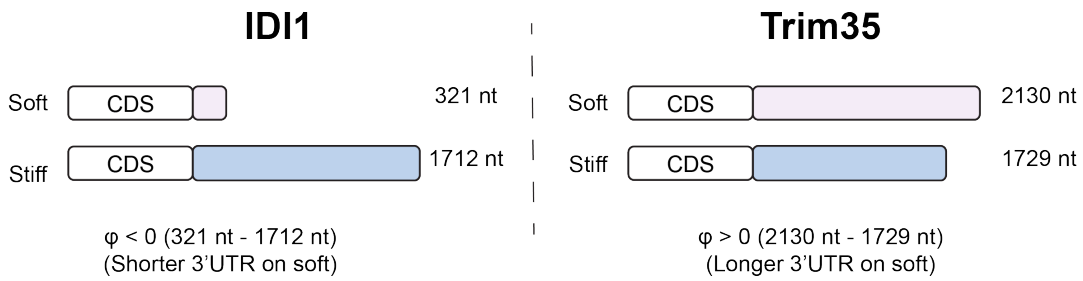

Figure B.1: Determining the change in 3'UTR length in NSCs in response to differentiating on a stiff substrate. The nucleotide length of the 3'UTR enriched on stiff substrate is compared to the one enriched on soft.

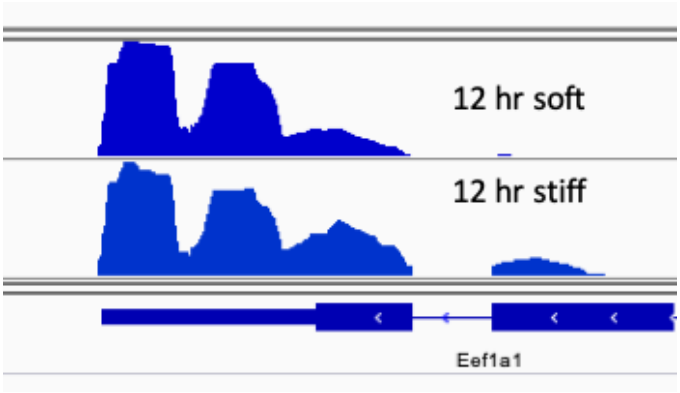

Figure B.2: There are more 3'UTR isoforms of eEF1A1 that are shorter in NSCs differentiating on stiff substrate relative those on soft. A shorter 3'UTR leads to a higher chance of them being translated. A longer 3'UTR results in the presence of more ARE sites, leading to less stable RNA.

a)

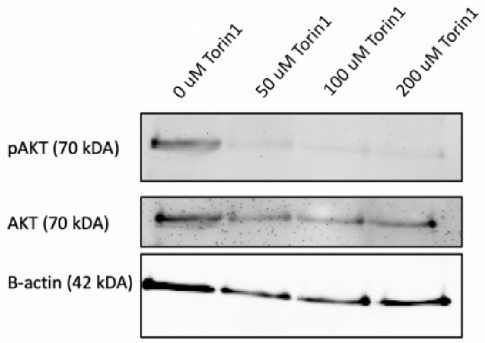

b)

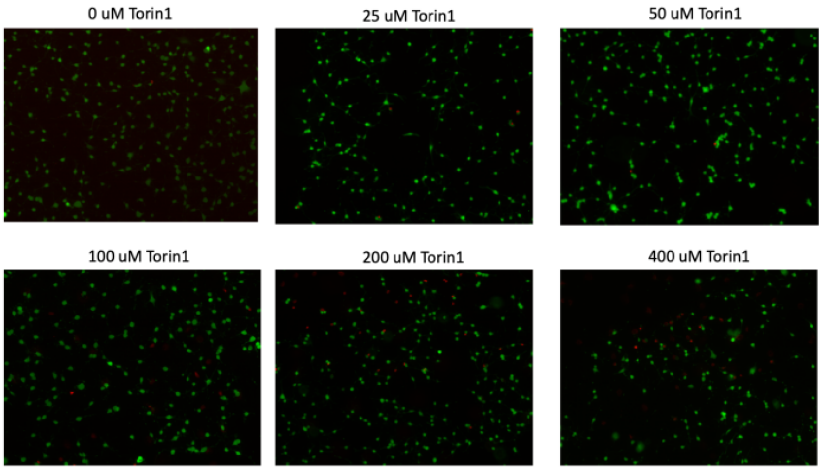

c)

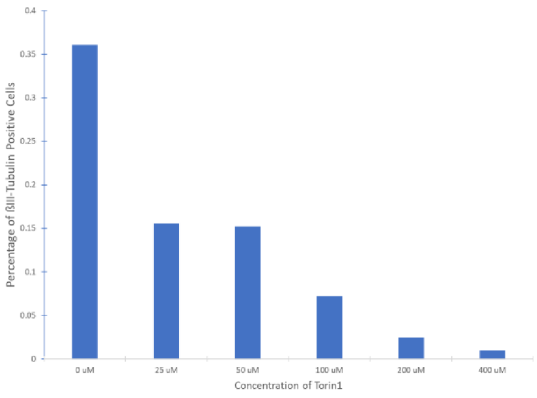

Figure B.3: Treating NSCs for 24 hours with Torin1, mTOR inhibitor. (A) Addition of Torin1 lowers pAKT activity while not influencing total AKT. pAKT is an indicator of mTOR activity) (B) Live/Dead assay showing adding Torin1 does not impact viability. C) Addition of Torin1 decreases neurogenesis.

Appendix C: Application of CRISPRi genome screen to identify novel factors involved in the mechanosensing of NSCs

C.1 Background

Previous work in our lab demonstrates that the stiffness of the brain matrix regulates neurogenesis. Specifically, when NSCs are cultured on soft substrates, there is an increase in neurogenesis, but when cultured on stiff substrates, neurogenesis decreases[35,36] . To elucidate this mechanism, we performed RNA sequencing (RNA-seq) to identify which genes are more highly expressed or repressed on either stiff or soft substrates. From the RNA-seq results, we identified that more genes are upregulated on stiff substrates compared to soft and that knocking down the expression of these genes leads to an increase of neurogenesis on stiff substrates. However, we still have yet to establish a relationship as to how stiffness is regulating the expression of these genes, and the activity of other players that differ in activity beyond the post-transcriptional level.

Recent advancements in genome engineering using CRISPR-Cas9 technology have allowed us to functionally annotate the genome and elucidate the role genes have in regulating cell behavior, directly linking the genotype of the cell to a phenotype of interest[120]. By using a catalytic inactive version of Cas9, referred to as dCas9, coupled with a Krab co-transcriptional repressor domain, we can transcriptionally silence gene expression without making changes to the DNA[121]. This dCas9-KRAB fusion system genetic perturbation technique is referred to as CRISPR interference (CRISPRi). With this technology, we performed a CRISPRi-genome wide screen to identify novel gene or genes that when knocked down, increase neurogenesis on stiff substrates.

C.2 Generating cell lines for performing CRISPRi knockdown screen

Development of mouse reporter line for selecting GFP+ (neurons) cells

To sort the cells that have undergone neurogenesis from other cell populations, I generated a GFP reporter line in mouse neural stem cells that fluorescence when cells express Tubb3, a common neuronal marker (Figure C.1). To assure that the GFP signal directly correlates with Tubb3 expression, I used CRISPR/Cas9 gene editing coupled with homology directed repair (HDR) to insert the cassette directly downstream of the Tubb3 gene. Thus, GFP expression is regulated by the endogenous Tubb3 promoter. An overview of the schematic can be seen in Figure C.2.

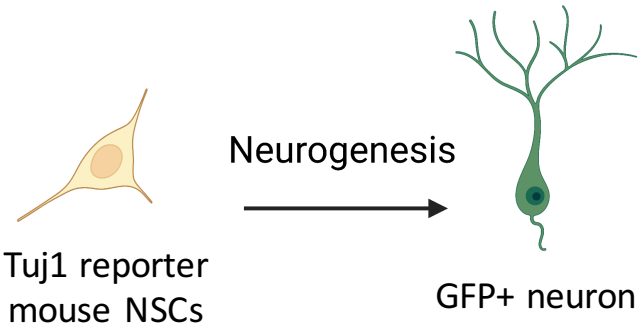

Figure C.1: Strategy for sorting neurons from population of differentiated NSCs.

Briefly, CRISPR/Cas9[122] is used to cut the double stranded DNA right before the stop codon, which increases the chances of HDR to occur. The pX330 (Addgene plasmid #42230) that encodes Cas9 machinery was used with a sgRNA (Table C.3) that targets the Tubb3 locus. A donor plasmid was also used that has to homology arms that perfectly align to the sequences surrounding the cut site as seen in Supplemental Figure C.2. The Oct-4-P2A-GFP plasmid (Addgene # 31938) was used and the homology arms that target the Oct4 gene were replaced with homology arms that target Tubb3. These arms were amplified from mouse genomic DNA (Primers used listed in Table C.3). Thus, through HDR, the cassette inserts itself in place of the stop codon (which is now at the end of the GFP sequence).

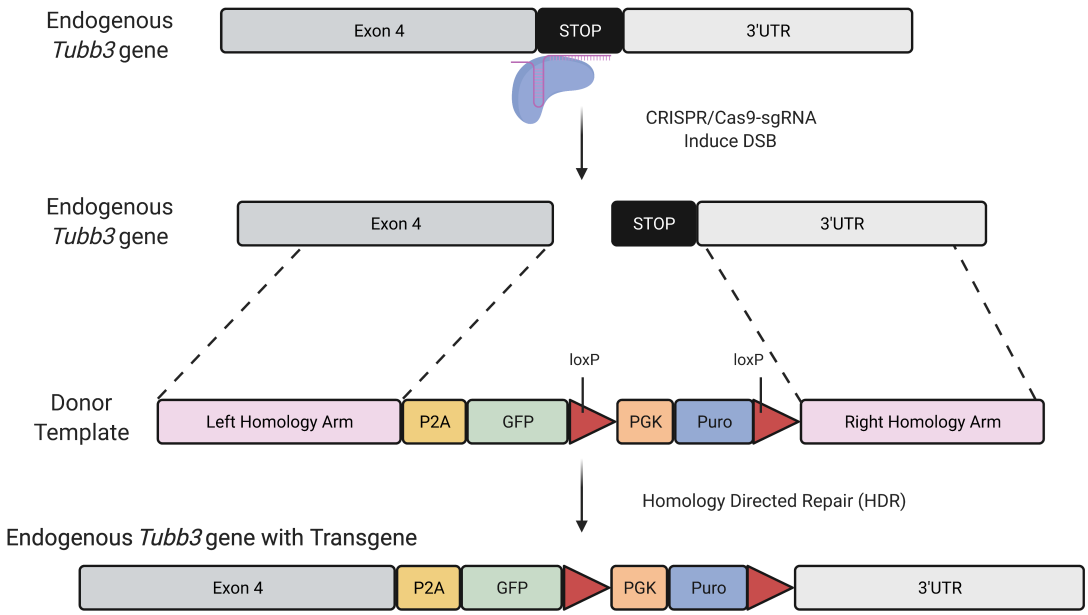

Figure C.2: Strategy to inserting GFP downstream of Tubb3 endogenous gene. Using CRISPR-Cas9 to induce a double stranded break (DSB), a donor construct provided by another plasmid was inserted to replace the stop codon.

To generate the reporter line, we nucleofected four million naïve mouse neural stem cells with 2.5 ug of pX330-Cas9-Tubb3-sgRNA plasmid and with 7.5 ug of the Tubb3-P2A-GFP donor plasmid. The following day we began selecting the cells with 0.6 ug/ml of puromyocin for one week prior and then sorted into cells onto a 96-well well using the serial dilution method[123]. The single-cells were cultured for approximately three weeks prior to expansion. The genomic DNA from each clonal cell was extracted and underwent genotyping analysis. Schematic of the genotyping strategy can be seen in in Figure C.3 with the primer sequences in the Table C.1.

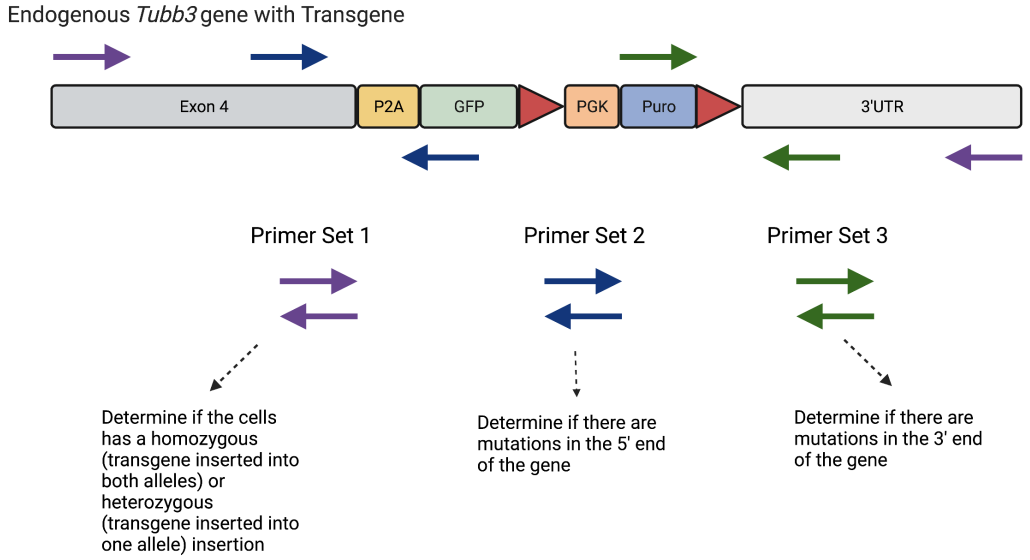

Figure C.3: Strategy for genotyping clonal cells for generating reporter line. Three sets of primers were designed to target different regions of the insert.

Primer Set	**Band Size**
Primer Set 1	3.5 kbp / 3.5 kbp and 600 bp (homozygous only / heterozygous)
Primer Set 2	1.3 kbp
Primer Set 3	1.2 kbp

Table C.1: Expected primer size of each of the primer sets used to genotype clonal cell lines.

Of the following 70 clonal reporter cells screened, only one had a successful insertion with no mutations in the 5' and 3' ends of the donor cassette (Primer Set 2 and

3) and was a homozygous insertion (Primer set 1). An example of the sequencing and gel results is seen in Figure C.4:

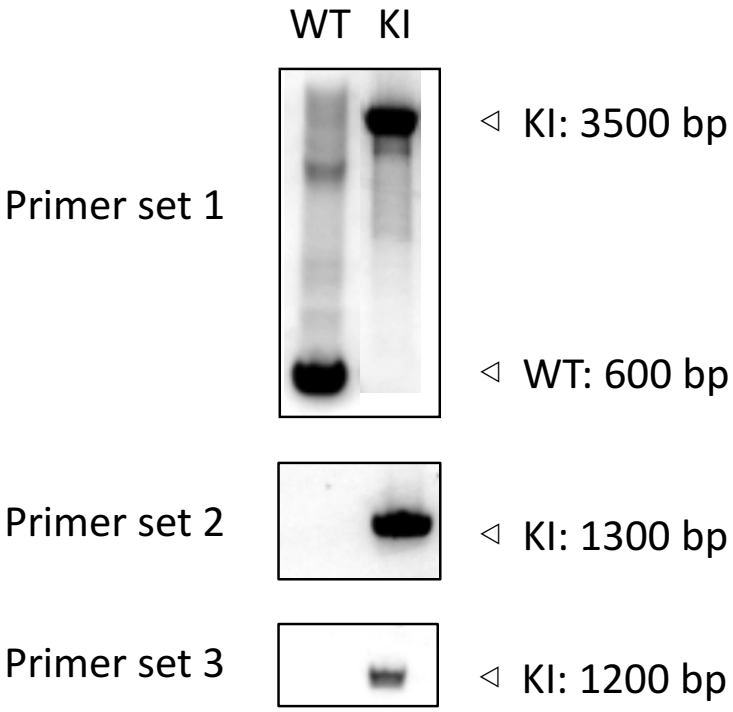

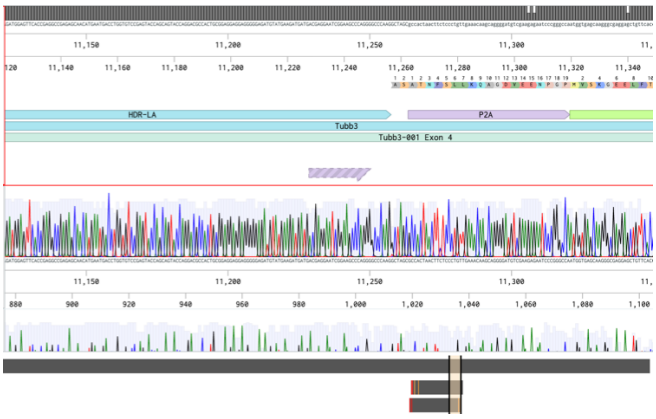

Figure C.4: Verifying genotyping results using Sanger Sequencing and PCR. Wildtype (WT) should only show one amplicon as seen in the top image. Primer set 1 indicates there is no insertion (since the band is 600 bp long). Knock-in (KI) shows three bands where there is amplification from Primer set 2 and primer set 3 where one primer binds to the foreign DNA and the other primer binds to the mouse genomic DNA. Second image below is example showing no mutations occurred during homologous directed recombination.

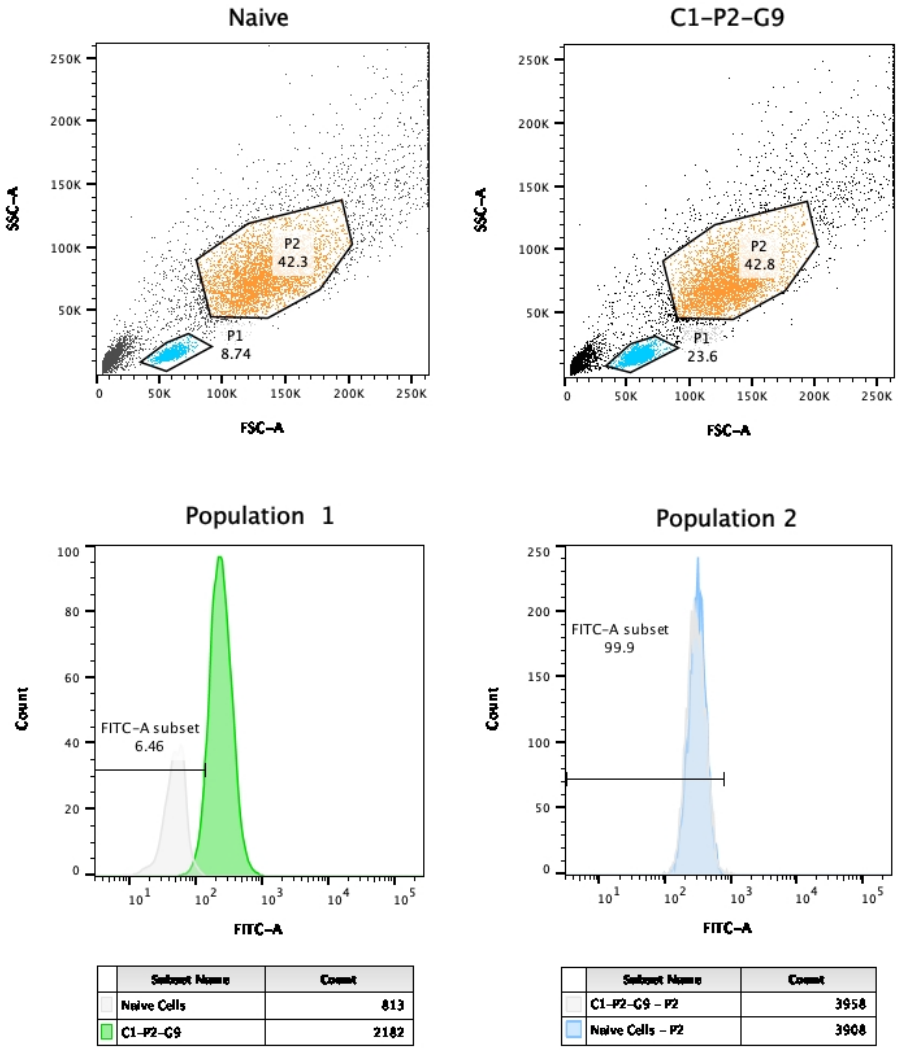

Figure C.5: FACS results verifying reporter line. Top images shows how each population from either Naïve and reporter (labeled C1-P2-G9) were gated. The bottom shows the fluorescence shift comparing reporter line to naïve. In Population 1, we see a shift in intensity signal in FITC-A, indicating the presence of GFP in C1-P2-G9.

We also verified there is GFP signal from these cells using FACS (Figure C.5.) and staining for another neuronal marker, doublecortin Figure C.6., which showed strong GFP colocalized in neurons. Thus, this reporter line was used for the continuation of the screen.

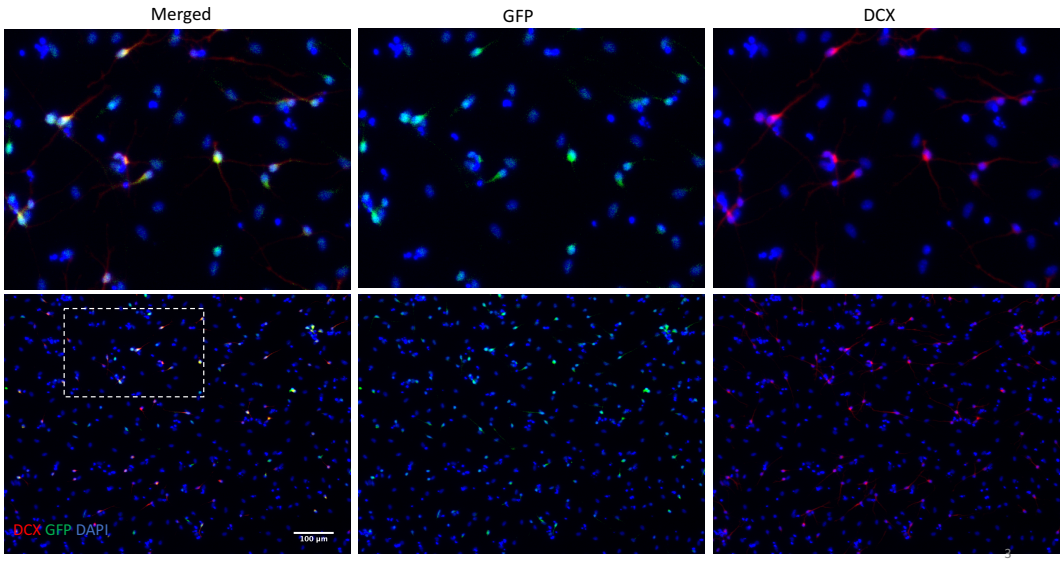

Figure C.6: Immunostaining images of NSCs differentiating after 6 days. Red = doublecortin, green = GFP, and blue = DAPI. Scale bar is 100 uM.

Lentiviral packaging of plasmid(s) encoding dCas9-KRAB fusion protein and the single guide RNA library

To generate the dCAS9-KRAB cell line, I first packaged a plasmid encoding this fusion protein complex (Addgene #83890) into lentivirus. I then cloned the sgRNA library (Addgene 83987), which consists of 3 sgRNA per gene along with 1000 non-targeting sgRNAs, into the pCRISPRia-v2 backbone (Addgene# 84832). Thus in total, approximately 109,000 sgRNAs were cloned into the plasmid. We then electroporated the sgRNA library into MegaX DH10B cells to determine the library diversity and determined an efficiency of more than 4800 colonies per sgRNA in the library. This efficiency is greater than the minimum coverage requirement (100 colonies per sgRNA) allowing us to move forward with this library.

C.3 In vitro selection screen for sgRNAs that knockdown genes that either enhance or suppress neurogenesis

A schematic of the selection strategy is presented in Supplemental Figure C.7:

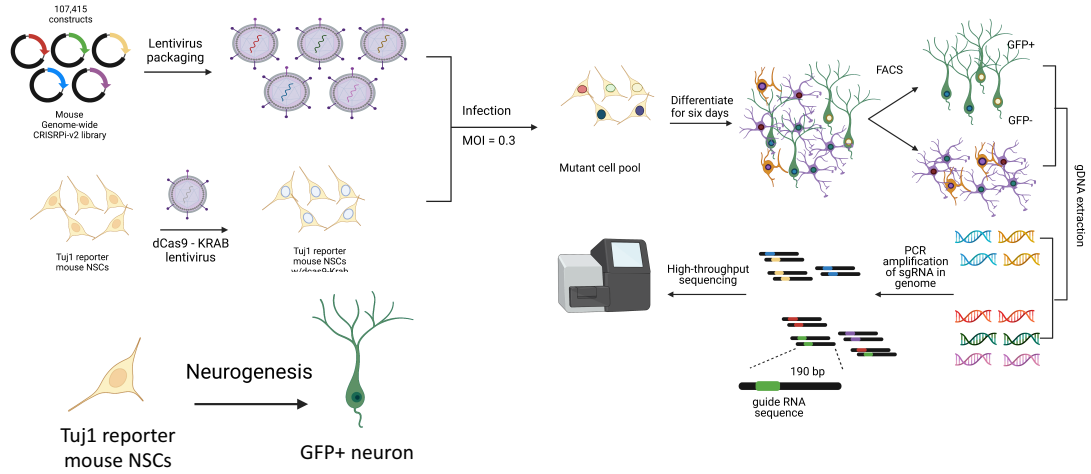

Figure C.7: Selection strategy for CRISPRi genome wide screen to determine genes that enhance neurogenesis.

The strategy is as follows:

1) I first infected the Tubb3-reporter mouse NSC lines with the lentiviruses packaging the dCas9-KRAB plasmid at a multiplicity of infection (MOI) of 1, and then selected using 100 ug/ml of hygromycin for approximately one week. Afterwards, we continued to maintain the cells in 50 ug/ml to assure that these cells were not contaminated by naïve NSCs.
2) We then packaged the sgRNA library into lentiviruses and infected them into the dCAS9-Krab mouse Tubb3-reporter NSC at a multiplicity of infection (MOI) of 0.3. We chose to do it a low MOI to assure only one copy of each sgRNA infects one cell. These cells were then FACS sorted for BFP (which is the selection marker for sgRNA library).
3) I then seeded the NSCs in multiple 15cm dishes at a confluence density of 10k/cm^2. After culturing overnight in proliferation conditions, we began differentiating them in mixed differentiation conditions (5 ng/ul of FGF2 + 1 uM retinoic acid). At the end of the 6 day differentiation time period, we harvested the cells and sorted for GFP+ and GFP- cells using FACS. We then extracted the genomic DNA and PCR amplified the region that contained information about the sgRNAs enriched in each condition. These were then sent off for deep sequencing at the Vincent J. Coates Genomic Sequencing Lab using NovaSeq 6000 (in 150 bp paired-end reads).

We performed this CRISPR screen twice to assure the results were consistent among biological replicates (Figure C.8.a). The results of the deep sequencing analysis were first trimmed using Cutadapt to eliminate the adapter sequences. The reads were then aligned using a fastq_to_counts.py source code which uses Bowtie alignment to align to reference table containing all the sgRNAs targeting the mouse genome[124]. Once we got the counts, we then determined the sgRNA and gene phenotype score and the p-values using process_experiments.py function[124]. The gene phenotype score of each gene is determined by averaging the read count of all the sgRNAs that target that specific gene for each replicate. This value is then averaged among both replicates.

A volcano plot depicting the results can be seen in Figure C.8.b. The results on the left side of the plot are those that when knocked down, suppress the expression of Tubb3. Thus these genes may be involved in enhancing the expression of Tubb3, and neurogenesis. The results on the right side of the plot are those that when knocked down, enhance the expression of Tubb3. Thus these genes are involved in suppressing the expression of Tubb3 and thus neurogenesis.

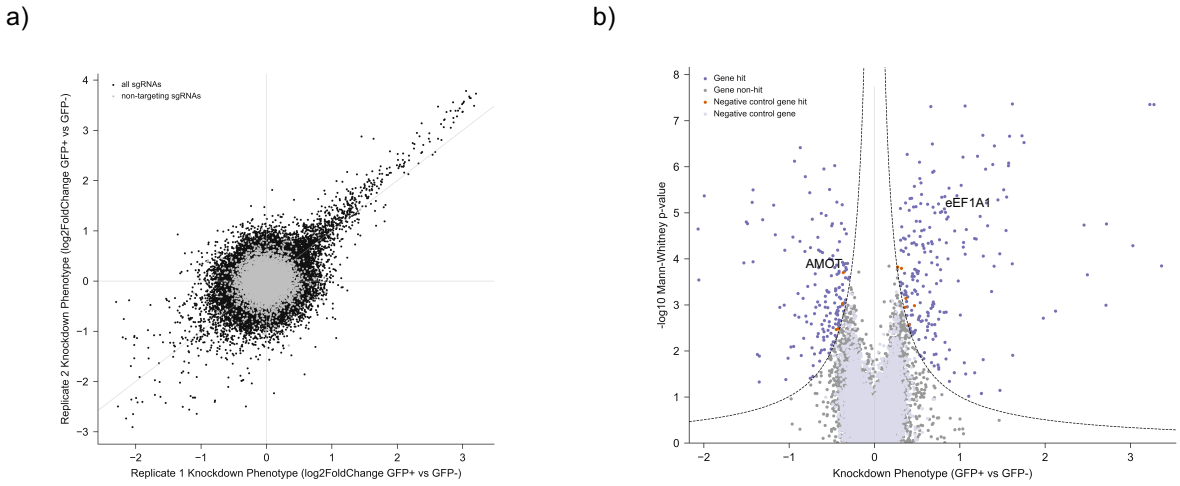

Figure C.8: CRISPRi genome screen results. (A) Scatter blot verifying the two biological replicates have similar sgRNA enrichment (GFP+ and GFP-) (B) Volcano plot showing the results of CRISPRi screen with the x-axis indicating the knockdown phenotype, which is the log2fold change of sgRNA expression between GFP+ vs GFP-, and the y-axis is the $\log_{10}p$-value. The left side of the plot represents genes that are important for neurogenesis (meaning knocking them down lowers neurogenesis) and the right side of the plot represents genes that suppress neurogenesis (meaning knocking them down enhances neurogenesis).

The way the analysis identifies hits is first comparing the fold change enrichment (also referred to as the gene phenotype score) of each gene found in the GFP+ and the GFP- populations. To determine the significance of the hits, the fold change among all the sgRNA is compared to the fold change of the negative control sgRNAs in each of the population. Thus the curve shows the p-value cut-off for the top hits (which is depicted by the dash line in the volcano plot). This approach allows us to only focus our attention

on the top hits from the screen. The results of the top genes from each population as seen below:

Table C.2 Gene identity, function, and phenotype score of the top 10 enriched genes from the GFP- population

Gene Name	Gene Symbol	Phenotype Score	Gene Function
Fry Like Transcription Coactivator	Fryl	-2.1782372	Involved in regulating cell polarity during morphogenesis and neuron projection. Also has roles in regulating the actin cytoskeleton and dendritic branching.
Plasminogen Activator, Urokinase	Plau	-2.078362	Encodes a secretase that converts zymogen plasminogen into active enzyme plasmin. While mostly studied in the context of blood coagulation, there is recent literature implicating its role in the Wnt signaling pathway[125].
Olfactory receptor 1000	Olfr1000	-2.0559506	A member of the olfactory receptor group mostly known for initiating a neuronal response to smell. These proteins are members of the G-protein-coupled receptor (GPCR) group.
Transmembrane protein 238	Tmem238	-1.4807463	Not much is known about this protein besides it's a transmembrane protein and interacts with Hnrnph1
Phosphatidylinositol-3,4,5-Triphosphate Dependent Rac Exchange Factor 2	Prex2	-1.4776331	Facilitates the exchange of GDP for GTP on Rac1
Neuramindase 2	Neu2	-1.4745996	Involved in a family of glucohydroytic enzymes which removes siiac acid residue from glycoproteins and glycolipids
Glycoprotein M6A	Gpm6a	-1.441394	Invoved in a multitude of pathways including mitogen-activated protein kinase (MAPK) pathway and Src signaling pathway. Speculated to pay a significant role in enabling calcium channel activity during stem cell differentiation and neuron migration. Inhibition of this gene through histone deacetylase 5 inhibits neurite elongation[126].
DnaJ Heat Shock Protein Family (Hsp40) Member B4	Dnajb4	-1.3295283	Has a multitude of roles in tumor suppression and binding to E-cadherin to target to plasma membrane.
Vascular endothelial Growth Factor B	Vegfb	-1.2985311	Involved in the family of proteins that regulate the formation of blood vessels and has been implicated to play a role in the survival of CNS-derived neurons. Furthermore, knockdown of this gene is shown to impair adult hippocampal neurogenesis[127]
Microfibril associated protein 4	Mfap4	-1.2885311	Has binding sites specifically for both collagen and carbohydrates and thought to be an extracellular protein involved in cell adhesion and other intracellular interactions

Table C.3 Gene identity, function, and phenotype score of the top 10 enriched genes from the GFP+ population

Gene Name	Gene Symbol	Phenotype Score	Gene Function
Transmembrane Protein 151a	Tmem151a	3.33548341	A transmembrane protein localized in the endoplasmic reticulum which plays a crucial role in Ca2+ mobilization and dynamics
Nicotinamide adenine dinucleotide (NAD) Synthetase 1	Nadsyn1	3.28489894	NAD is involved in metabolic redox reactions and involved in protein in posttranslational modifications. NAD Synthetase catalyzes the final step of NAD biosynthesis from nicotinic acid adenine dinucleotide
SCY1 Like Pseudokinase 2	Scyl2	3.21579851	The protein encoded by this gene regulates clathrin-dependent trafficking at the plasma membrane. Also has functions in the Wnt signaling pathway by targeting frizzled 5 (Fzd5)
Notch Receptor 1	Notch1	3.16449785	Encodes a protein that is involved in the NOTCH family of proteins. Notch signaling pathway is an evolutionary conserved pathway that regulates the interactions between other cell types through Notch ligand interaction. Inactivation of Notch signaling has been shown to induce neurogenesis but depletes NSC population[20].
Olfactory receptor 544	Olfr544	2.80609287	Regulates cellular energy and metabolism
G Protein-Coupled Receptor 21	Gpr21	2.80601045	A member of the G-protein-coupled recetor family which activates signaling pathways in response to extracellular stress. The protein translated from this gene is shown to activate Gq signaling transduction pathway and mobilize calcium.
Ring Finger Protein 157	Rnf157	1.63167091	Involved in enabling ubiquitin protein ligase activity. Prevents apoptosis and promotes survival of neurons through ubiquitination of APBB1 for its degradation.
Interleukin 1 Receptor Associated Kinase 1	Irak1	1.59472811	Interacts with the interleukin-1 receptor and plays a role in innate immune response against foreign pathogens. Through interactions with protein BAP31, Irak1 modulates inflammatory cytokines and cognitive impairment induced by neuroinflammation.
Transformation related protein 53	Trp53	2.166070439	The protein (p53) encoded by this gene responds to cellular stress to target genes that induce cell cycle arrest, apoptosis, senescence, DNA repair, or changes in overall cellular metabolism. Other work has shown that knockdown of this gene results towards biased in neuronal precursors[128].
Heme oxygenase 1	Hmox1	2.0931798	This gene encodes a protein involved in heme catabolism and one of the cytoprotective enzymes induced by many stimuli including oxidative stress.

C.4 Discussion and Future work

Overall, the CRISPR screen served as a way to validate some previous results from the lab in linking the cues emitted from substrate stiffness to NSC fate commitment. For example, Angiomotin (AMOT) showed up as a hit in the GFP- population. Previous work in our lab showed that knockdown of AMOT resulted in a suppression of neurogenesis (using Tubb3 expression to measure neurogenesis) on both soft and stiff substrates and that the rescue of the protein increased neurogenesis[67]. Furthermore, eEF1A1 showed up as a hit in the GFP+ population, meaning when knocked down, increases Tubb3 expression (and thereby neurogenesis). As discussed in Chapter 2, eEF1A1 was found to be upregulated on stiff substrates relative to soft and its expression suppresses neurogenesis.

However, another protein our lab has studied, YAP[40] was not found to be differentially expressed in either of the populations. There could be several reasons as to why. One reason could be that we used mouse NSCs in this study and these cells may not respond in the same manner to mechanical cues as rat neural stem cells (the cell type used in that paper). We can test this hypothesis by either seeing if we see YAP upregulation on stiff substrates versus soft substrates or if YAP knockdown in mouse NSCs influences neurogenesis to the same degree as they do in rat neural stem cells.

CRISPR screens serve as way to identify novel candidates involved in a regulating a phenotype of interest in a more high-throughput manner. Some of the top hits listed in Table C.2 and C.3 have not been exploded in the context of NSC fate commitment or mechanobiology and thus would be interesting to further investigate their involvement in either of those fields. Some interesting hits (such as *Neu2* and *Olfri544*) are involved in metabolism which is a process involved in both mechanotransduction and stem cell fate commitment. However, it is not yet known whether if influencing metabolism influences the ability of stiffness cues to regulate NSC fate commitment.

Furthermore, some of the hits identified from the screen have been identified to play a prominent role in NSC fate commitment. One example is *Vegfb* which previous work has shown that knockdown of this gene decreases NSC differentiation to neurons[127]. This gene showed up in the GFP- population, and verifying this gene is important for regulating neurogenesis. Two other genes heavily studied to be involved in neurogenesis showed up in GFP+ population. One of these genes, *Notch1*, serves as a receptor for Notch ligands and involved in the Notch signaling pathway. When knocked down, there is an overall increase in neurogenesis[20], similar to our CRISPR screen results. Interestingly, *Notch1* has been explored as mechanosensor in adult arteries, serving a way to fluid sense shear stress in the vascular wall of heart valves[129]. In addition, Trp53 gene which expresses p53 also has been involved in regulating neurogenesis. Knockdown of this gene results in both an increase in proliferation, and neuronal differentiation[128]. This gene has also been heavily studied in the context of cancer, specifically brain tumors, as mutations of this gene result in aberrant expression of genes involved in cell cycle arrest, apoptosis, etc[130,131]. Thus, fundamental understanding of p53 will further advance our knowledge in not only brain development, but also tumorigenesis.

One of the biggest drawbacks of the setup of the screen is that the genes we identified in the GFP- population are those we propose are important for neurogenesis (because knocking them down results in no Tubb3 expression). However, these genes could just be involved in regulating the fate to other lineages or enhance proliferation/impair differentiation. Similarly, this can be said for the GFP+ population where some of the hits may just influence the transition from stem cells to neurons cells but not influence their fate. Lastly, our setup to identify neurons is based on the paradigm that Tubb3 is expressed in the neurons. However, some of the hits either in the GFP- and GFP+ population may just regulate the expression of Tubb3, and not neurogenesis. A follow up verification study of the hits is necessary to corroborate whether they do influence fate commitment, and not just Tubb3 expression. This can using another marker for immature neurons such as double-cortin (DCX).

Another caveat with our screen results is that we do not know if the hits identified from the screen are associated with the mechanosensation of NSC differentiation to neurons. The CRISPR screen was conducted on a stiff substrate, and while we know that on stiff substrates there is a suppression of neurogenesis, we do not know if the hits identified are involved in the mechanosensation of NSC to neurons or just involved in regulating neurogenesis. While it is promising that two hits (AMOT and eEF1A1) showed up in these results that have been explored in the mechanosensation of NSC differentiation, we need to further validate whether any of the other hits identified do so as well. One way is to measure the expression or activity level of any of these hits or any downstream effectors of the hits (if the hit is a transcription factor or kinase) and determine whether we see any differences among soft versus stiff substrate. We also do have RNA sequencing data of NSCs cultured on soft versus stiff substrates (both in 2D and 3D) during early differentiation. We could determine whether any of the hits are involved in regulating the expression of some of the differentially expressed mRNA transcripts identified in these RNA-seq results. In addition, more future work for this project includes combining the hits (after they are validated) to see if they work together mechanistically to dictate fate commitment by regulating the mechanosensation of NSCs.

C.5 Supplementary Material

Table C.4: Primer sequences used to generate and verify reporter line

Primer Name	Sequence (5’ to 3’)
Tubb3-sgRNA_FWD	CACCG**AGCTGCGAGC AAC TTCACTT**
Tubb3-sgRNA_REV	CACCGAGCTGCGAGCAACTTCACTT
Tubb3_L-HA-FWD	TCAC**CCTGCAGG**GGGGCACAGGCTCAGGCATG
Tubb3_L-HA-REV	AGCAGCTAGCCTTGGGCCCCTGGGCTTCCG
Tubb3_R-HA-FWD	GGGCGGCGCGCCAGTTGCTCGCAGCTGGGGTG
Tubb3_R-HA-FWD	GTAG**GCGGCCGC**GGAAGAATGCTGGATATGAG

Table C.5: Primer sequences used for genotyping analysis

Primer name	Sequence (5’ to 3’)

Tubb3-PS1_FWD	AGA TGT CGT GCG GAA AGA GT
Tubb3-PS1-REV	GAA CTT CAG GGT CAG CTT GC
Tubb3-PS2_FWD	GCC TGA AGA ACG AGA TCA GC
Tubb3-PS2_REV	ATG GAG CCA GTA CAG GGT TG
Tubb3-PS3-FWD	GTC AAG GTA GCC GTG TGT GA
Tubb3-PS3-REV	TCT CCA ATA CCA GGC AGA GG

References

(1) Altman, J.; Das, G. D. Autoradiographic and Histoloaical Evidence of Postnatal Hippocampal Neurogenesis in Rats. *J. Comp. Neurol.* **1965**, *125*, 319–336.

(2) Eriksson, P. S.; Perflieva, E.; Bjork-Eriksson, T.; Alborn, A.-M.; Nordborg, C.; Peterson, D. A.; Gage, F. H. Neurogenesis in the Adult Human Hippocampus. *Nat. Med.* **1998**, *4* (11), 1313–1317.

(3) Sorrells, S. F.; Paredes, M. F.; Cebrian-silla, A.; Sandoval, K.; Qi, D.; Kevin, W.; James, D.; Mayer, S.; Chang, J.; Auguste, K. I.; et al. Human Hippocampal Neurogenesis Drops Sharply in Children to Undetectable Levels in Adults. *Nature* **2018**, *555*, 377–381.

(4) Lucassen, P. J.; Fitzsimons, C. P.; Salta, E.; Maletic-savatic, M. Adult Neurogenesis, Human after All (Again): Classic, Optimized, and Future Approaches. *Behav. Brain Res.* **2020**, *381* (May 2019), 112458.

(5) Boldrini, M.; Fulmore, C. A.; Tartt, A. N.; Dwork, A. J.; Mann, J. J.; Boldrini, M.; Fulmore, C. A.; Tartt, A. N.; Simeon, L. R.; Pavlova, I.; et al. Short Article Human Hippocampal Neurogenesis Persists throughout Aging Short Article Human Hippocampal Neurogenesis Persists throughout Aging. *Cell Stem Cell* **2018**, 589–599.

(6) Moreno-Jiménez, E. P.; Flor-García, M.; Terreros-Roncal, J.; Rábano, A.; Cafini, F.; Pallas-bazarra, N.; Ávila, J.; Llorens-martín, M. Adult Hippocampal Neurogenesis Is Abundant in Neurologically Healthy Subjects and Drops Sharply in Patients with Alzheimer ' S Disease. *Nat. Med.* **2019**, *25* (April), 554–560.

(7) Alam, M. J.; Kitamura, T.; Saitoh, Y.; Ohkawa, N.; Kondo, T.; Inokuchi, K. Adult Neurogenesis Conserves Hippocampal Memory Capacity. *J. Neurosci.* **2018**, *38* (31), 6854–6863.

(8) Dupret, D.; Revest, J.; Koehl, M.; Giorgi, F. De; Abrous, D. N. Spatial Relational Memory Requires Hippocampal Adult Neurogenesis. *PLoS One* **2008**, *3* (4).

(9) Mu, Y.; Gage, F. H. Adult Hippocampal Neurogenesis and Its Role in Alzheimer ' S Disease. *Mol. Neurodegenration* **2011**, *6*, 1–9.

(10) Sanai, N.; Tramotin, A. D.; Quinones-Hinojosa, A.; Barbaro, N. M.; Gupta, N.; Kunwar, S.; Lawton, M. T.; McDermott, M. W.; Parsa, A. T.; Verdugo, J. M.-G.; et al. Unique Astrocyte Ribbon in Adult Human Brain Contains Neural Stem Cells but Lacks Chain Migration. *Nature* **2004**, *427* (February), 740–744.

(11) Basak, O.; Taylor, V. Stem Cells of the Adult Mammalian Brain and Their Niche. *Cell. Mol. Life Sci.* **2009**, *66*, 1057–1072.

(12) Aimone, J. B.; Li, Y.; Lee, S. W.; Clemenson, G. D.; Deng, W.; Gage, F. H.; Jb, A.; Li, Y.; Sw, L.; Gd, C.; et al. REGULATION AND FUNCTION OF ADULT NEUROGENESIS : FROM GENES TO COGNITION. *Physiol. Rev.* **2014**, *94*, 991–1026.

(13) Mosher, K. I.; Schaffer, D. V. Influence of Hippocampal Niche Signals on Neural Stem Cell Functions during Aging. *Cell Tissue Res.* **2018**, *371* (1), 115–124.

(14) Lie, D.-C.; Colamarino, S. A.; Song, H.-J.; Désiré, L.; Mira, H.; Consiglio, A.; Lein, E. S.; Jessberger, S.; Lansford, H.; Dearie, A. R.; et al. Wnt Signalling Regulates Adult Hippocampal Neurogenesis. *Nature* **2005**, *437* (7063), 1370–1375.

(15) Shetty, A. K.; Hattiangady, B.; Shetty, G. A. Stem / Progenitor Cell Proliferation Factors FGF-2 , IGF-1, and VEGF Exhibit Early Decline During the Course of Aging in the Hippocampus : Role of Astrocytes. *Glia* **2005**, *51* (January), 173–186.
(16) Yousef, H.; Morgenthaler, A.; Schlesinger, C.; Bugaj, L.; Irina, M.; Schaffer, D. V; Biology, C. Age-Associated Increase in BMP Signaling Inhibits Hippocampal Neurogenesis. *Stem Cells* **2016**, *33* (5), 1577–1588.
(17) Mathieu, C.; Sii-felice, K.; Fouchet, P.; Etienne, O.; Haton, C.; Mabondzo, A.; Boussin, F. D.; Mouthon, M. Endothelial Cell-Derived Bone Mo Rphogenetic Proteins Control Proliferation of Neural Stem/ Progenitor Cells. *Mol. Cell. Neurosci.* **2008**, *38*, 569–577.
(18) Meyers, E. A.; Gobeske, K. T.; Bond, A. M.; Jarrett, J. C.; Peng, C.; Kessler, J. A. Increased Bone Morphogenic Protein Signaling Contributes to Age-Related Declines in Neurogenesis and Cognition. *Neurobiol. Aging* **2017**, 164–175.
(19) Gobeske, K. T.; Das, S.; Bonaguidi, M. A.; Weiss, C.; Radulovic, J.; John, F.; Kessler, J. A. BMP Signaling Mediates Effects of Exercise on Hippocampal Neurogenesis and Cognition in Mice. *PLoS One* **2009**, *4* (10).
(20) Imayoshi, I.; Sakamoto, M.; Yamaguchi, M.; Mori, K.; Kageyama, R. Essential Roles of Notch Signaling in Maintenance of Neural Stem Cells in Developing and Adult Brains. *J. Neurosci.* **2010**, *30* (9), 3489–3498.
(21) Ashton, R. S.; Conway, A.; Pangarkar, C.; Bergen, J.; Lim, K.; Shah, P.; Bissell, M.; Schaffer, D. V. Astrocytes Regulate Adult Hippocampal Neurogenesis through Ephrin-B Signaling. *Nat. Neurosci.* **2012**, *15* (10), 1399–1406.
(22) Jiao, J.; Feldheim, D. A.; Chen, D. F. Ephrins as Negative Regulators of Adult Neurogenesis in Diverse Regions of the Central Nervous System. *Proc. Natl. Acad. Sci.* **2008**, *105* (25), 8778–8783.
(23) Sibbe, M.; Kuner, E.; Althof, D.; Frotscher, M. Stem- and Progenitor Cell Proliferation in the Dentate Gyrus of the Reeler Mouse. **2015**, 3–11.
(24) Yu, C.; Griffiths, L. R.; Haupt, L. M. Exploiting Heparan Sulfate Proteoglycans in Human Neurogenesis — Controlling Lineage Specification and Fate. *Front. Integr. Neurosci.* **2017**, *11* (October), 1–15.
(25) Veríssimo, C. P.; Carvalho, S.; Jorge, F.; Campanati, L.; Moura-neto, V.; Coelho-aguiar, J. D. M. Laminin and Environmental Cues Act in the Inhibition of the Neuronal Differentiation of Enteric Glia in Vitro. *Front. Neurosci.* **2019**, *13* (September), 1–13.
(26) Su, W.; Matsumoto, S.; Sorg, B.; Sherman, L. S. Distinct Roles for Hyaluronan in Neural Stem Cell Niches and Perineuronal Nets. *Matrix Biol.* **2019**, *78–79*, 272–283.
(27) Adil, M. M.; Vazin, T.; Ananthanarayanan, B.; Rodrigues, G. M. C.; Rao, A. T.; Kulkarni, R. U.; Miller, E. W.; Kumar, S.; Schaffer, D. V. Engineered Hydrogels Increase the Post-Transplantation Survival of Encapsulated hESC-Derived Midbrain Dopaminergic Neurons. *Biomaterials* **2017**, *136*, 1–11.
(28) Ballios, B. G.; Cooke, M. J.; Donaldson, L.; Coles, B. L. K.; Morshead, C. M.; Kooy, D. Van Der; Shoichet, M. S. A Hyaluronan-Based Injectable Hydrogel Improves the Survival and Integration of Stem Cell Progeny Following Transplantation. *Stem Cell Reports* **2015**, *4* (6), 1031–1045.
(29) Luque, T.; Kang, M. S.; Schaffer, D. V; Kumar, S. Microelastic Mapping of the

Rat Dentate Gyrus. *R. Soc. Open Sci.* **2016**, *3*, 1–7.
(30) Chatelin, S.; Constantinesco, A.; Willinger, R. Fifty Years of Brain Tissue Mechanical Testing : From in Vitro to in Vivo Investigations. *Biorheology* **2010**, *47* (January), 255–276.
(31) Cheng, S.; Clarke, E. C.; Bilston, L. E. Rheological Properties of the Tissues of the Central Nervous System : A Review. *Med. Eng. Phys.* **2008**, *30*, 1318–1337.
(32) Rojas-Fernandez, A.; Herhaus, L.; Macartney, T.; Lachaud, C.; Hay, R. T.; Sapkota, G. P. Rapid Generation of Endogenously Driven Transcriptional Reporters in Cells through CRISPR/Cas9. *Sci. Rep.* **2015**, *5* (1), 9811.
(33) Antonovaite, N.; Beekmans, S. V; Hol, E. M.; Wadman, W. J. Regional Variations in Stiffness in Live Mouse Brain Tissue Determined by Depth-Controlled Indentation Mapping. *Sci. Rep.* **2018**, No. August, 1–11.
(34) Ryu, Y.; Iwashita, M.; Lee, W.; Uchimura, K.; Kosodo, Y.; Carver, C. M. A Shift in Tissue Stiffness During Hippocampal Maturation Correlates to the Pattern of Neurogenesis and Composition of the Extracellular Matrix. *Front. Aging Neurosci.* **2021**, *13* (July), 1–10.
(35) Saha, K.; Keung, A. J.; Irwin, E. F.; Li, Y.; Little, L.; Schaffer, D. V; Healy, K. E. Substrate Modulus Directs Neural Stem Cell Behavior. *Biophys. J.* **2008**, *95* (9), 4426–4438.
(36) Keung, A. J.; De Juan-Pardo, E. M.; Schaffer, D. V.; Kumar, S. Rho GTPases Mediate the Mechanosensitive Lineage Commitment of Neural Stem Cells. *Stem Cells* **2011**, 1886–1897.
(37) Baek, J.; Lopez, P. A.; Lee, S.; Kim, T. Egr1 Is a 3D Matrix – Specific Mediator of Mechanosensitive Stem Cell Lineage Commitment. *Sci. Adv.* **2022**, *8*.
(38) Hodge, R. G.; Ridley, A. J. Regulating Rho GTPases and Their Regulators. *Nat. Rev.* **2016**, *17*.
(39) Yang, C.; Tibbitt, M. W.; Basta, L.; Anseth, K. S. Mechanical Memory and Dosing Influence Stem Cell Fate. *Nat. Mater.* **2014**, *13* (6), 645–652.
(40) Rammensee, S.; Kang, M. S.; Georgiou, K.; Kumar, S.; Schaffer, D. V. Dynamics of Mechanosensitive Neural Stem Cell Differentiation. **2017**, 497–506.
(41) Dupont, S.; Morsut, L.; Aragona, M.; Enzo, E.; Giulitti, S.; Cordenonsi, M.; Zanconato, F.; Digabel, J. Le; Forcato, M.; Bicciato, S.; et al. Role of YAP / TAZ in Mechanotransduction. **2011**.
(42) Darnell, M.; Gu, L.; Mooney, D. Biomaterials RNA-Seq Reveals Diverse Effects of Substrate Stiffness on Mesenchymal Stem Cells. *Biomaterials* **2018**, *181*, 182–188.
(43) Darnell, M.; Neil, A. O.; Mao, A.; Gu, L.; Rubin, L. L.; Mooney, D. J. Material Microenvironmental Properties Couple to Induce Distinct Transcriptional Programs in Mammalian Stem Cells. *Proc. Natl. Acad. Sci.* **2018**, *115* (36).
(44) Gage, F. H.; Temple, S. Neural Stem Cells: Generating and Regenerating the Brain. *Neuron* **2013**, *80* (3), 588–601.
(45) Bond, A. M.; Ming, G.; Song, H. Review Adult Mammalian Neural Stem Cells and Neurogenesis : Five Decades Later. *Stem Cell* **2015**, *17* (4), 385–395.
(46) Zhao, C.; Deng, W.; Gage, F. H. Mechanisms and Functional Implications of Adult Neurogenesis. *Cell* **2008**, *132* (4), 645–660.
(47) Morrison, J. H.; Hof, P. R. Life and Death of Neurons in the Aging Brain. *Science*

(80-.). **1997**, *278*, 412–419.
(48) Oliveira, N. B. De; Irioda, A. C.; Elias, P.; Stricker, F.; Mogharbel, B. F.; Silva, D.; Dziedzic, M.; Athayde, K.; Carvalho, T. De. Natural Membrane Differentiates Human Adipose-Derived Mesenchymal Stem Cells to Neurospheres by Mechanotransduction Related to YAP and AMOT Proteins. *Membranes (Basel).* **2021**, *11* (687), 5–8.
(49) Zhao, B.; Li, L.; Lu, Q.; Wang, L. H.; Liu, C.; Lei, Q.; Guan, K. Angiomotin Is a Novel Hippo Pathway Component That Inhibits YAP Oncoprotein. *Genes Dev.* **2011**, *25*, 51–63.
(50) Murray, J. W.; Edmonds, B. T.; Liu, G.; Condeelis, J. Bundling of Actin Filaments by Elongation Factor 1 α Inhibits Polymerization at Filament Ends. *J. Cell Biol.* **1996**, *135* (5), 1309–1321.
(51) Mateyak, M. K.; Kinzy, T. G. eEF1A : Thinking Outside the Ribosome. *J. Biol. Chem.* **2011**, *285* (28), 21209–21213.
(52) Li, D.; Wei, T.; Abbott, C. M. The Unexpected Roles of Eukaryotic Translation Elongation Factors in RNA Virus Replication and Pathogenesis. *Microbiol. Mol. Biol. Rev.* **2013**, *77* (2), 253–266.
(53) Mickleburgh, I.; Chabanon, H.; Nury, D.; Fan, K.; Burtle, B.; Chrzanowska-lightowlers, Z.; Hesketh, J. Elongation Factor 1 a Binds to the Region of the Metallothionein-1 mRNA Implicated in Perinuclear Localization — Importance of an Internal Stem – Loop. **2006**, 1397–1407.
(54) Liu, G.; Grant, W. M.; Persky, D.; Latham, V. M.; Singer, R. H.; Condeelis, J. Interactions of Elongation Factor 1α with F-Actin and β-Actin mRNA: Implications for Anchoring mRNA in Cell Protrusions. *Mol. Biol. Cell* **2002**, *13* (2), 579–592.
(55) Gross, S. R.; Kinzy, T. G. Translation Elongation Factor 1A Is Essential for Regulation of the Actin Cytoskeleton and Cell Morphology. *Nat. Struct. Mol. Biol.* **2005**, *12* (9).
(56) Yue, J.; Shukla, R.; Accardi, R.; Zanella-cleon, I.; Siouda, M.; Cros, M.; Krutovskikh, V.; Hussain, I.; Niu, Y.; Hu, S.; et al. Cutaneous Human Papillomavirus Type 38 E7 Regulates Actin Cytoskeleton Structure for Increasing Cell Proliferation through CK2 and the Eukaryotic Elongation Factor 1A. *J. Vi* **2016**, No. October, 8477–8494.
(57) Love, M. I.; Huber, W.; Anders, S. Moderated Estimation of Fold Change and Dispersion for RNA-Seq Data with DESeq2. *Genome Biol.* **2014**, *15* (12), 1–21.
(58) Pantano, L. DEGreport: Report of DEG Analysis. New Jersey, NJ: R package version 1.20.0. 2019.
(59) Kendall, M. G. *Rank Correlation Methods, 2nd Ed.*; Hafner Publishing Co.., 1955.
(60) Pearson, K. Notes on Regression and Inheritance in the Case of Two Parents. *Proc. R. Soc. London* **1895**, *58*, 240–242.
(61) Caraglia, M.; Budillon, A.; Vitale, G.; Lupoli, G.; Tagliaferri, P.; Abbruzzese, A. Modulation of Molecular Mechanisms Involved in Protein Synthesis Machinery as a New Tool for the Control of Cell Proliferation. **2000**, *3936*, 3919–3936.
(62) Snape, N.; Li, D.; Wei, T.; Jin, H.; Lor, M.; Rawle, D. J.; Spann, K. M.; Harrich, D. The Eukaryotic Translation Elongation Factor 1A Regulation of Actin Stress Fibers Is Important for Infectious RSV Production. **2018**, 1–10.

(63) Allen, W. E.; Jones, G. E.; Pollard, J. W.; Ridley, A. J. Rho, Rac and Cdc42 Regulate Actin Organization and Cell Adhesion in Macrophages. *J. Cell Sci.* **1997**, *720*, 707–720.
(64) Yue, J.; Shukla, R.; Accardi, R.; Zanella-cleon, I.; Siouda, M.; Cros, M.; Krutovskikh, V.; Hussain, I.; Niu, Y.; Hu, S.; et al. Cutaneous Human Papillomavirus Type 38 E7 Regulates Actin Cytoskeleton Structure for Increasing Cell Proliferation through CK2 and the Eukaryotic Elongation Factor 1A. *J. Virol.* **2016**, *85* (17), 8477–8494.
(65) Ishizaki, T.; Uehata, M.; Tamechika, I.; Keel, J.; Nonomura, K.; Medicine, F.; Discovery, D. Pharmacological Properties of Y-27632 ,a Specific Inhibitor of Rho-Associated Kinases. *Mol. Pharmacol.* **2000**, *57*, 976–983.
(66) Kovacs, M.; Toth, J.; Hetenyi, C.; Malnasi-Csizmadia, A.; Sellers, J. R. Mechanism of Blebbistatin Inhibition of Myosin II *. *J. Biol. Chem.* **2004**, *279* (34), 35557–35563.
(67) Kang, P. H.; Schaffer, D. V; Kumar, S.; Discher, D. Angiomotin Links ROCK and YAP Signaling in Mechanosensitive Differentiation of Neural Stem Cells. *Mol. Biol. Cell* **2020**.
(68) Andersen, G. R.; Pedersen, L.; Valente, L.; Chatterjee, I.; Kinzy, T. G.; Kjeldgaard, M.; Nyborg, J.; Vej, G. W. Structural Basis for Nucleotide Exchange and Competition with tRNA in the Yeast Elongation Factor Complex eEF1A : eEF1B ␣. *Mol. Cell* **2000**, *6*, 1261–1266.
(69) Jakobsson, M. E.; Malecki, J.; Falnes, P. Regulation of Eukaryotic Elongation Factor 1 Alpha (eEF1A) by Dynamic Lysine Methylation. *RNA Biol.* **2018**, *15* (3), 314–319.
(70) Vlasenko, D. O.; Novosylna, O. V.; Negrutskii, B. S.; El'skaya, A. V. Truncation of the A,A∗,A' Helices Segment Impairs the Actin Bundling Activity of Mammalian eEF1A1. *FEBS Lett.* **2015**, *589* (11), 1187–1193.
(71) Baser, A.; Skabkin, M.; Martin-villalba, A. Neural Stem Cell Activation and the Role of Protein Synthesis. *Brain Plast.* **2017**, *3*, 27–41.
(72) Forester, C. M.; Zhao, Q.; Phillips, N. J.; Urisman, A.; Chalkley, R. J.; Oses-prieto, J. A. Revealing Nascent Proteomics in Signaling Pathways and Cell Differentiation. *Proc. Natl. Acad. Sci.* **2018**, *115* (10), 2353–2358.
(73) Simpson, L. J.; Tzima, E.; Reader, J. S. Mechanical Forces and Their Effect on the Ribosome and Protein Translational Machinery. *Cells* **2020**, 1–12.
(74) Perez, W. B.; Kinzy, T. G. Translation Elongation Factor 1A Mutants with Altered Actin Bundling Activity Show Reduced Aminoacyl-tRNA Binding and Alter Initiation via eIF2a Phosphorylation *. *J. Biol. Chem.* **2014**, *289* (30), 20928–20938.
(75) Moro, A.; Driscoll, T. P.; Boraas, L. C.; Armero, W.; Kasper, D. M.; Baeyens, N.; Jouy, C.; Mallikarjun, V.; Swift, J.; Ahn, S. J.; et al. MicroRNA-Dependent Regulation of Biochemical Genes Establishes Tissue Stiffness Homeostasis. *Nat. Cell Biol.* **2019**, *21* (March), 348–358.
(76) Pasquinelli, A. E. MicroRNAs and Their Targets : Recognition , Regulation and an Emerging Reciprocal Relationship. *Nat. Publ. Gr.* **2012**, *13* (April), 271–282.
(77) Prasanth, S. G.; Prasanth, K. V; Stillman, B. Orc6 Involved in DNA Replication , Chromosome Segregation , and Cytokinesis. *Science (80-.).* **2002**, *297* (August),

1026–1032.
(78) Koff, A.; Giordano, A.; Desai, D.; Yamashita, K.; Harper, J. W.; Elledge, S.; Nishimoto, T.; Morgan, D.; Franza, B. R.; Roberts, J. M. Formation and Activation of a Cyclin E-cdk2 Complex During the G1 Phase of the Human Cell Cycle. *Science (80-.).* **1992**, *257* (September), 1689–1694.
(79) Ohnuma, S.; Harris, W. A. Neurogenesis and the Cell Cycle. *Neuron* **2003**, *40*, 199–208.
(80) Peltier, J.; Ormerod, B. K.; Schaffer, D. V. Isolation of Adult Hippocampal Neural Progenitors. *Methods Mol. Biol.* **2010**, *621* (6), 57–63.
(81) Andrews, S. FastQC: A Quality Control Tool for High Throughput Sequence Data [Online]. Available online at: http://www.bioinformatics.babraham.ac.uk/projects/fastqc/.
(82) Bushnell, B. BBMap. Available online at sourceforge.net/projects/bbmap/.
(83) Kim, D.; Langmead, B.; Salzberg, S. L. HISAT: A Fast Spliced Aligner with Low Memory Requirements. *Nat. Methods* **2015**, *12* (4), 357–360.
(84) Anders, S.; Pyl, P. T.; Huber, W. Genome Analysis HTSeq — a Python Framework to Work with High-Throughput Sequencing Data. **2015**, *31* (2), 166–169.
(85) Huang, D. W.; Sherman, B. T.; Lempicki, R. A. Systematic and Integrative Analysis of Large Gene Lists Using DAVID Bioinformatics Resources. *Nat. Methods* **2008**, *4* (1), 44–57.
(86) Peltier, J.; Schaffer, D. V. Viral Packaging and Transduction of Adult Hippocampal Neural Progenitors. **2010**, *621* (6), 103–116.
(87) Schindelin, J.; Arganda-carreras, I.; Frise, E.; Kaynig, V.; Longair, M.; Pietzsch, T.; Preibisch, S.; Rueden, C.; Saalfeld, S.; Schmid, B.; et al. Fiji : An Open-Source Platform for Biological-Image Analysis. *Nature* **2019**, *9* (7).
(88) Carpenter, A. E.; Jones, T. R.; Lamprecht, M. R.; Clarke, C.; Kang, I. H.; Friman, O.; Guertin, D. A.; Chang, J. H.; Lindquist, R. A.; Moffat, J.; et al. CellProfiler: Image Analysis Software for Identifying and Quantifying Cell Phenotypes. *Genome Biol.* **2006**, *7* (10).
(89) Moore, M. J.; Proudfoot, N. J. Pre-mRNA Processing Reaches Back to Transcription and Ahead to Translation. *Cell* **2009**, *136* (4), 688–700.
(90) Darnell, J. E.; Wall, R.; Tushinski, R. J. An Adenylic Acid-Rich Sequence in Messenger RNA of HeLa Cells and Its Possible Relationship to Reiterated Sites in DNA. *Proc. Natl. Acad. Sci.* **1971**, *68* (6), 1321–1325.
(91) Edmonds, M.; Vaughan, M. H.; Nakazato, H. Polyadenylic Acid Sequences in the Heterogeneous Nuclear RNA and Rapidly-Labeled Polyribosomal RNA of HeLa Cells : Possible Evidence for a Precursor Relationship. *Proc. Natl. Acad. Sci.* **1971**, *68* (6), 1336–1340.
(92) Lee, S. Y.; Mendeckif, J.; Brawermant, G. A Polynucleotide Segment Rich in Adenylic Acid in the Rapidly-Labeled Polyribosomal RNA Component of Mouse Sarcoma 180 Ascites Cells Biochemistry : *Proc. Natl. Acad. Sci.* **1971**, *68* (6), 1331–1335.
(93) Hardy, J. G.; Norbury, C. J. Cleavage Factor Im (CFIm) as a Regulator of Alternative Polyadenylation. *Biochem. Soc. Trans.* **2016**, *44* (4), 1051–1057.
(94) Derti, A.; Garrett-engele, P.; Macisaac, K. D.; Stevens, R. C.; Sriram, S.; Chen, R.;

Rohl, C. A.; Johnson, J. M.; Babak, T. A Quantitative Atlas of Polyadenylation in Five Mammals. *Genome Res.* **2012**, *22*, 1173–1183.
(95) Tian, B.; Manley, J. L. Alternative Polyadenylation of mRNA Precursors. *Nat. Rev. Mol. Cell Biol.* **2016**, *18* (1), 18–30.
(96) O'Brien, J.; Hayder, H.; Zayed, Y.; Peng, C. Overview of microRNA Biogenesis, Mechanisms of Actions, and Circulation. *Front. Endocrinol. (Lausanne)*. **2018**, *9* (AUG), 1–12.
(97) Zhou, Z.; Chen, P.; Zhou, Y.; Zhou, Z.; Qu, J.; He, L.; Zhu, Y.; Yang, S.; Zhang, F.; Guo, T.; et al. Stiff Matrix Instigates Type I Collagen Biogenesis by Mammalian Cleavage Factor I Complex- Mediated Alternative Polyadenylation Find the Latest Version : Stiff Matrix Instigates Type I Collagen Biogenesis by Mammalian Cleavage Factor I Complex-Mediated Al. **2020**, *5* (3).
(98) Flavell, S. W.; Kim, T.; Gray, J. M.; Harmin, D. A.; Hemberg, M.; Hong, E. J.; Markenscoff-papadimitriou, E.; Bear, D. M.; Greenberg, M. E. Genome-Wide Analysis of MEF2 Transcriptional Program Reveals Synaptic Target Genes and Neuronal Activity-Dependent Polyadenylation Site Selection. *Neuron* **2008**, *60* (6), 1022–1038.
(99) Weng, T.; Wagner, E. J.; Blackburn, M. R.; Weng, T.; Ko, J.; Masamha, C. P.; Xia, Z.; Xiang, Y.; Chen, N.; Molina, J. G.; et al. Cleavage Factor 25 Deregulation Contributes to Pulmonary Fibrosis through Alternative Polyadenylation. *J. Clin. Invest.* **2019**, *129* (5), 1984–1999.
(100) Ko, J.; Mills, T.; Huang, J.; Chen, N.; Mertens, T. C. J.; Collum, S. D.; Lee, G.; Xiang, Y.; Han, L.; Zhou, Y.; et al. Transforming Growth Factor B1 Alters the 3'-UTR of mRNA to Promote Lung Fibrosis. *J. Biol. Chem.* **2019**, *294* (43), 15781–15794.
(101) Blair, J. D.; Hockemeyer, D.; Doudna, J. A.; Bateup, H. S.; Floor, S. N.; Blair, J. D.; Hockemeyer, D.; Doudna, J. A.; Bateup, H. S.; Floor, S. N. Widespread Translational Remodeling during Human Neuronal Differentiation Resource Widespread Translational Remodeling during Human Neuronal Differentiation. *Cell Rep.* **2017**, *21* (7), 2005–2016.
(102) Chang, J.; Zhang, W.; Yeh, H.; Jong, E. P. De; Jun, S.; Kim, K.; Bae, S. S.; Beckman, K.; Hwang, T. H.; Kim, K.; et al. mRNA 3'-UTR Shortening Is a Molecular Signature of mTORC1 Activation. *Nat. Commun.* **2015**, *6* (7218).
(103) Morgan, J. T.; Murphy, C. J.; Russell, P. What Do Mechanotransduction, Hippo, Wnt , and TGF B Have in Common ? YAP and TAZ as Key Orchestrating Molecules in Ocular Health and Disease. *Exp. Eye Res.* **2013**, *115*, 1–12.
(104) Signaling, C.; Brumbaugh, J.; Stefano, B. Di; Wang, X.; Hu, G.; Shi, Y.; Hochedlinger, K. Nudt21 Controls Cell Fate by Connecting Alternative Polyadenylation to Chromatin Signaling. *Cell* **2018**, *172* (1–2), 106–109.e21.
(105) Alcott, C. E.; Yalamanchili, H. K.; Ji, P.; Heijden, M. E. Van Der; Saltzman, A.; Elrod, N.; Lin, A.; Leng, M.; Bhatt, B.; Hao, S.; et al. Partial Loss of CFIm25 Causes Learning Deficits and Aberrant Neuronal Alternative Polyadenylation. *Elife* **2020**, *9*, 1–30.
(106) Harrison, B. J.; Park, J. W.; Gomes, C.; Petruska, J. C.; Sapio, M. R.; Iadarola, M. J.; Chariker, J. H.; Rouchka, E. C. Detection of Differentially Expressed Cleavage Site Intervals Within 3 ′ Untranslated Regions Using CSI-UTR Reveals Regulated

Interaction Motifs. *Front. Genet.* **2019**, *10* (March), 1–15.
(107) Wouters, K.; Gorp, P. J. Van; Bieghs, V.; Gijbels, M. J.; Duimel, H.; Dieter, L.; Kruchten, R. Van; Maeda, N.; Staels, B.; Bilsen, M. Van; et al. Dietary Cholesterol, Rather than Liver Steatosis, Leads to Hepatic Inflammation in Hyperlipidemic Mouse Models of Nonalcoholic Steatohepatitis. *Hepatology* **2008**, *48* (31), 474–486.
(108) Bridge, A. J.; Pebernard, S.; Ducraux, A.; Nicoulaz, A.; Iggo, R.; Conant, G. C.; Wagner, A. Induction of an Interferon Response by RNAi Vectors in Mammalian Cells. *Nat. Genet.* **2003**, *34* (3), 263–264.
(109) Robinson, J. T.; Thorvaldsdottir, H.; Winckler, W.; Guttman, M.; Lander, E. S.; Getz, G.; Mesirov, J. P. Integrative Genomics Viewer. **2012**, *29* (1), 24–26.
(110) Lytle, J. R.; Yario, T. A.; Steitz, J. A. Target mRNAs Are Repressed as Efficiently by microRNA-Binding Sites in the 5' UTR as in the 3' UTR. *Proc. Natl. Acad. Sci.* **2007**, *104* (23).
(111) Plotnikova, O.; Baranova, A.; Skoblov, M. Comprehensive Analysis of Human microRNA – mRNA Interactome. **2019**, *10* (October), 1–11.
(112) Li, Z.; Kupcsik, L.; Yao, S.; Alini, M.; Stoddart, M. J. Mechanical Load Modulates Chondrogenesis of Human Mesenchymal Stem Cells through the TGF-B Pathway. *J. Cell. Mol. Med.* **2010**, *14* (6), 1338–1346.
(113) Romo, L.; Ashar-patel, A.; Pfister, E.; Aronin, N.; Romo, L.; Ashar-patel, A.; Pfister, E.; Aronin, N. Alterations in mRNA 3 ' UTR Isoform Abundance Accompany Gene Expression Changes in Human Huntington's Disease Brains. *Cell Rep.* **2017**, *20* (13), 3057–3070.
(114) Orengo, J. P.; Chambon, P.; Metzger, D.; Mosier, D. R.; Snipes, G. J.; Cooper, T. A. Expanded CTG Repeats within the DMPK 3' UTR Causes Severe Skeletal Muscle Wasting in an Inducible Mouse Model for Myotonic Dystrophy. *Proc. Natl. Acad. Sci.* **2008**, *105* (7), 2646–2651.
(115) Masamha, C. P.; Xia, Z.; Yang, J.; Albrecht, T. R.; Li, M.; Shyu, A.; Li, W.; Wagner, E. J. CFIm25 Links Alternative Polyadenylation to Glioblastoma Tumour Suppression. *Nature* **2014**, *510*.
(116) Robertson, M. J.; Peltier, J.; Schaffer, D. V. In Vivo Analysis of Engrafted Adult Hippocampal Neural Progenitors. *Methods Mol. Biol.* **2010**, *621* (6), 57–63.
(117) Cyrus, R.; Patel, N. R. A Network Algorithm for Performing Fisher ' S Exact Test in R × c Contingency Tables. *J. Am. Stat. Assoc.* **1983**, *1459*.
(118) Benjamini, Y.; Hochberg, Y. Controlling the False Discovery Rate: A Practical and Powerful Approach to Multiple Testing. *J. R. Stat. Soc. Ser. B* **1995**, *57* (1).
(119) Taylor, S.; Wakem, M.; Dijkman, G.; Alsarraj, M.; Nguyen, M. A Practical Approach to RT-qPCR — Publishing Data That Conform to the MIQE. *Methods* **2010**, *50* (4), S1–S5.
(120) Sanjana, N. E.; Shalem, O.; Zhang, F. Improved Vectors and Genome-Wide Libraries for CRISPR Screening. *Nat. Methods* **2014**, *11* (8), 783–784.
(121) Qi, L. S.; Larson, M. H.; Gilbert, L. A.; Doudna, J. A.; Weissman, J. S.; Arkin, A. P.; Lim, W. A. Repurposing CRISPR as an RNA-Guided Platform for Sequence-Specific Control of Gene Expression. *Cell* **2013**, *152* (5), 1173–1183.
(122) Ran, F. A.; Hsu, P. D.; Wright, J.; Agarwala, V.; Scott, D. A.; Zhang, F. Genome Engineering Using the CRISPR-Cas9 System. **2013**, *8* (11), 2281–2308.

(123) Sharpe, P. T. *Methods of Cell Separation*; Elsevier Science, 1988.
(124) Gilbert, L. A.; Horlbeck, M. A.; Adamson, B.; Villalta, J. E.; Chen, Y.; Whitehead, E. H.; Guimaraes, C.; Panning, B.; Ploegh, H. L. Genome-Scale CRISPR-Mediated Control of Gene Repression and Activation. *Cell* **2014**, *159* (3), 647–661.
(125) Li, J.; Fan, H.; Zhou, X.; Xiang, Y.; Liu, Y. Prognostic Signi Fi Cance and Gene Co-Expression Network of PLAU and PLAUR in Gliomas. *Front. Oncol.* **2022**, *11* (January), 1–13.
(126) Gu, X.; Fu, C.; Lin, L.; Liu, S.; Su, X.; Li, A.; Wu, Q.; Jia, C.; Zhang, P.; Chen, L.; et al. miR-124 and miR-9 Mediated Downregulation of HDAC5 Promotes Neurite Development through Activating MEF2C-GPM6A Pathway. *J. Cell. Physiol.* **2016**, *233*, 673–687.
(127) Sun, Y.; Jin, K.; Childs, J. T.; Xie, L.; Mao, X. O.; Greenberg, D. A. Vascular Endothelial Growth Factor-B (VEGFB) Stimulates Neurogenesis : Evidence from Knockout Mice and Growth Factor Administration. *Dev. Biol.* **2006**, *289*, 329–335.
(128) Bragado, P.; Valle, I.; Cuevas, E.; Lazaro, I.; Martin, C.; Cigudosa, J. C.; Silva, A. p53 REGULATES THE SELF-RENEWAL AND DIFFERENTIATION OF NEURAL PRECURSORS. *Neuroscience* **2009**, *158* (4), 1378–1389.
(129) Mack, J. J.; Mosqueiro, T. S.; Archer, B. J.; Jones, W. M.; Sunshine, H.; Faas, G. C.; Briot, A.; Aragón, R. L.; Su, T.; Romay, M. C.; et al. NOTCH1 Is a Mechanosensor in Adult Arteries. *Nat. Commun.* **2017**, *8*, 1–18.
(130) Mantovani, F.; Collavin, L. Mutant p53 as a Guardian of the Cancer Cell. *Cell Death Differ.* **2019**, *26*, 199–212.
(131) Ozaka, T.; Nakagawara, A. Role of p53 in Cell Death and Human Cancers. *Cancers (Basel)*. **2011**, *3*, 994–1013.